Formation and evolution of nearshore sandbar patterns

Marije W. J. Smit

PROPOSITIONS

pertaining to the thesis

The formation and evolution of nearshore sandbar patterns

by

M.W.J. Smit

Delft, January 18, 2010

1. The evolution of the nearshore zone depends strongly on the existing topography and rarely on the concurrent offshore wave conditions.
2. Hydrodynamics can only play a major role in short-term evolution when the initial bathymetry is alongshore uniform or when the conditions are extreme.
3. Highly evolved bed features maintain their own environment.
4. Successfully validating a model with observed morphological changes only, does not imply a correct representation of the physical processes.
5. Technical knowledge can not contribute to coastal safety without proper management and policy implementation.
6. Better models alone will not reduce the number of beach goers drowning in rip currents, education is at least as important.
7. Like a morphological system, society responds more unanimous to extreme conditions than to calm conditions.
8. Review comments are like paddling out through the surf: it is a good training in endurance and skill, so that at times you easily find your way through and can catch a wave.
9. This is something in between.
10. The difference between waiting and writing is only a letter.

These propositions are considered defendable and as such have been approved by the supervisors Prof.dr.ir M.J.F. Stive and Prof.dr.ir A.J.H.M. Reniers.

STELLINGEN

behorende bij het proefschrift

The formation and evolution of nearshore sandbar patterns

van

M.W.J. Smit

Delft, 18 januari 2010

1. De evolutie van de brandingszone is sterk afhankelijk van de bestaande topografie en zelden van de huidige golfcondities.
2. De hydrodynamica kan alleen sturend zijn in ontwikkeling op de korte termijn, als de initiële bodem kustlangs uniform is of de optredende energie extreem groot.
3. Ver ontwikkelde bodem patronen houden zichzelf in stand.
4. Het succesvol valideren van een morfologisch model met alleen morfologische veranderingen, betekent nog niet dat de fysische processen goed gerepresenteerd worden.
5. Technische kennis draagt niets bij aan kustveiligheid zonder goed management en uitvoering van beleid.
6. Betere modellen op zich zullen het aantal strandgangers dat in muistromen verdrinkt niet reduceren, onderwijs is minstens zo belangrijk.
7. Net als een morfologisch systeem, reageert een samenleving eensgezinder op extreme condities dan op kalme condities.
8. Commentaar is net als uitpeddelen door de branding: het is een goede training in uithoudingsvermogen en vaardigheid, opdat je er soms gemakkelijk doorheen komt en een golf kunt pakken.
9. Dit is iets er tussenin.
10. Het verschil tussen wachten en schrijven is slechts een paar letters.

Deze stellingen worden opponeerbaar en verdedigbaar geacht en zijn als zodanig goedgekeurd door de promotoren Prof.dr.ir M.J.F. Stive en Prof.dr.ir A.J.H.M. Reniers.

Formation and evolution of nearshore sandbar patterns

Formation and evolution of

nearshore sandbar patterns

PROEFSCHRIFT

ter verkrijging van de graad van doctor
aan de Technische Universiteit Delft,
op gezag van de Rector Magnificus prof.dr.ir. J.T. Fokkema,
voorzitter van het College voor Promoties,
in het openbaar te verdedigen op maandag 18 januari 2010 om 12.30 uur

door

Marije Welmoed Joanne SMIT
ingenieur civiele technologie en management
geboren te Berlijn

Dit manuscript is goedgekeurd door de promotoren:
Prof.dr.ir. M.J.F. Stive
Prof.dr.ir. A.J.H.M. Reniers

Samenstelling promotiecommissie:

Rector Magnificus	voorzitter
Prof.dr.ir. M.J.F. Stive	Technische Universiteit Delft, promotor
Prof.dr.ir. A.J.H.M. Reniers	University of Miami (Verenigde Staten), promotor
Prof.dr.ir. J.A. Roelvink	Technische Universiteit Delft
Dr. G.B. Ruessink	Universiteit Utrecht
Prof.dr. H. de Swart	Universiteit Utrecht
Dr. G. Symonds	CSIRO Marine and Atmospheric Research, Perth (Australië)
Prof.dr.ir. W.S.J. Uijttewaal	Technische Universiteit Delft

This research has been funded by the Dr.Ir. Cornelis Lely Foundation and the ONR-funded Beach Wizard project (N000140510266).

Front cover:	Scheveningen, The Netherlands
Back cover:	Scheveningen, The Netherlands
	Kijkduin, The Netherlands
	Peniche, Portugal
	Palm Beach, NSW, Australia (twice)

All pictures by Marije W.J. Smit

Printed by Ipskamp Drukkers BV, the Netherlands

ISBN 978-90-9025032-8

The electronic version of this publication can be found at http://repository.tudelft.nl

Abstract

The aim of this study is to understand whether hydrodynamic processes or geometrical characteristics play a dominant role in the response of the nearshore sandbar system to hydrodynamic conditions. To that end a depth-averaged (2DH) process-based model has been used to compute the morphological evolution of nearshore sandbars.

The morphological evolution was computed for an initially alongshore uniform beach profile with two bars with an alongshore length of 7 km, forced with constant hydrodynamic conditions over a period of two weeks. The computations aimed to investigate the evolution of the system. It was found that an identical initial cross-shore profile responds distinctly different to different constant hydrodynamic conditions, showing the role of the hydrodynamic conditions. The length scales of the bars (corresponding to rip channel distances) increased with increasing alongshore velocities and increasing depths of the bar crests. The length scales ranged from 300-700 m for the inner and 600-2000 m for the outer bar. The response time of the system was in the order of days and depends linearly on the local wave height, the alongshore current, the steepness of the bar and inversely on the active volume of the bar. Bars with a smaller volume were found to respond quicker. To speed up the morphological computations, the initial alongshore uniform bathymetries were perturbed with a random seed in the order of cm. Different seedings resulted in different locations of the evolving features, while maintaining the length scales corresponding to the forcing condition.

The role of the antecedent morphology was further investigated with computations with an increasing level of initial morphological variability. A high level of variability is for example formed by deep rip channels. With deeply imprinted bathymetrical patterns, the resulting hydrodynamical patterns prohibited the evolution of new patterns. This prohibited the adaptation toward length scales that would match the concurrent forcing conditions if the initial bathymetry would have been alongshore uniform. Only if the level of variability is small (smaller than O 0.5 m), the patterns adjusted toward the expected length scales. This was found for both evolutions with increasing as well as decreasing energy levels.

This explains why observed nearshore bar patterns rarely match the concurrent conditions. The antecedent level of variability is often high, which inhibits complete adaptation. Further, the

forcing conditions rarely persist for periods of time that are long enough for a system to evolve towards the corresponding length scales even if the initial variability would have been minimal.

A hindcast was performed of an observed morphological evolution at Palm Beach, New South Wales, Australia, during a ten day period including a storm event. Palm Beach is a pocket beach of about 2 km length. During the event, the wave energy increased from moderate to storm levels, subsequently decreasing again to moderate conditions. The observed morphological variability changed from a single barred beach with rip channels toward a reset morphology (no alongshore variability) during the storm with subsequently newly evolving rip channels during the quieter post-storm conditions. The initial bathymetries used for the model computations were inferred from video-observations of the dissipation patterns. The effect of wave groups, wave asymmetry, long wave induced sediment stirring, the amount of turbulence and the rate of morphological change was tested in creating and hindcasting the observed patterns.

It was found that these processes affect the magnitude and pace of morphological evolution. With optimal settings, the model including all mentioned processes forecasted a morphological evolution with decreasing variability during the storm event -similar to the observations. However, the observed amount of increase in bathymetrical variability after the storm event could not be matched in magnitude by the model. In general, best matches with observations were obtained for computations with a duration of up to three days. Within this period the different process settings only clearly changed the morphological evolution when the storm event was included within this period.

Excluding wave groups resulted in the evolution of slightly shorter length scales. During the storm event an offshore bar formed and subsequent evolution was small and occurred both near the shore (wave groups have a diffusive effect in shallow water) and in deeper water. Computations starting after the storm event showed very little difference in morphological evolution whether wave groups were included or not. Excluding wave asymmetry resulted in shoreward migration of the shoreline and very little morphological evolution after all initial features had been erased. Long wave induced sediment stirring has a large diffusive effect on the evolving morphological features. Excluding this stirring resulted in the evolution of extreme shore-attached features. When the turbulent diffusion in the model was decreased, similar types of features evolved, though at slightly different rates and moments. Increasing the rate of morphological change resulted in the evolution of increased, mainly shore-attached, morphological variability.

It was found that obtaining the correct pace and magnitude of morphological evolution is crucial for the level of success. If an event would encompass only an increasing or decreasing level of energy, it could be modelled. However, maintaining the correct pace and magnitude of evolution throughout a storm event has not been achieved with the currently tested model formulations and settings. This indicates that the model formulations need improvement. It is

suggested that improving the description of the diffusion, including improving the turbulence description, can improve the model's capabilities. This does not only require improved model formulations, but also increased knowledge of the turbulence processes in the nearshore zone.

The location of evolving features was found to be highly sensitive to the location and depth of imprint of features in the initial bathymetry. As this is rarely available to the required degree of accuracy, it is not expected that the exact location of features will be predicted correctly. However, the length scales and level of variability could be hindcasted if optimal settings are found, process descriptions improved (e.g. the diffusion) and if the model is morphologically calibrated both for evolutions with increasing and decreasing wave energy.

In conclusion, morphological evolution of nearshore sandbar patterns is found to be influenced by the initial morphology in two ways. First, if the initial variability is low, local hydrodynamic forcings -determined by the off-shore conditions and the local geometry- and their duration will determine the length scale. The location of initially small perturbations -order of cm- influences the location of rip channels. Second, if the initial morphology has a high level of variability, the bathymetry will remain the same due to the occurring hydrodynamic circulations which are reinforced by the incoming waves. Only an event with extreme energy may cause changes in the morphology in this case.

The hydrodynamics seem to have a rather small role in changing the patterns of a bathymetry in case there is a significant level of variability: they reinforce existing patterns and are only capable of drastically changing existing patterns when the energy level is extremely high. They do affect the length scales and the response time in case of small initial variability.

Using a morphological model requires accurate calibration of both the hydrodynamics as well as of the morphodynamics. Different nearshore processes have different effects with various magnitudes at different locations in the nearshore zone. Obtaining the correct balance between processes which amplify or damp existing patterns throughout an event with varying energy levels is currently a challenge. However, hindcasting either an up-state or a down-state morphological evolution is possible.

Samenvatting

Het doel van deze studie is te begrijpen in hoeverre hetzij de hydrodynamische processen dan wel de geometrische kenmerken dominant zijn in de reactie van kustnabije zandbank systemen op hydrodynamische condities. Hiertoe is een dieptegemiddeld (2DH) procesgebaseerd model gebruikt om de morfologische ontwikkeling van kustnabije zandbanken te berekenen.

De morfologische ontwikkeling is berekend voor een initieel kustlangs uniform profiel met twee banken van 7 km lengte kustlangs, welke geforceerd werd met constante hydrodynamische condities gedurende twee weken. De berekeningen hadden tot doel de ontwikkeling van het systeem te onderzoeken. Uit de resultaten bleek dat een identiek initieel kustdwars profiel onderscheidend anders reageert op verschillende hydrodynamische condities, wat de rol aantoont van de hydrodynamische condities. De lengteschalen van de banken (de afstanden tussen muigaten) namen toe met toenemende kustlangse stroomsnelheden en toenemende diepte van de top van de bank. De lengte schalen waren 300-700 m voor de binnenste en 600-2000 m voor de buitenste bank. De reactietijd van het systeem was in de orde van dagen en hangt lineair af van de lokale golfhoogte, de kustlangse stroomsnelheid, de steilheid van de bank en tegengesteld met het actieve volume van de bank. Banken met een kleiner volume bleken sneller te reageren. Om de morfologische berekeningen te versnellen, zijn de initiële kustlangs uniforme profielen verstoord met een willekeurige verticale variatie in de orde van cm. Verschillende variaties resulteerden in andere lokaties van de ontwikkelende vormen, terwijl de lengteschalen bleven passen bij de forceringsconditie.

De rol van de antecedente morfologie is verder onderzocht met berekeningen met een toenemend niveau van initiële variabiliteit. Een hoog variabiliteitsniveau wordt bijvoorbeeld gevormd door diepe muigaten. Diepe bathymetrische patronen resulteren in hydrodynamische patronen welke de ontwikkeling van nieuwe patronen verhinderen. Dit verhindert de aanpassing naar lengteschalen welke overeen zouden komen met de optredende forceringscondities, zoals ze op zouden treden wanneer de initële bodem kustlangs uniform was geweest. Alleen wanneer het variabiliteitsniveau laag is (kleiner dan O 0,5 m), pasten de patronen zich aan naar de verwachte lengteschalen. Dit werd gevonden voor ontwikkelingen met zowel toenemende als met afnemende energieniveau's.

Dit verklaart waarom geobserveerde zandbank patronen zelden overeenkomen met de optredende condities. Vaak is het antecedente variabiliteitsniveau hoog, wat een volledige aanpassing verhindert. Verder duren de forceringscondities zelden lang genoeg opdat een systeem zich kan aanpassen aan de bijbehorende lengteschalen, zelfs als het initiële variabiliteitsniveau minimaal zou zijn geweest.

Een hindcast is uitgevoerd van een geobserveerde morfologische ontwikkeling van Palm Beach, New South Wales, Australië, van tien dagen, welke een storm bevatte. Palm Beach is een pocket beach van 2 km lengte. Gedurende de periode nam de golfenergie toe van gematigd naar storm niveau om vervolgens af te nemen naar gematigde condities. De geobserveerde morfologische variabiliteit veranderde van een enkel bank systeem met muigaten naar een reset-morfologie (geen kustlangse variabiliteit) gedurende de storm met vervolgens nieuw ontwikkelende muigaten gedurende de kalmere post-storm condities. De initiële bathymetrieën welke in het model gebruikt werden, zijn verkregen uit video-observaties van de dissipatiepatronen. Het effect van golfgroepen, golfasymmetrie, sediment opwoeling ten gevolge van lange golven, de mate van turbulentie en de mate van morfologische verandering is getest in het creëren en hindcasten van de geobserveerde patronen.

Deze processen bleken de grootte en het tempo van de morfologische ontwikkeling te beïnvloeden. Met optimale instellingen voorspelde het model wat alle genoemde processen bevatte, een morfologische ontwikkeling met afnemende variabiliteit gedurende de storm -vergelijkbaar aan de observaties. Echter, de geobserveerde toename in bathymetrische variabiliteit na de storm werd niet in de juiste mate voorspeld door het model. Over het algemeen werden de beste overeenkomsten met de observaties gevonden voor berekeningen met een duur tot drie dagen. Binnen deze periode veranderden de verschillende proces-instellingen de morfologische ontwikkeling alleen wanneer de storm binnen deze periode viel.

Het uitsluiten van golfgroepen resulteerde in de ontwikkeling van iets kortere lengteschalen. Gedurende de storm vormde zich een bank uit de kust en de opeenvolgende ontwikkeling was klein en vond plaats zowel nabij de kust (golfgroepen hebben een diffusief effect in ondiep water) als in dieper water. Berekeningen welke na de storm begonnen, vertoonden weinig verschil in de morfologische ontwikkeling wanneer golfgroepen wel of niet werden meegenomen. Het uitsluiten van golfasymmetrie resulteerde in kustwaartse migratie van de kustlijn en zeer kleine morfologische ontwikkeling nadat alle initiële vormen waren uitgewist. De opwoeling van sediment ten gevolge van lange golven heeft een groot diffusief effect op de zich ontwikkelende morfologische vormen. Wanneer dit effect werd uitgesloten, ontwikkelden zich extreme aan de kust gebonden vormen. Wanneer de turbulente diffusie in het model was verlaagd, ontwikkelden zich gelijksoortige vormen, alhoewel in verschillend tempo en op verschillende momenten. Het verhogen van de mate van morfologische verandering resulteerde in de ontwikkeling van verhoogde, voornamelijk aan de kust gebonden morfologische variabiliteit.

Het verkrijgen van het juiste tempo en grootte van morfologische ontwikkeling werd bevonden cruciaal te zijn voor de mate van succes. Wanneer een gebeurtenis alleen een toenemend of alleen een afnemend niveau van energie behelst, kan het worden gemodelleerd. Echter, het behouden van het correcte tempo en de correcte grootte van ontwikkeling gedurende een storm gebeurtenis werd niet bereikt met de huidig geteste model formuleringen en instellingen. Dit duidt erop dat de model formuleringen verbetering behoeven. Er wordt voorgesteld dat een verbetering van de diffusie beschrijving, inclusief verbetering van de turbulentie beschrijving, de prestaties van het model kan verbeteren. Dit vereist niet alleen verbeterde model formuleringen, maar ook verbeterde kennis van de turbulentie processen in de kustnabije zone.

De lokatie van de zich ontwikkelende vormen bleek zeer gevoelig voor de lokatie en diepte van de vormen in de initiële bathymetrie. Daar deze zelden beschikbaar zijn in de vereiste mate van nauwkeurigheid, wordt niet verwacht dat de lokatie van vormen correct kan worden voorspeld. Echter, de lengteschalen en het variabiliteitsniveau zullen kunnen worden gehindcast wanneer optimale instellingen gevonden worden, procesbeschrijvingen verbeterd worden (zoals de diffusie) en als het model morfologische gecalibreerd is voor zowel ontwikkelingen met toenemende als met afnemende golfenergie.

Tenslotte werd er gevonden dat de morfologische ontwikkeling van patronen van kustnabije zandbanken op twee manieren wordt beinvloed door de initiële morfologie. Ten eerste, indien de initiële morfologie laag is, bepalen de lokale hydrodynamische forceringen -bepaald door de off-shore condities en de lokale geometrie- en de duur van deze forceringen, de lengteschalen. De lokatie van initieel kleine verstoringen -orde cm- beinvloedt de lokatie van muigaten. Ten tweede, indien de initiële morfologie een hoog variabiliteitsniveau heeft, blijft de bathymetrie gelijk ten gevolge van de optredende hydrodynamische circulaties welke worden versterkt door de inkomende golven. Alleen een gebeurtenis met extreme energie kan in dit geval de morfologie veranderen.

De hydrodynamische condities blijken een relatief kleine rol te hebben in het veranderen van patronen van een bathymetrie wanneer er een significant variabiliteitsniveau is: ze versterken de bestaande patronen en kunnen bestaande patronen alleen in grote mate wijzigen wanneer het energie niveau extreem hoog is. Ze beïnvloeden wel de lengteschalen en reactietijden in het geval van kleine initiële variabiliteit.

Het gebruik van een morfologisch model vereist nauwkeurige calibratie van zowel de hydrodynamica als de morfodynamica. Verschillende kustnabije processen hebben verschillende effecten van verscheidene grootte op verschillende lokaties in de kustnabije zone. Het verkrijgen van de correcte balans tussen processen met versterkende en dempende effecten gedurende een gebeurtenis met variërende energieniveau's is momenteel een uitdaging. Echter, het hindcasten van ofwel een up-state ofwel een down-state morfologische ontwikkeling is mogelijk.

Contents

Chapter 1

Introduction

Nearshore sandbars are common features along sandy coasts. These bars may be shore-parallel, possibly with crescent-like shapes, they may be oblique or shore-attached. Their patterns are generally not preserved in time. It seems that when they change, this happens in response to offshore wave conditions. The exact interaction between the offshore wave forcing and the local bathymetrical (sub-aqueous bed level) configuration and thus impact on the hydrodynamics and sediment transport, is not yet fully understood.

The current work aims to increase the understanding of the behaviour of sandbars in response to wave conditions and to investigate to what extent the behaviour is intrinsically determined by the properties of the system itself.

Increasing knowledge of the coastal zone will result in a safer use of the coastal zone: both for local recreation purposes as well as for coastal defense of the hinterland.

1.1 Background

This thesis concerns the behaviour of nearshore sandbars, bars that occur in water depths of about 0.5 m to 6 m which are situated tens to hundreds of meters offshore. The emphasis is on the behaviour of these bars on spatial scales up to a few kilometers and time scales of days to weeks. These bars are affected by several interacting processes. Waves in the nearshore zone may break, resulting in both currents and turbulence, bringing sediment in the water column, which is transported by the currents. This can result in accretion or erosion of existing features which presence feeds back to the water motion. Below, the main known processes, occurring in the nearshore zone, relevant for this thesis, are briefly introduced.

1.1.1 Waves and currents

Wind blowing over the ocean generates waves. These waves travel and when approaching the shore, entering shallow water, they will reshape (shoal). When the wave height is about 80%

of the water depth, the waves will break, dissipating their energy. In case there is a nearshore bar (Figure 1.1), the wave may already break when reaching the bar -depending on the wave height and the water depth over the bar. If the wave height is small, the wave will travel over the bar and break when it reaches shallower water near the beach. When there are multiple bars and the incoming waves are large, the waves may break on the outer bar (the bar located most offshore), dissipating most of their energy offshore. The remaining waves will continue on-shore, possibly breaking when reaching the inner bar or when reaching the shoreline. The presence of nearshore bars thus decreases the wave energy which actually reaches the dry beach and therefore the wave energy which directly affects the visible part of the coastal defense. The area where waves are breaking and are influenced by the bathymetry is called the surf zone.

Wave fields are generally described using the statistics of the incoming incident waves. In the field, the propagating wind waves reorder into wave trains (wave groups). These result in water level set-down (set-up) at the location of the higher (lower) short waves, resulting in a bound long wave. The bound long waves have periods of around 20 to 200 s (while individual incident short waves have periods up to 20 seconds). Waves with such large periods are also referred to as infragravity waves.

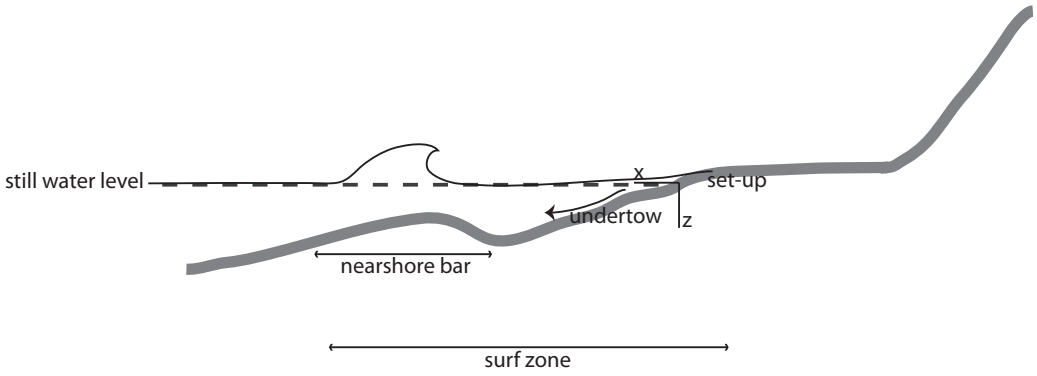

Figure 1.1: Cross-shore profile of the nearshore zone showing relevant definitions, processes and parameters.

When waves travel into shallower water, they break, lose energy and their height decreases. This results in a gradient in the radiation stress. This gradient is balanced by a slope of the mean water surface, resulting in wave set-up near the shoreline (Figure 1.1). The mass of water carried shoreward by the breaking waves in a surf zone will be compensated by a seaward return flow, often referred to as the undertow (Svendsen, 1984). When obliquely incident waves (i.e. waves approaching the shore under an angle) break, the changes in alongshore directed momentum generate an alongshore current.

Rip currents are another type of offshore directed currents. They result from alongshore water level gradients (in space), either induced by the topography (Figure 1.2) or due to spatial variations in the wave field (for example low frequency motions) (e.g. Symonds and Ranasinghe, 2000), resulting in transient rips (e.g. Johnson and Pattiaratchi, 2004). In the case of a

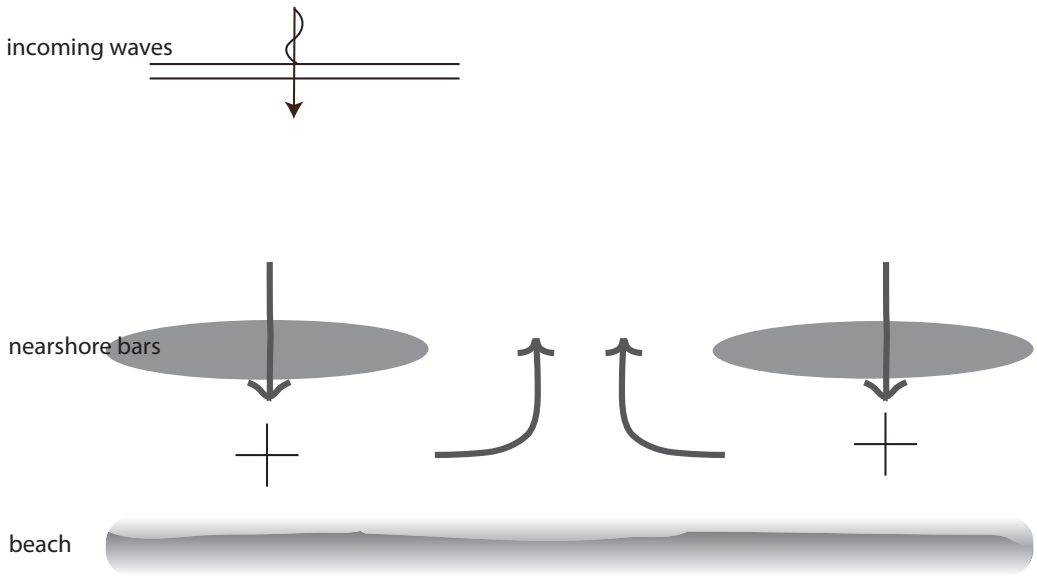

Figure 1.2: Top view of incoming waves and the resulting alongshore variable wave set-up (indicated with the +) near the shoreline, resulting in rip currents in the rip channels in between the shoals.

topographically induced rip current, the coast may for example have a single bar, intersected by rip channels. Due to the different water depths, the water level set-up due to the incoming waves will vary in the alongshore. The lowest set-up will occur over the rip channel, resulting in currents toward this location, and thus off to sea. These rip currents can reach velocities up to 1 m/s, forming a serious hazard for users of the coastal zone, whether it be coastal scientists doing field work or swimmers, when they get unintentionally caught by a rip. On the other hand, users like surfers who intend to get past the surf zone use the rip currents to allow an easier way to deeper water with unbroken waves. The danger lies in the fact that the unaware swimmer thinks to enter a quiet part of the ocean -where no waves are breaking- and opt to swim in a falsely looking safe area. However, the lack of breaking waves is due to the deeper rip channel, where a rip current may take the swimmer off to sea. Rip currents currently lead to drownings at almost any beach around the world. Users of the coast should therefore be trained in both the danger of rip currents and correct response when caught in a rip (Appendix 1). Life guards are trained on the presence of rip currents and public awareness is raised in some places. The ability to predict the location and occurrence of rip currents will enable a safer use of the coastal zone, see MacMahan et al. (2006) for a review of rip currents.

Compared to the effects of individual waves and wave groups, the water level in the nearshore area varies also on a larger time and spatial scale: due to the tide. The tidal effects are not taken into account in this thesis, as it was found from test computations that, although including tides affect instantaneous hydrodynamic patterns, they did not alter the morphodynamic results for

the investigated beaches (which have a tidal range of 1 m).

1.1.2 Sediment transport

Sediment in the water, for example due to turbulence as a result of wave breaking, will be transported by the nearshore currents. Erosion and accretion of the nearshore area occurs when there is a gradient in sediment transport. No change occurs when:

$$\frac{\delta S_x}{\delta x} + \frac{\delta S_y}{\delta y} = 0$$

with $S_{x,y}$ = sediment transport, x, y is respectively the cross-shore and alongshore direction and location.

Sediment transport is generally described as a function of the velocity (e.g. v^3, with v the velocity). Several processes affect this transport. First the amount of sediment that is in suspension (in the water column), which is affected by the turbulence. Turbulence brings sediment into suspension, and also has a diffusive effect on nearshore patterns. Further in the nearshore zone, the wave crests are shorter and higher and the wave troughs are longer and flatter, called wave asymmetry, which affects the sediment transport. The orbital motion under the crest is relatively high and results in onshore transport. Under the trough the velocities are smaller resulting in smaller offshore transport. The net effect of wave asymmetry is typically onshore sediment transport.

When accounting for the effect of wave groups, the sediment transport is affected as well as the hydrodynamics. In the nearshore area, the long wave results in water level set-down at the location of the higher short waves. At the locations of high short waves, more sediment is stirred up, which is then transported offshore due to the bound infragravity wave induced offshore current resulting in net offshore transport.

The above described processes give a synoptic overview of processes affecting nearshore sediment transport and which are included in (parts of) the current work.

1.2 Observed and modelled bar behaviour

Nearshore bar patterns have been observed to vary in time. Wright and Short (1984) combine incoming wave energy with the type of coast (reflective to dissipative), to explain whether the response will be slow (low energy, reflective) or fast (high energy, dissipative coast) and whether erosion or accretion will occur. Further, they define a down-state sequence of 6 beach states ranging from dissipative to reflective. They based their analysis on observed behaviour at Australian beaches. Lippmann and Holman (1990) extended the work by Wright and Short

(1984) by distinguishing two extra classes. They defined a sequence of eight beach states, based on four characteristics of the morphology (existence or absence of a bar, dominant bar scaling, longshore variability, trough). They based their analysis on a two year data-set of video images of Duck, North Carolina, USA. Different types of behaviour have been observed at different coasts, also the response time seems to vary at different coasts. Van Enckevort et al. (2004) hypothesized that the volume of the bars played a role in the response time of the system. They used video-based information, using the Argus video-system (e.g. Holman and Stanley, 2007). Video images allow observations with high resolution in both time and space. The dissipation patterns (occurring at locations with shallower depths, i.e. at the bar crest locations) are analysed in time, combining those with information of the incoming wave energy and the local beach characteristics. In most field-based analyses, it was aimed to couple the beach state or characteristics to the concurrent hydrodynamic conditions. However, clear links could not be found (e.g. Holman et al., 2006; Turner et al., 2007). In general, nearshore systems are analysed using the length scales (i.e. alongshore rip channel distances), the level of variability, the offshore location of the bar and/or the mean cross-shore profile.

Next to using field observations, nearshore bar behaviour is analysed using various types of models. Edge wave template models aimed to show the relationship between the standing edge waves and observed length scales (e.g. Bowen and Inman, 1971; Holman and Bowen, 1982). However, this relationship is in fact not found in the field and in later modelling work it was shown that the standing edge waves are not the causing factor in the evolution of crescentic bars (e.g. Reniers et al., 2004).

Linear stability analyses are performed aiming to investigate the length scales of the fastest growing mode. However, the lack of correlation between time series of observed concurrent hydrodynamic conditions and occurring length scales (e.g. Holman et al., 2006) as well as the high level of variability in length scales at any given moment in time (e.g. Van Enckevort et al., 2004), may affect how the results of these models can be interpreted and used. Morphological modelling with process-based models has been under development in the past decades (e.g. Reniers et al., 2004; Grunnet et al., 2004; Castelle et al., 2005). These models include physical descriptions of the nearshore processes, including waves, currents and sediment transport. As some processes are either not fully understood or too complex to describe physically (with the current computational capacities), the effect of these processes is included using parameterizations or empirical descriptions. Morphological models can be done in one dimension (only cross-shore evolution), 2DH (depth-averaged, 3D morphological evolution), or fully three-dimensional (3D). The latter includes the information of velocity profiles, which are not uniform over the depth of the water column.

Another type of models are aggregated models which describe the behaviour of the coast using certain key parameters. For example by linking the incoming wave height with the cross-shore bar location, and looking for a relationship which explains the variability (Plant et al., 2006).

The required model parameters are based on data.

From these different attempts in understanding nearshore bar behaviour it seems that more factors than only offshore wave conditions play a role in the morphological response. Calvete et al. (2007) showed that for several cases with shore-normal waves, the cross-shore profile was more important than the incoming wave height in determining the response of the system. It has also been observed that at certain beaches, a large storm has hardly any effect, while a storm with similar energy at another beach resulted in large morphological changes. To conclude, the exact links and roles of concurrent hydrodynamic conditions and several properties of the concurrent geometry in the response of nearshore bar systems are not yet fully understood.

1.3 Research questions

This thesis aims to improve the understanding of nearshore bar behaviour and specifically the role of hydrodynamic conditions and antecedent morphology. We would like to understand which processes are crucial to incorporate into a process-based model in order to be able to hindcast and predict morphological bar behaviour.

The main research question addressed in this thesis is:

Why does an observed nearshore bar pattern look the way it does?

We hypothesize that the response of a nearshore bar system is a function of both the hydrodynamics and the concurrent morphology. In fact we would like to know when precisely the observed pattern is a function of the concurrent hydrodynamic conditions or the antecedent bathymetry or a mix thereof.

This question is split into three subquestions:

- How would a nearshore bar system evolve if it would have a constant forcing and an initially alongshore uniform profile?
  - what is the role of the hydrodynamic conditions?
  - what is the role of the geometry?
- What is the role of the antecedent morphology?
- Which processes are dominant in creating the observed patterns?

1.4 Approach

1.4.1 Method

The research questions are approached by using a depth-averaged process-based numerical morphological model (2DH).

The model includes wave transformation. The nearshore currents are computed based on the radiation stresses due to the waves, using the non-linear shallow water equations. With these currents, using the advection-diffusion equation and the equilibrium concentration as obtained with a transport equation, the sediment transport is computed. The changes in the bed level per flow time step are computed (using the bed-level continuity equation). Then the wave transformation over the new bed level is computed (Figure 1.3). The processes that are specifically included for the different chapters are summarized in Table 1.1.

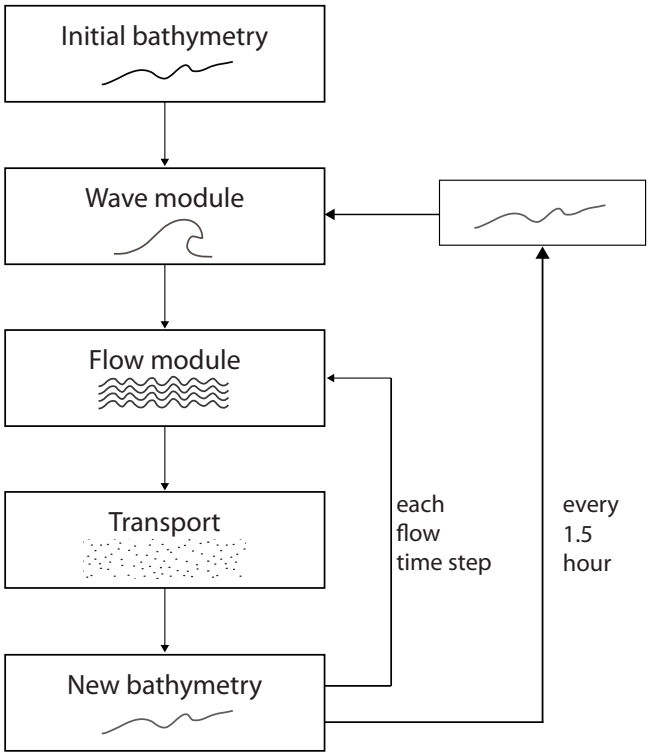

Figure 1.3: Set-up of the process based model with basic process description.

1.4.2 Structure

The intention of the system is the response the system would show if it would have a constant forcing and no morphologically induced restrictions, other than those due to the initially alongshore uniform profile. This is investigated using computations of the morphological evolution of an alongshore uniform double barred beach, which is forced with sixteen different constant hydrodynamic conditions (Chapter 2). The resulting morphological patterns are analysed using

process/setting/condition	Chapter 2	Chapter 3	Chapter 4
short waves	x	x	x
wave groups			x
roller effects			x
undertow			x
wave asymmetry			x
no tide	x	x	x
diffusion	constant	constant	f(turbulence, depth)
time varying conditions		x	x
observation-based bathymetry			x
idealised bathymetry	x	x	

Table 1.1: Processes and settings included in the 2DH process-based models used in chapter 2, 3 and 4; x indicates that the process/setting is included.

the evolving length scales and bathymetrical variability. Their evolution in time is followed, resulting in measures for the intended length scales and the response times of the system. These have been determined for two different initial cross-shore profiles, to investigate the role of the cross-shore geometry in the evolving length scales and response times of the system. These are determined as a function of the hydrodynamical conditions. Further, five different initial perturbations (order cm) have been used to test their effect on the evolving features. This approach gives insight in the intention of the system as a function of both the initial geometry and the hydrodynamic conditions.

Chapter 3 includes the results of numerical modelling tests with various levels of variability in the initial morphology. This allows investigation of the role of the level of variability on the level of adaptation toward changing hydrodynamic conditions. When does a bathymetry evolve toward the template corresponding with the concurrent hydrodynamic conditions, i.e. when is the morphological evolution dependent on the hydrodynamic condition alone?

In Chapter 4 the role of various processes in morphological evolution and the capability to model these processes is investigated. An observed morphological evolution of 10 days throughout a storm event was hindcasted using a model with various process and parameter settings. The evolution was computed starting from different start dates, giving insight in how long the morphological evolution could be hindcasted and what the role was of the initial bathymetry, the conditions in the following evolution and whether different processes play a more or less dominant role in different parts of the morphological evolution. Video-based observations have been used to obtain the initial bathymetries for this morphological evolution and to compare the computed evolution with the observed.

In Chapter 5 (Synthesis) the findings are discussed and compared with other literature, resulting in conclusions, discussion and recommendations.

Chapter 2

The morphological response of a nearshore double sandbar system to constant wave forcing

M.W.J. Smit[1*], A.J.H.M. Reniers[1,2], B.G. Ruessink[3], J.A. Roelvink[4,5]

This chapter is based on a paper published in Coastal Engineering 55 (2008), p. 761-770.

1. Delft University of Technology, faculty of Civil Engineering and Geosciences, PO Box 5048, 2600 GA Delft, The Netherlands; MWJS is currently affiliated with The Netherlands Institute of Ecology (NIOO-KNAW), PO Box 140, 4400 AC Yerseke, The Netherlands
2. Rosenstiel School of Marine and Atmospheric Science (RSMAS) University of Miami, 4600 Rickenbacker Causeway, FL 33149-1098, Miami, USA
3. Utrecht University, Faculty of Geosciences, Department of Physical Geography, Institute of Marine and Atmospheric Research, Heidelberglaan 2, 3584 CS Utrecht, The Netherlands
4. UNESCO-IHE, PO Box 3015, 2601 DA Delft, The Netherlands
5. Deltares, PO Box 177, 2600 MH Delft, The Netherlands

*Corresponding author. Tel.: +31 113 577470; Fax: + 31 113 573616. E-mail address: M.Smit@nioo.knaw.nl (M.W.J. Smit).

Abstract

Results of 2DH morphodynamic computations are presented to quantify the temporal evolution of the crescentic patterns emerging in a double nearshore bar system in response to constant wave boundary forcing. Sixteen different conditions varying both offshore wave height and angle of wave incidence were applied. The mean length scales of the emerging irregular crescentic patterns are linearly proportional to the local longshore velocity over the inner and outer bar. For similar longshore velocities, the length scales of the outer bar are larger than of the inner bar. This is explained by accounting for the difference in water depth above the bar crest. The variable morphological response times can be explained by including additional bathymetrical parameters. The active volume of the bar, defined by the breaker index, plays an important role in this response time. With larger active volumes the bar responds more rapidly to identical

boundary conditions. Also, bars with a smaller total volume respond more quickly. This faster response is due to the steeper active volume of the bars. Different initial perturbations resulted in different locations of the emerging features, showing that their location is sensitive to the initial bathymetry. However, the range in length scales and response times due to the different perturbations was significantly smaller than those obtained for the different hydrodynamic conditions. Based on the present findings we hypothesize that morphological length scales in the field are rarely in equilibrium with the concurrent offshore wave height and angle of incidence owing to the slow response of the sandbars under constant conditions relative to the stochastic nature of natural wave forcing.

Keywords: double nearshore bar system, process-based model, length scale, response time, morphology, rhythmicity

2.1 Introduction

Analyses of nearshore sandbar observations show a wide range of morphological variability. The sandbar patterns vary from linear, shore parallel (reset-morphology) to undulating or crescentic, in part welded to the beach. These patterns can be found in both single and multiple bar systems (Van Enckevort et al., 2004). In general, high energy conditions lead to straightening of the bars, while during lower energy conditions the bars break up to form crescents, sometimes intersected by rip channels (Wright and Short, 1984).

Attempts to correlate the prevailing hydrodynamic conditions to observed rip spacings have not yet led to conclusive explanations (Holman et al., 2006). This may be caused by the relatively slow response of crescentic patterns and rips relative to the variability in the forcing, implying that rip spacings are rarely in equilibrium with the actual wave conditions (Plant et al., 2006). Wright and Short (1984) stated that the rate of the morphodynamic response to low-energy events is slower than to high-energy events. The rapid changes in natural wave conditions may therefore prohibit the beach to evolve to the beach states matching the actual conditions. This means that the observed beach states are more likely correlated to a sequence of past conditions than to the actual conditions. This dependence of the actual morphology on past conditions is not only a function of the duration and intensity of the wave conditions but also related to the fact that the time required to evolve from one beach state to the next is proportional to the volume of sand that needs to be redistributed (Wright and Short, 1984). In addition, Calvete et al. (2007) point out that slight variations in the characteristics of cross-shore depth profiles, such as water depth above the crest, rather than the offshore wave conditions can be more important for rip channel spacing.

Hence, in order to understand why the actual bathymetry exhibits a certain morphological pattern, one needs to know the following. First: what is the intention of the system, i.e. how would

the morphological system respond if a hydrodynamic condition would persist for an infinite period? Second: how long does it take for the system to develop this morphological response? Thirdly: what is the effect of the antecedent morphology on the morphological evolution?

This paper focuses on the first two items by means of a depth-averaged process-based (2DH) model. To that end the computed morphological response of a double barred beach to a large range of hydrodynamic conditions is examined in space (spatial patterns) and time (evolution). Both the angle of wave incidence and the wave height are varied. This is in contrast with earlier work (e.g. Deigaard et al., 1999; Damgaard et al., 2002) where generally either the wave heights or the angles of wave incidence were varied. We apply each condition sufficiently long to reach a quasi-steady state in length scales and bed variability.

The effect of the antecedent morphology is addressed here to a lesser extent. The self-organizing morphological response in our model is promoted by the selective growth of a small (order of cm) random vertical perturbation of the bathymetry. It is important that the trends in the morphological response are due to different offshore wave conditions rather than a result of the interaction of the perturbed initial bathymetry and the applied offshore condition. Therefore, we use five different initial perturbations for each hydrodynamic condition to test that the trends are significantly different to the range in results due to different initial perturbations.

Field observations of double barred systems show inner and outer bar patterns to be different for the same offshore wave conditions (e.g. Van Enckevort et al., 2004). This is tested and analysed here further by using a double barred bathymetry in the computations. Van Enckevort et al. (2004) additionally suggested that increased bar volume leads to increased response times. Therefore, for a selected set of hydrodynamic conditions, computations with 2 different profiles are analysed.

To understand nearshore bar behaviour, others have analysed their model results on the computed length scales (lengths of the crescents or rip channel distances), cross-shore variability, migration and growth rates of the features, combined with the applied hydrodynamics. Studies of single barred systems based on linear stability analyses showed for example that for obliquely incident waves, the length scales increase with increasing trough area and increasing longshore current velocities (Deigaard et al., 1999). For shore normal incident waves Damgaard et al. (2002) found that the length scales remained unchanged with increasing wave height, only the growth rate increased, whereas Calvete et al. (2007) found increasing length scales for increasing wave heights. An advantage of 2DH morphodynamic models over linear stability analysis is that they allow for temporal and alongshore variations in crescent lengths (e.g. Damgaard et al., 2002; Reniers et al., 2004; Smit et al., 2004), consistent with Van Enckevort et al. (2004) who observed variations in the field upto a factor 2 in the wavelength and amplitude of individual crescents at any moment in time. The modelling study by Reniers et al. (2004) for example, predicts a variation which agrees with the measurements presented by Holman et al. (2006). Klein and Schuttelaars (2006) who investigated the morphodynamic evolution of double barred

beaches for both the linear and non-linear regime, found that the spacings predicted with the linear stability analysis are only observed during the exponential growth phase of the non-linear experiments. In the dynamic phase, multiple modes span the bed features. The present modelling approach also allows for the non-linear evolution of the beach patterns resulting in quasi-rhythmic patterns.

The applied model set-up and equations are introduced in Section 2.2. Section 2.3 explains the method of analysis and describes the results. In Section 2.4 the results are discussed and compared with work by others. Conclusions are drawn in the final section.

2.2 Method

2.2.1 Model set-up

The numerical model, a research version of Delft3D (www.deltares.nl, Roelvink and Van Banning, 1994; Lesser et al., 2004; Reniers et al., 2004), consists of coupled modules for simulating short waves, currents, sediment transport and bed level update.

Wave Module

The wave propagation, breaking and corresponding radiation stresses are computed with SWAN (Booij et al., 1999). The waves are described with a two-dimensional wave action density spectrum $N(\sigma,\theta)$, defined as the energy density spectrum divided by the relative frequency σ as observed in a reference frame moving with the current velocity, θ being the angle of wave incidence. The corresponding spectral action balance equation is

$$\frac{\partial N}{\partial t} + \frac{\partial c_x N}{\partial x} + \frac{\partial c_y N}{\partial y} + \frac{\partial c_\sigma N}{\partial \sigma} + \frac{\partial c_\theta N}{\partial \theta} = \frac{S}{\sigma} \tag{2.1}$$

with c_x,c_y, c_σ and c_θ the propagation velocities in x-, y-, σ - and θ -space respectively, t being time. $S(\sigma,\theta)$ is the source/sink term, representing the effects of generation, dissipation and non-linear wave-wave interactions as function of frequency and direction. Default settings were used throughout the present study.

Flow Module

The flow driven by radiation stress gradients is calculated with the non-linear depth-averaged shallow water equations. Delft3D-flow solves the Navier-Stokes equations for an incompressible fluid, under the shallow water and the Boussinesq assumptions. In the vertical momentum equation the vertical accelerations are neglected, which leads to the hydrostatic pressure equation. The corresponding depth-averaged continuity equation is

$$\frac{\partial \eta}{\partial t} + \frac{\partial u(d+\eta)}{\partial x} + \frac{\partial v(d+\eta)}{\partial y} = 0 \tag{2.2}$$

and the momentum equations in horizontal direction are given by

$$\frac{\partial u}{\partial t} + u\frac{\partial u}{\partial x} + v\frac{\partial u}{\partial y} + g\frac{\partial \eta}{\partial x} + \frac{\tau_x - F_x}{\rho(d+\eta)} - \nu_t\left(\frac{\partial^2 u}{\partial x^2} + \frac{\partial^2 u}{\partial y^2}\right) = 0 \tag{2.3}$$

$$\frac{\partial v}{\partial t} + u\frac{\partial v}{\partial x} + v\frac{\partial v}{\partial y} + g\frac{\partial \eta}{\partial y} + \frac{\tau_y - F_y}{\rho(d+\eta)} - \nu_t\left(\frac{\partial^2 v}{\partial x^2} + \frac{\partial^2 v}{\partial y^2}\right) = 0 \tag{2.4}$$

in which d is the water depth with respect to mean sea level (MSL), g is gravitational acceleration, $F_{x,y}$ are the x- and y-component of external forces due to waves computed with SWAN, u and v are the depth-averaged velocity components in x- and y-direction respectively, ρ is the mass density of water, $\tau_{x,y}$ are the cross- and longshore components of the bed shear stress, ν_t is the turbulent eddy viscosity and η is the water level with respect to MSL.

Sediment Module

The suspended sediment transport is modelled with a depth-averaged, advection diffusion equation

$$\frac{\partial}{\partial t}hC + \frac{\partial}{\partial x}hCu + \frac{\partial}{\partial y}hCv - \frac{\partial}{\partial x}D\frac{\partial hC}{\partial x} - \frac{\partial}{\partial y}D\frac{\partial hC}{\partial y} = \frac{hC_{eq} - hC}{T_s} \tag{2.5}$$

in which h is the local water depth, C is the depth averaged sediment concentration, D= 0.5 m^2/s is the horizontal diffusion coefficient, C_{eq} is the depth averaged equilibrium concentration and T_s is the adaptation time, representing the vertical diffusion of the sediment.

The equilibrium concentration (C_{eq}) is the suspended transport (S_s) divided by the local water depth and velocity magnitude. The value of S_s is computed using Bijker (1971) which takes into account the effect of wave stirring.

The bed load (S_b), which is adjusted every flow timestep, is also computed according to Bijker (1971).

$$S_b = bD_{50}\frac{q}{Ch}\sqrt{g}\,(1-\varepsilon_{por})\,\mathrm{e}^{A_r} \tag{2.6}$$

with $b = 2$, Ch is the Chézy coefficient using Manning $Ch = h^{1/6}/0.026$, D_{50} is the mean grain diameter (D_{50} = 150 μm), q is the flow velocity magnitude, A_r is a dimensionless parameter including the shear stress due to currents and waves and $\varepsilon_{por} = 0.4$, the porosity of the sea bed. The bed load transport is adjusted for effects of the bed slope in the direction of the sediment

transport, following Bagnold (1966) and Ikeda (1982) for the longitudinal and transverse slope effects.

To compute the new bottom, the bed level continuity equation is applied,

$$(1 - \varepsilon_{por}) \frac{\partial z_b}{\partial t} + \frac{\partial S_x}{\partial x} + \frac{\partial S_y}{\partial y} = 0 \tag{2.7}$$

in which z_b is bed level, $S_{x,y}$ are the combined bed load and suspended load transport rates in x- and y-direction. For further details, refer to Lesser et al. (2004) and the Delft3D manual (www.deltares.nl).

No specific cross-shore effects, like undertow, are taken into account in this paper. Also, the present computations do not include sediment transport in the wave direction due to wave skewness or asymmetry. We assume that these effects, while important for the longer term modelling profile, evolve slowly relative to bar rhythmicity. Given the incomplete physical description of the cross-shore sediment transport processes the computed cross-shore migration of the bars is not analysed. The cross-shore migrations of the evolving crescents, however, do limit the duration of our computations as the shoals ultimately weld to the coast.

The transport and bottom changes are calculated for each flow time step, with a morphological factor to speed up the computations (Roelvink, 2006), assuming that the flow field does not change significantly within that period (equal to the flow time step times the morphological factor). For the present computations a morphological factor of 15 was used. This means that for every flow step of 6 s, the morphological adjustment over a period of 1.5 minutes is calculated. This loop is done 60 times (which in this case corresponds to 1.5 hour morphologically), after which the waves are recomputed with the latest bathymetry.

2.2.2 Initial bathymetry and grid

The initial bathymetry is based on a measured cross-section at Egmond aan Zee, the Netherlands (Figure 2.1). This measured cross-section is applied over a length of 7000 m to obtain an alongshore-uniform stretch of coast.

The model area has a width of 1200 m cross-shore. A small (order of 1 cm) random perturbation is applied over the whole model area to reduce the time needed to start the morphological evolution. Initial computations showed that a different seed of the perturbation resulted in slightly different patterns in the bathymetry. This raised the question whether applying different perturbations would result in different conclusions about the effects of the angle of wave incidence. To investigate the range in resulting patterns, five different random perturbations were created for each hydrodynamic condition. Computations were carried out on a 15x15 m grid; a denser grid did not alter the results.

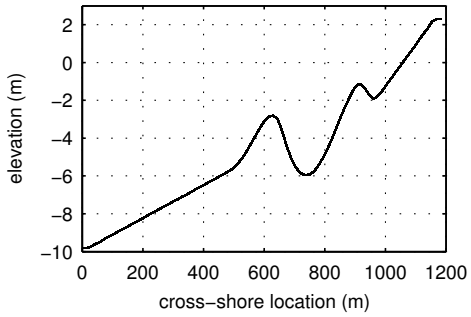

Figure 2.1: Elevation (relative to mean sea level) versus cross-shore location as used in the simulations.

2.2.3 Model settings: boundary conditions

On the wave grid, the waves are incident at the seaward boundary only. The wave grid is larger than the flow grid, hence the waves are incident on both the lateral and seaward boundaries of the hydrodynamic grid. The lateral hydrodynamic boundaries of the flow model are defined as zero water level gradients perpendicular to the shore normal. The seaward boundary is a zero water level boundary. The bottom boundaries are defined as zero depth gradients on the lateral boundaries.

2.2.4 Computational settings

All computations are carried out for fourteen days. The used model settings result in net onshore bar movement, thus prohibiting the possibility to extend computations for much longer as the evolving shoals would have welded to the shoreline. The wave height in all computations is set at the offshore boundary. The wave period in all computations is six seconds. Tide is not included in the computations.

To investigate the effect of the angle of wave incidence (θ), computations were done with four angles of wave incidence ranging from shore normal to 30° (with a 10° step size). Four wave heights were chosen to investigate the effect of the significant wave height (H_s): 1 m, 1.5 m, 2 m and 2.5 m. The directional wave spreading is constant at 30°. Five different initial perturbations were applied for each hydrodynamic condition to investigate the stochastic nature of the morphological response of the system. Thus sixteen hydrodynamic conditions were applied, each with five different initial perturbations, resulting in eighty computations in total.

2.3 Results

All applied offshore wave forcings resulted in crescentic bar evolution with an example ($\theta = 10°$ and $H_s = 1.5$ m) given in Figure 2.2b. This example shows a clear response of the inner bar and

a weaker response of the outer bar for this hydrodynamic condition. The length scales on the inner bar are all considerably smaller than the length scales on the outer bar and vary in the alongshore. The resulting development of the bars for other conditions show similar variations in length scales. The exact length scales and response times of the patterns however, varied for the various wave heights and angles of wave incidence.

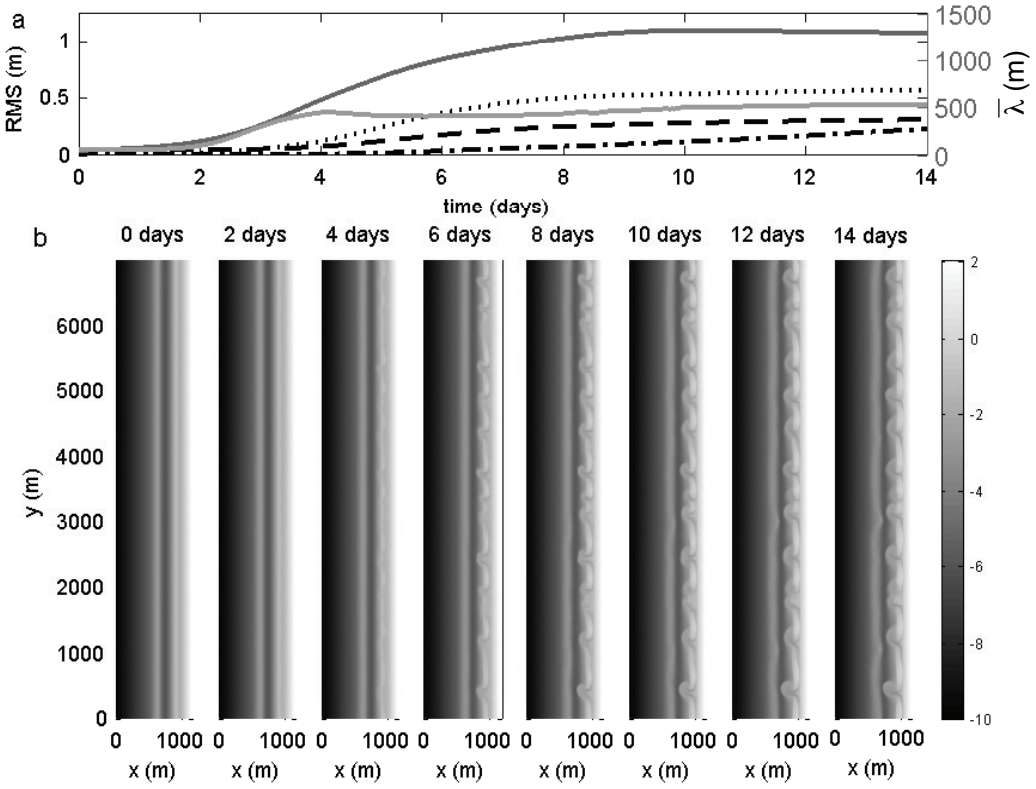

Figure 2.2: a: Evolution of *RMS* for a computation with $H_s = 1.5$ m, $\theta = 10^o$, for the whole area (dashed line), inner bar (dotted line) and outer bar (dash-dotted line) and evolution of inner bar $\overline{\lambda}$ (light grey) and outer bar $\overline{\lambda}$ (dark grey). b: Bathymetrical development of bottom with perturbation 1, with $H_s = 1.5$ m and $\theta = 10^o$, colorbar indicates elevation in m (light is shallow, dark is deep).

The following describes the definition for the length scale, the morphological development and the response time of the system. The trends of these parameters for all conditions are then analysed.

2.3.1 Length scale definition

The length scale is quantified using the contours of the bathymetry. The geographical location of these contours is used in a Fourier analysis to obtain an objective quantitative value of the length scales observed in the computations (Figure 2.3).

For this length scale analysis, long uninterrupted signals, representing the longshore variability are desired. Depth contours give two possible problems, interrupted contours and multiple-

valued signals (i.e. more than one cross-shore value per alongshore location). The first can be caused by interaction of the depth contours of the two bars or by defining a too shallow contour value, which does not occur continuously alongshore. To avoid this, first, the mean depth is computed over the inner bar area. Next, the contour is computed at a value of this mean depth minus two times the standard deviation of the depths in the inner bar area (Figure 2.3b). This contour value accounts for the alongshore variation in depth which will be larger at later stages of the morphological evolution. The same is done for the outer bar. If a contour does not cover the whole model area, or if it exists of several small parts, the longest stretch is chosen for the analysis, with a required minimum length of 750 m.

The second possible problem, a multiple-valued signal, is caused by the occasionally alongshore skewed appearance of the emerging crescents. At alongshore locations where this original contour signal has two cross-shore values, the double cross-shore values are cut out to obtain a single-valued signal (Figure 2.3b), used in the Fourier analysis (Figure 2.3c). The resulting Fourier transform is weighted with the variance ($(Fzy)^2$) per wavenumber (k_y [m^{-1}]), resulting in the weighted length scale ($\overline{\lambda}$). A $\overline{\lambda}$ value was computed for each computation and each time step.

$$\overline{\lambda} = \frac{\int (Fzy)^2 dk_y}{\int k_y (Fzy)^2 dk_y} \tag{2.8}$$

In other studies, length scales were frequently determined manually. Van Enckevort et al. (2004), however developed an automated method based on the maximum dissipation over the bar as seen in time-exposure video images. Our method gives similar length scales to their method (Appendix C).

2.3.2 Morphological development

The degree of morphological change within an area is quantified as the root mean square value (RMS [m]) of the differences between the actual depth and the corresponding alongshore mean depth at each timestep. The RMS is computed for three areas, the whole model domain and for the inner and outer bar areas, defined by 225 m wide sections around the bar crest.

The RMS values for one computation ($H_s = 1.5$ m, $\theta = 10^o$), with the corresponding bathymetries at 0, 2, 4, 6, 8, 10, 12 and 14 days respectively, are shown in Figure 2.2. For the whole area, the RMS value initially shows exponential growth followed by a saturation stage. After 10 days, the variation of the bathymetry does not alter anymore. The exact patterns might still change location, however. In this computation, the final inner bar RMS value is reached earlier than the outer bar value. Also, the inner bar RMS values are larger than those of the outer bar, implying that for this computation the inner bar shows a larger response than the outer bar. Further, the outer bar RMS is still increasing, implying that the outer bar patterns are not saturated at the end of the computation.

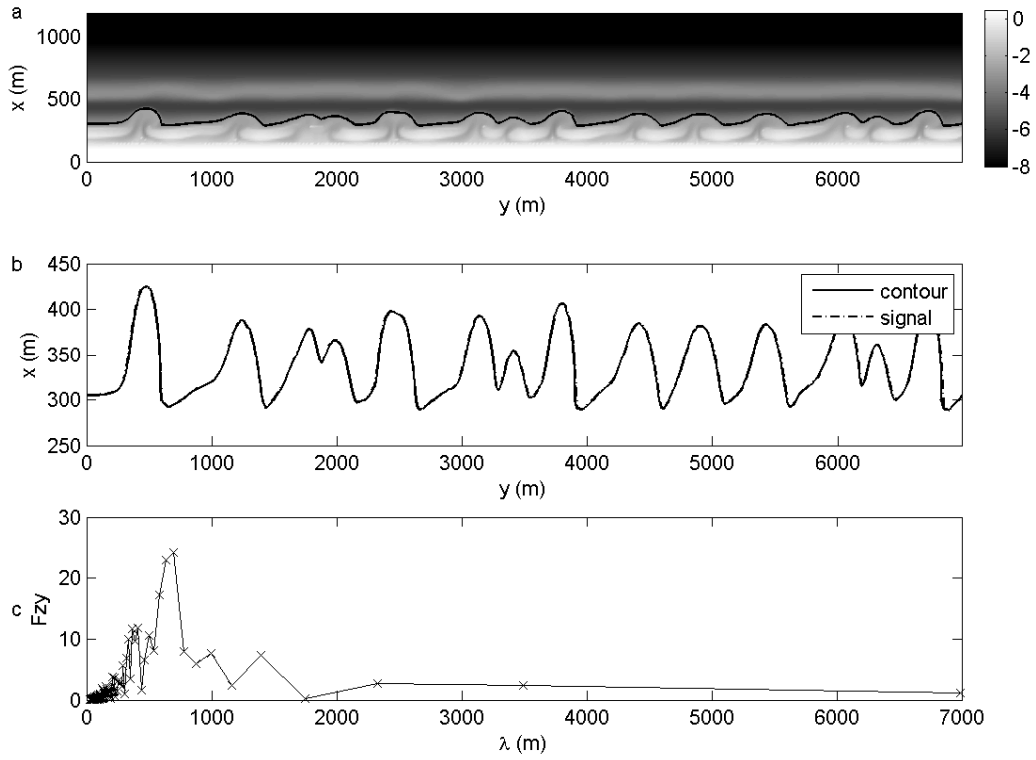

Figure 2.3: a: Bathymetry with the contour indicated on the inner bar as used for the length scale definition, same signal is shown in b with corresponding single-valued signal as used for the Fourier transform, which spectrum (Fzy versus λ) is shown in c. The figures correspond with 10 days of morphological response to H_s =1.5 m, $\theta = 10^o$.

The inner bar $\overline{\lambda}$ starts evolving after two days, while the *RMS* value is still small. In the following two days, $\overline{\lambda}$ evolves to about 575 m, at which it remains for the remainder of the computation. The outer bar $\overline{\lambda}$ shows similar development starting at a later moment and growing to a larger value (i.e. longer length scale).

When looking at the bathymetrical development (Figure 2.2b) of this computation we see that the inner bar indeed responds stronger to the applied wave conditions than the outer bar and that the outer bar patterns develop later than the inner bar patterns. After 6 days the inner bar patterns remain the same whereas the outer bar patterns are still developing. It is apparent that the length scales start evolving while the morphological evolution is still small (e.g. at 3 days for the inner bar). The bars seem to reach a (weighted) length scale at this early stage, which then remains constant with time.

2.3.3 All conditions

The evolution of the *RMS* and of the inner- and outer bar $\overline{\lambda}$ for all offshore wave conditions based on the same initial bathymetrical perturbation is presented in Figure 2.4 (The bathymetrical evolution of these 16 conditions are included in Appendix B). As can be seen, large angles and small wave heights (upper right hand corner) result in relatively low *RMS* values. Also, the moment at which the final *RMS* value is reached for the whole area is postponed for larger θ. In fact, for large θ, fourteen days of morphological evolution are not enough to reach an equilibrium value. For the computations with obliquely incident waves and large wave height, the *RMS* decreases after reaching a peak value. The results further indicate that the outer bar response is larger than the inner bar response, especially for the larger wave heights.

Initially, the inner bar $\overline{\lambda}$ increases rapidly, when the *RMS* is still small. For the oblique angles this is followed by a slight decrease in $\overline{\lambda}$. In general, the final $\overline{\lambda}$ ($\overline{\lambda}_{end}$) is reached before the *RMS* has reached its saturation value. This indicates that the weighted equilibrium length scales in the system develop at an early stage, with only small bathymetrical changes at first and are then maintained when the features develop further. For some conditions however (e.g. H_s = 2.5 m, $\theta = 10^o$, outer bar), the $\overline{\lambda}$ still changes slightly after 14 days.

The outer bar $\overline{\lambda}_{end}$ generally exceeds the inner bar $\overline{\lambda}_{end}$ (see Figure 2.4). For the more oblique waves and larger wave heights, the length scales on the outer bar evolve at an earlier stage in the computations than the length scales on the inner bar. This does not necessarily seem to correspond to a more rapid evolution of the *RMS* of the outer bar. Note that the $\overline{\lambda}_{end}$ is generally reached earlier on the inner bar, implying that it takes longer for the outer bar to evolve towards the intended length scales. This might be due to the larger bar volume and greater water depth above the outer bar.

The small wobbles in the $\overline{\lambda}$-evolution are due to the previously mentioned variable lengths of the contours due to possible interactions of the bar contours. In general, the length scales on

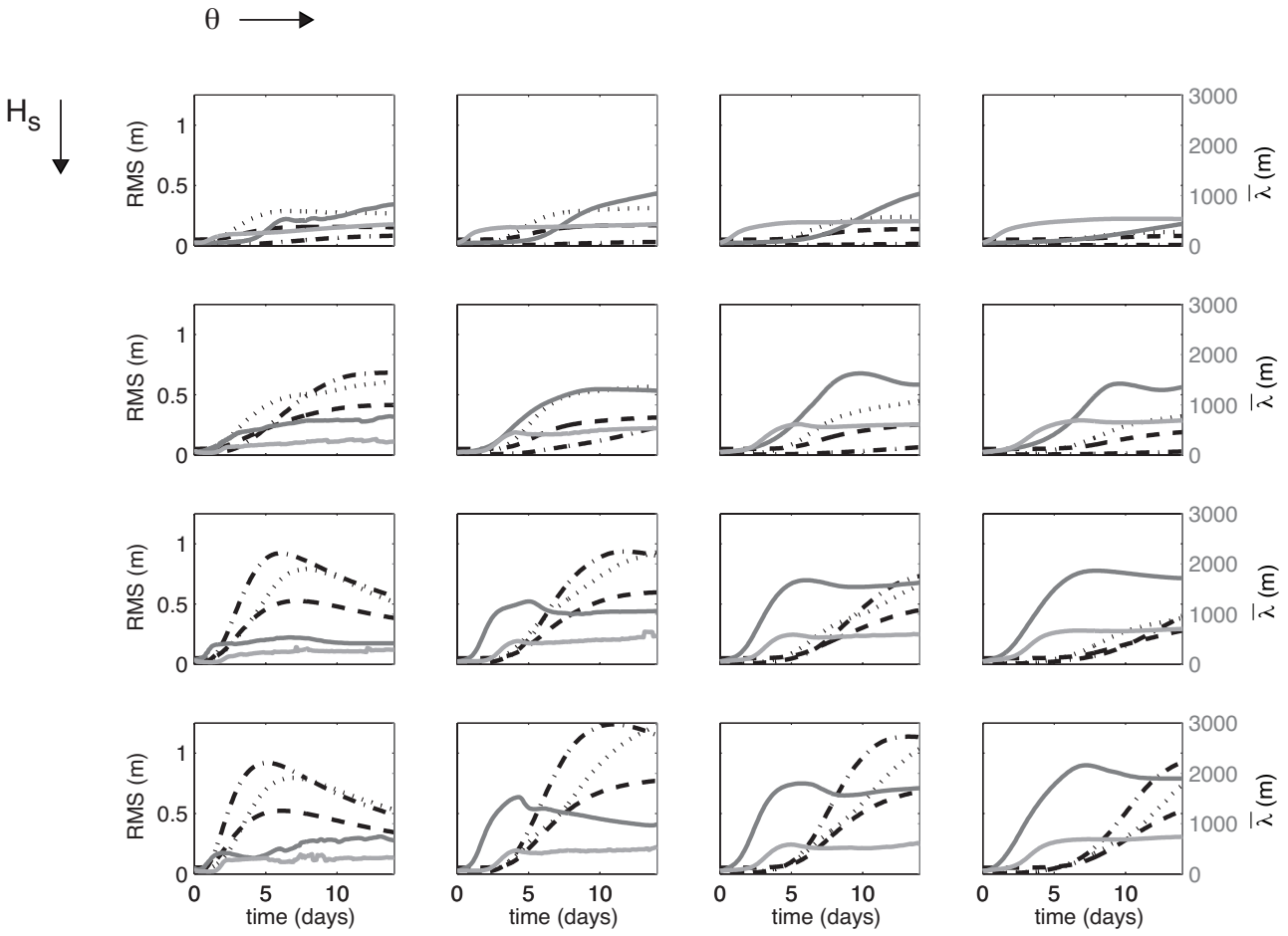

Figure 2.4: Evolution of *RMS* (black) of the whole area (dashed), inner bar (dotted line), outer bar (dash dotted line), inner bar $\overline{\lambda}$ (light grey) and outer bar $\overline{\lambda}$ (dark grey) for 16 hydrodynamic conditions: rows (left to right) correspond to increasing θ ($0^o, 10^o, 20^o, 30^o$), columns (top to bottom) to increasing H_s (1, 1.5, 2, 2.5 m). All computations had identical initial perturbation.

the outer bar are more easily detected, resulting in smoother lines, as the seaward side of the outer bar, which does not interact with other features, is used for this analysis. The inner bar contours, however, might interact with either the shore or the outer bar. These interactions are omitted from the analysis, but this might result in smaller lengths of the used contour, resulting in a slightly wobbling length scale evolution (e.g. normal waves, with $H_s = 1.5$ m). This especially holds for the shore-normal cases that show the emergence of outer bar crescents with a large cross-shore amplitude (first column in Figure 2.4).

The morphological evolution of the emerging three-dimensional patterns in all simulations can be described by a sequence of initial development, growth and saturation. The growth takes place due to the reinforcement of the hydrodynamics and the evolving bed patterns. The currents are onshore over the shoals, followed by longshore currents in the inner trough and offshore directed currents in the rip channels. These rips can be oblique when the waves are obliquely incident. Instead of an ongoing deepening of the rips and heightening of the shoals, this morphological evolution reaches a saturated state. This is shown in Figure 2.4 by the levelling off of the *RMS* evolution for the whole area. Garnier et al. (2006) suggests that saturation is reached due to the balance between the positive feedback between flow and morphology and the diffusive effect of down-slope sediment transport.

2.3.4 Length scale analysis

The inner- and outer bar $\overline{\lambda}_{end}$ for all 16 simulations are shown in Figure 2.5 as a function of the offshore wave height. Each data marker represents the mean of five computations with identical hydrodynamic conditions, but five different initial bathymetrical perturbations. The vertical lines around each data marker are the standard deviation from this mean. Computations with identical hydrodynamic conditions but different initial perturbations of the bathymetry give similar length scales of the evolving features, even though these features evolve at different locations and may evolve in slightly different ways and with slightly different length scales. The resulting range in length scales due to different perturbations is however smaller than the range due to different hydrodynamic conditions. Nonetheless, we find that exact patterns and rip channel locations are sensitive to the initial bathymetrical conditions, indicating the difficulty in deterministically predicting local alongshore variability in nearshore bar behaviour (see also Calvete et al., 2007).

As can be seen in Figure 2.5a, the inner bar $\overline{\lambda}_{end}$ increases with wave angle for a given wave height and, except for shore-normal waves, the inner bar $\overline{\lambda}_{end}$ also increases with the wave height itself for a fixed wave angle. For the same wave height and angle, the outer bar $\overline{\lambda}_{end}$ are larger than the inner bar $\overline{\lambda}_{end}$ (compare Figure 2.5a with Figure 2.5b).

As can be deduced from Figure 2.5b, outer bar $\overline{\lambda}_{end}$ also increases with the angle of wave incidence for the same wave height. For conditions with small wave heights and oblique angles

of wave incidence, the outer bar (whose crest is at 2.8 m depth) is hardly affected by the waves and as a result the outer bar bathymetry did not evolve. The length scales on the outer bar from these computations (with $RMS < 0.09$ m) were therefore not computed.

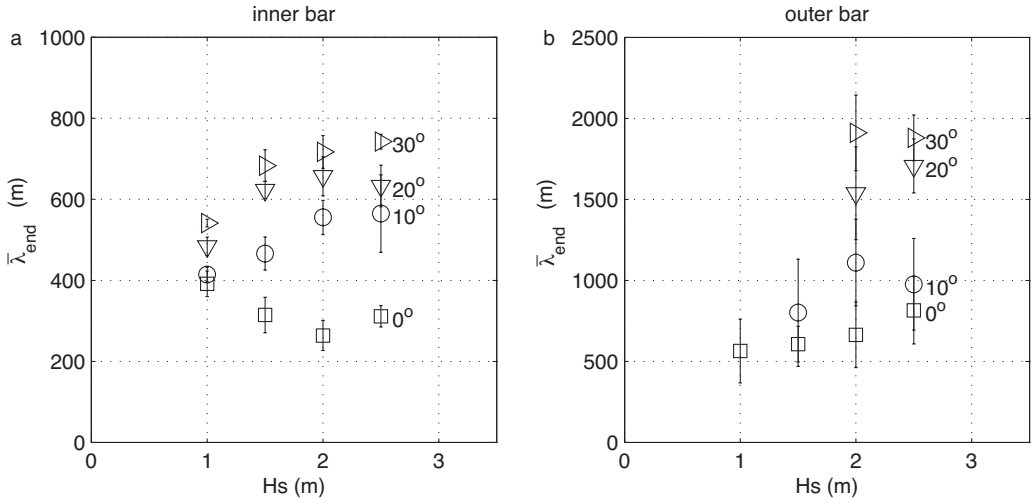

Figure 2.5: Mean of the $\overline{\lambda}_{end}$ for 5 initial perturbations on inner bar (a) and outer bar (b) versus H_s. Different markers indicate different θ. The vertical lines are $\pm$ 1 standard deviation. For computations with RMS <0.09 m the $\overline{\lambda}_{end}$ are not included.

In Figure 2.5 $\overline{\lambda}_{end}$ is presented as a function of the *offshore* wave height and angle. However, the wave height and angle of wave incidence on the bar crests will be different from the offshore values because of wave shoaling, breaking and refraction. To examine how $\overline{\lambda}_{end}$ depends on local hydrodynamical characteristics, the wave height, angle of incidence and alongshore current velocity (V_y) at the bar crests at t=0 were determined and correlated with $\overline{\lambda}_{end}$. The strongest correlation was found for $\overline{\lambda}_{end}$ and V_y (Figure 2.6a). The observed linear dependence of $\overline{\lambda}_{end}$ and V_y is consistent with Deigaard et al. (1999), who investigated the effect of oblique waves on a single bar system. They found that by varying the geometry of the trough and a number of flow parameters, a V_y increase gave an increase in the preferred wavelength of the evolving patterns.

In more detail, the outer bar $\overline{\lambda}_{end}$ are larger than the inner bar $\overline{\lambda}_{end}$ (Figure 2.6a) for the same V_y and increase more with increasing V_y. To examine whether this behaviour is related to the differences in the local water depth, 1.1 m and 2.8 m for the inner and outer bar respectively, $\overline{\lambda}_{end}$ is plotted as function of $V_y h_{crest}$ which collapses both $\overline{\lambda}_{end}$-V_y relationships on a single line (with h_{crest} = depth over the bar crest, Figure 2.6b).

The computed length scales correspond well with the local waterdepth at the bar crest multiplied by the mean alongshore velocity ($V_y h_{crest}$). This measure is indicative of the momentum associated with the longshore current ($\rho h_{crest} V_y$) and therefore suggests that the deceleration of the longshore current may be an important parameter in the determination of the length scales of the rip spacing. The velocity field on an alongshore quasi rhythmically-varying bar crest

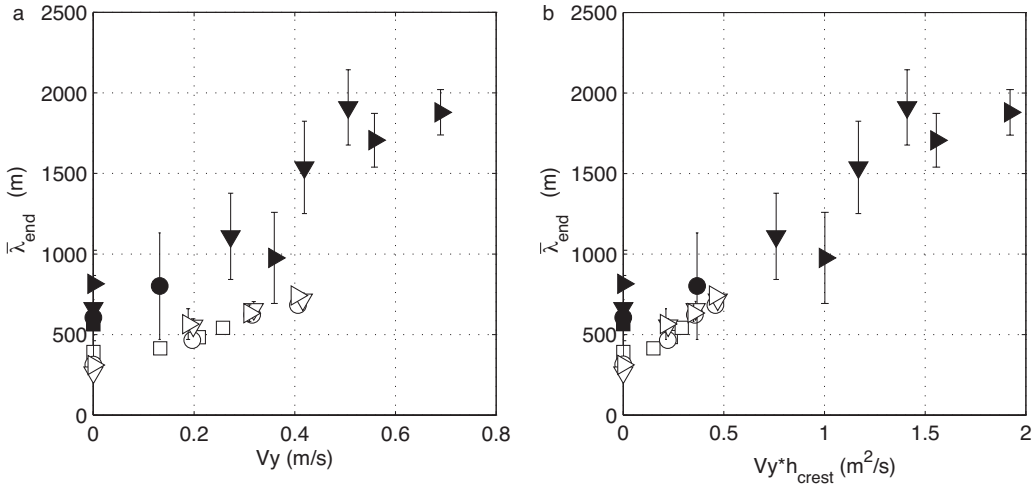

Figure 2.6: a: $\overline{\lambda}_{end}$ versus V_y on the inner (white) and outer (solid) bar. b: $\overline{\lambda}_{end}$ versus $V_y h_{crest}$ for inner (white) and outer (solid) bar. The markers indicate offshore H_s ($\square$= 1 m, $\circ$ = 1.5 m, $\bigtriangledown$ = 2 m, $\triangleright$ = 2.5 m).

displays a meandering character. If we assume that in the deceleration area the wave forcing is minimal and the stationary flow is governed by friction only, the wave-averaged alongshore momentum balance, Equation 2.4, can be written as:

$$\rho h v \frac{\partial v}{\partial y} = -\tau_y \tag{2.9}$$

Using a simple expression for the bottom shear stress, we obtain:

$$h v \frac{\partial v}{\partial y} = -c_f v \left| v \right| \tag{2.10}$$

which can also be written as:

$$\frac{1}{v}\frac{\partial v}{\partial y} = -\frac{c_f}{h} \tag{2.11}$$

provided $v > 0$. The corresponding velocity for a freely decelerating flow then becomes:

$$v(y) = V_{y,crest} e^{-\frac{c_f y}{h}} \tag{2.12}$$

where $V_{y,crest}$ corresponds to the longshore current velocity at the bar crest. Assuming that the longshore current velocity has to reduce to a velocity at which the sand is no longer picked up by the flow, V_{crit}, the corresponding length scale (L_y) can be retrieved:

$$L_y = -\frac{h}{c_f y} \ln \frac{V_{crit}}{V_{y,crest}} \tag{2.13}$$

Using $c_f = 0.0035$ (common value for the longshore current friction parameter) and using the critical velocity as a fit parameter, $V_{crit} = 0.055$m/s (being close to the critical shields velocity)

the predicted length scales are in agreement with the computed $\overline{\lambda}_{end}$ for obliquely incident wave conditions (Figure 2.7). This explains why the outer bar has larger length scales: the bar crest is at a larger depth, meaning that the water needs more time to decelerate, in which it travels further for the same flow alongshore pattern (driven by either circulation cells or directly by the longshore current).

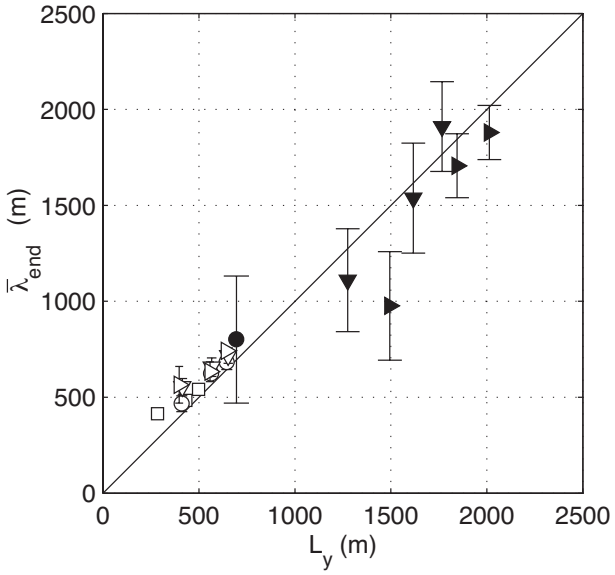

Figure 2.7: $\overline{\lambda}_{end}$ versus L_y on the inner (white) and outer (solid) bar. The markers indicate offshore H_s ($\square$= 1 m, $\circ$ = 1.5 m, $\bigtriangledown$ = 2 m, $\triangleright$ = 2.5 m) for obliquely incident waves only.

2.3.5 Response times

The response time (T_{resp}) of the system is defined here as the moment at which the *RMS* curve has its first deflection point, that is, when the rate of change starts to decrease. The response time is computed for the *RMS* of the inner bar and the outer bar area seperately. T_{resp} of the inner bar is similar for the different offshore wave heights (Figure 2.8), while T_{resp} decreases with wave height on the outer bar. For increasing offshore angles of wave incidence, T_{resp} increases for both inner and outer bar.

To understand why the inner and outer bar T_{resp} are different for the same offshore wave height and angle, T_{resp} has been analysed as functions of the local wave height, angle of wave incidence, dissipation, long shore current and orbital velocities as computed on the bars. In addition, we defined a bathymetrical parameter, termed the active volume (Vol_a, Figure 2.9). The active volume is defined by the volume of the bar where the breaker index ($\gamma = H_s/h$ with h = local water depth) is larger than 0.3. When waves break at larger depth, the turbulent motion affects a larger part of the bar. It is expected that when a larger part of the bar is mobilized, the bar evolves more rapidly.

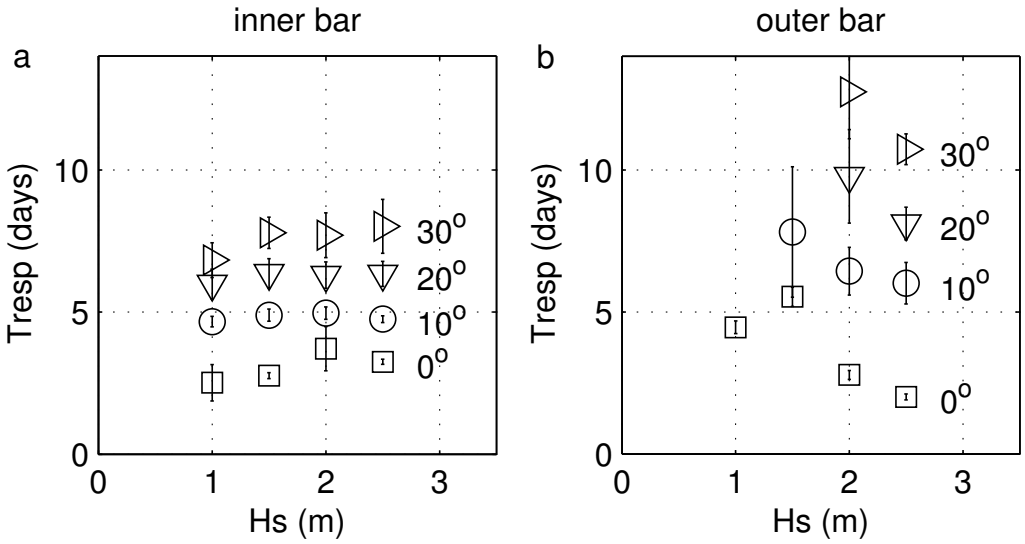

Figure 2.8: T_{resp} of the inner bar area (a) and outer bar area (b) versus offshore H_s. Different markers indicate different angles of wave incidence.

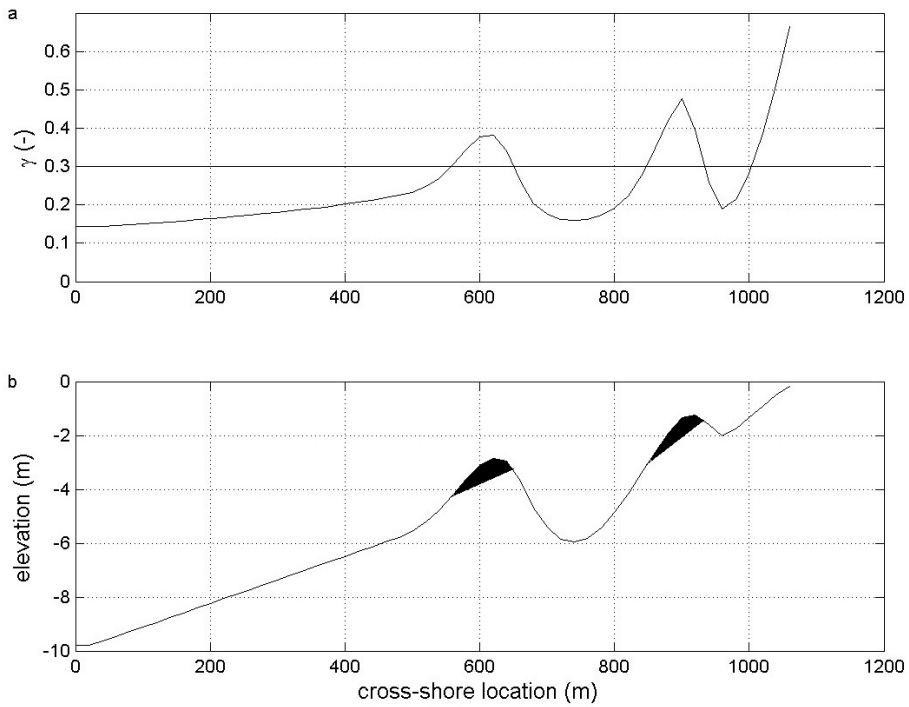

Figure 2.9: a: Breaker index versus cross-shore location. b: Elevation versus cross-shore location, shaded areas indicating the active volume of outer and inner bar. Used computation: $H_s = 2$ m, $\theta = 20^{\circ}$.

We found that T_{resp} is well correlated to the local wave height multiplied by the local V_y divided by Vol_a (Figure 2.10). A physical explanation for this dependence can be inferred from examing the alongshore sediment transport rate in combination with the active volume. Using the simpler transport formulation of Bailard (1981) to estimate the alongshore sediment transport rate:

$$S_y \approx C_1 u_{rms}^2 V_y \tag{2.14}$$

where C_1 is a dimensional scaling coefficient. Using linear wave theory to obtain the near-bed orbital velocity (u_{rms}) and assuming shallow water wave conditions Equation 2.14 can be rewritten to:

$$S_y \approx C_1 g H_{rms}^2 h V_y \tag{2.15}$$

At breaking the local water depth and the incident wave height are correlated through γ which then gives:

$$S_y \approx C_1 g \gamma H_{rms} V_y \tag{2.16}$$

The response time is then obtained by dividing Vol_a with the sediment transport rate obtained from Equation 2.16. Unfortunately Vol_a and $H_{rms}V_y$ are not independent where for instance both Vol_a and V_y depend on the offshore H_{rms}. This leads to the counterintuitive result that a larger sediment transport rate leads to a longer response time (Figure 2.10), which is explained by the concurrent smaller increase in the active volume.

2.3.6 Effect of different bar volume

To test whether bar volume affects the response time, as suggested by Van Enckevort et al. (2004), the results of the Egmond profile were compared with the results for a profile with smaller bar volumes but with bar positions and depths identical to the Egmond profile. Both the on- and offshore slopes of the bars of Profile 2 have a steeper profile than in the original Egmond profile (Figure 2.11). The initial bathymetry of Profile 2 was perturbed with the same five initial perturbations as the Egmond profile.

The morphological response ($\overline{\lambda}_{end}$ and T_{resp}) was compared for $H_s = 2$ m and all four wave angle settings. As an example, Figure 2.12 shows the *RMS* evolution for both the Egmond profile (black) and Profile 2 (grey) for $H_s = 2$ m and $\theta = 10^o$. As can be seen, Profile 2 starts to evolve at about 2 days earlier than the Egmond profile, consistent with Van Enckevort et al. (2004)'s suggestion. Also for the other wave angles Profile 2 responded faster than the Egmond profile. The length scales of Profile 2 develop faster as well.

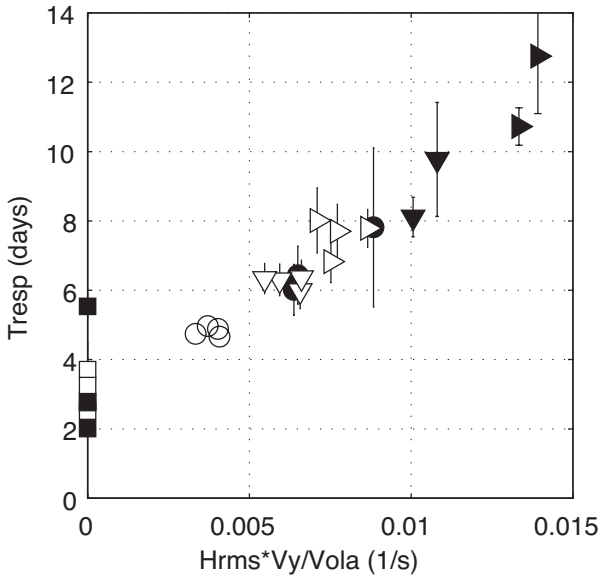

Figure 2.10: T_{resp} for both inner (white) and outer (solid) bar versus local $H_{rms}V_y/Vol_a$. Markers indicate the offshore θ ($\square = 0^o, \circ = 10^o, \bigtriangledown = 20^o, \triangleright = 30^o$).

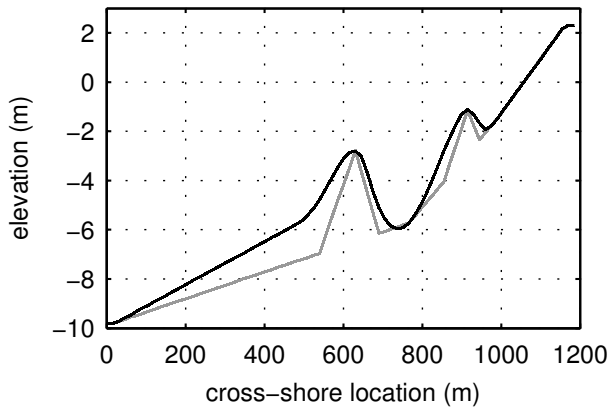

Figure 2.11: Elevation (relative to mean sea level) versus cross-shore location for the original Egmond profile (black) and Profile 2 (grey).

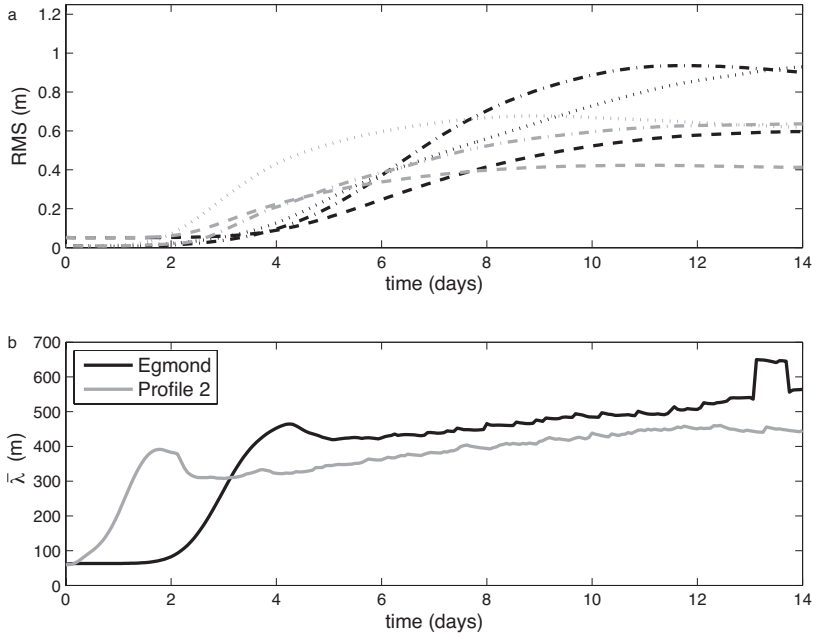

Figure 2.12: a: Evolution of *RMS* for Egmond profile (black) and Profile 2 (grey), for whole (dashed), inner (dotted) and outer bar (dash-dotted) area. b: Evolution of inner bar $\overline{\lambda}$ for both profiles.

The computed length scales for both the inner and outer bar, $\overline{\lambda}_{end}$, for Profile 2 are consistent with the results for the Egmond profile (Figure 2.13) being a function of the local longshore current velocity and water depth. Also the predicted length scales (Equation 2.13) show a good fit with the computed $\overline{\lambda}_{end}$. There is one outlier for the outer bar length scales where the computed length scale is significantly shorter than the corresponding Egmond length scale. This can be explained by the fact that for this condition, the inner bar interacts with the outer bar, caused by the large cross-shore amplitude of the evolving features of the inner bar. The fact that this does not occur for the Egmond profile is related to the more rapid response time of Profile 2 which is discussed next.

For both inner and outer bar holds that the response times of the Egmond profile are larger (Figure 2.14a), thus showing a slower response of the Egmond system. Figure 2.14a accounts for the absolute active volume of the bar. To understand the different response times for the two profiles, we accounted for the steepness of the active part of the bar by taking into account the ratio of the width (W) and the height of the active part of the bar (H_t). It is expected that if the active part becomes wider, with the same height, it will take longer to respond. Figure 2.14b shows the response times as a function of the local hydrodynamic conditions ($H_{rms}V_y$) times the ratio W/H_t (i.e. the reciprocal of the steepness) divided by the active volume of the bar (Vol_a). The outer and inner bars of both profiles then show similar response times, thus illustrating the importance of the shape of the active part of the bar volume. The active part of the bars of Profile 2 were steeper than for the Egmond profile for similar local hydrodynamic conditions, thus resulting in a quicker response.

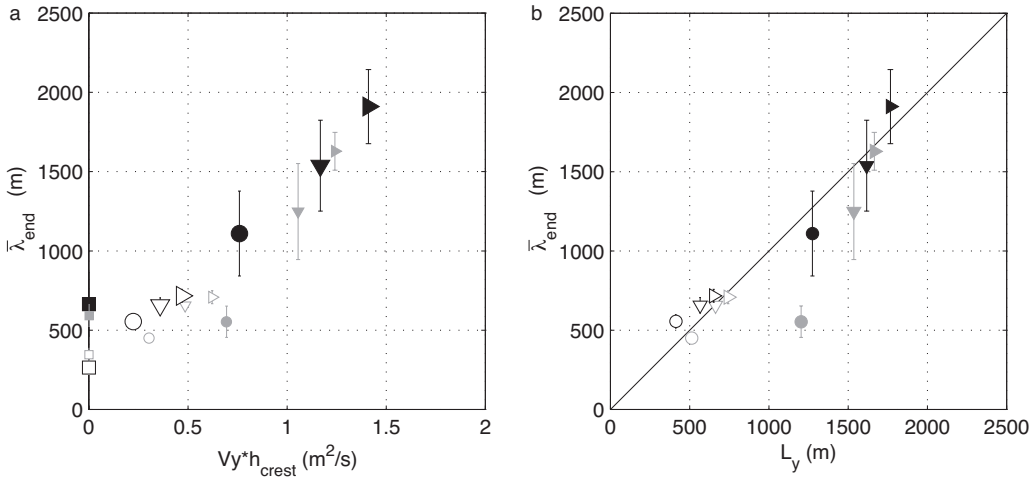

Figure 2.13: a: $\overline{\lambda}_{end}$ versus the local $V_y h_{crest}$ on the inner (white) and outer (solid) bar for both Egmond (black large markers) and Profile 2 (grey small markers). Results of 20 computations covering 4 hydrodynamic conditions viz. offshore $H_s = 2$ m, $\theta = 0^o(\square), 10^o(\circ), 20^o(\triangledown), 30^o(\triangleright)$.b: $\overline{\lambda}_{end}$ versus L_y for obliquely incident waves only (same markers as a).

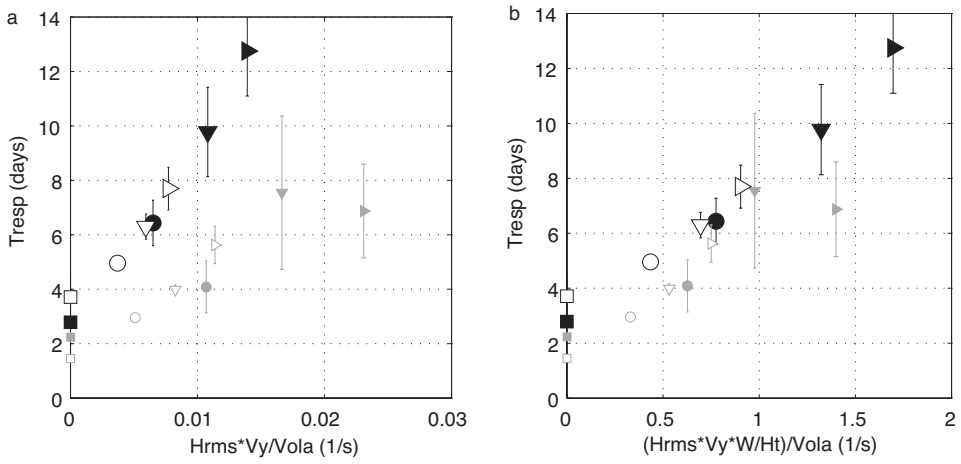

Figure 2.14: T_{resp} (days) versus the local wave height multiplied by the local V_y divided by the active volume (a) and multiplied with W/H_t (b) for both Egmond (large black markers, white and solid for inner and outer bar) and Profile 2 (small grey markers, white and solid for inner and outer bar). Results of 20 computations covering 4 hydrodynamic conditions viz. $H_s = 2$ m, $\theta = 0^o(\square), 10^o(\circ), 20^o(\triangledown), 30^o(\triangleright)$.

Calvete et al. (2007) discuss the sensitivity of rip channel spacing and time scales to the initial geometry for shorenormal waves using a linear stability analysis based model. With their results they recommend that a rip channel predictor should fully account for the shape of the underlying bathymetry. This agrees with our findings that a combination of local nearshore conditions, cross-profile parameters and condition dependent profile parameters explain the length scales and response times. A direct comparison is however not possible due to the inclusion of V_y in our parameters which make them suitable for obliquely incident waves only.

2.4 Discussion

The modelling results presented here compare well to other modelling studies. Deigaard et al. (1999) found in their linear stability analysis of a single barred coast that for increasingly oblique angles of wave incidence, the length scale of the fastest growing mode increased as well. With the offshore angle of wave incidence increasing from 10° to 40°, the length scale increased from 1000 m to 1200 m. This trend corresponds to the work presented in the current paper. However, the values found by Deigaard et al. are higher than the values found here, which might be explained by the differences in cross-shore profile, sediment parameterization and the different definition of the length scale.

Van Enckevort et al. (2004) hypothesized that observed differences in response times of different systems are due to the difference in volumes of the bars. Systems with a larger volume of sand would respond slower than systems with a smaller volume. In simulations with two different profiles, with different volumes of sand in the bars, we found that indeed the bars with the smaller volume responded more rapidly. Even when the local wave height and longshore current were similar, the bars would respond quicker, as the active part of the smaller volume bar was steeper than for the profile with the larger total bar volume.

Studies of video-based observations from Palm Beach (Holman et al., 2006) and the Gold Coast (Turner et al., 2007) found no correlation between the rip spacing and offshore H_{rms}. Also other work, concerning observations of smaller morphological features, viz. ripples, show that ripple parameters (e.g. wavelength and ripple height) are often not in equilibrium with the hydrodynamic forcing (Traykovski, 2007). The current work confirms that the response times of the system (order of days) are large compared to the variability of the hydrodynamic conditions, thus preventing the system to develop morphology that corresponds to the current conditions. This process can be understood further by taking into account the antecedent morphology. In this paper only the random initial perturbations were varied. This showed that the range in results due to these different initial perturbations was smaller than the range due to different hydrodynamic forcings. The different initial perturbations did result in different locations of rip patterns, but the trends in length scales and response times were similar. However, for antecedent morphological features with significant amplitudes, this consistency

in trends most likely does not hold (Calvete et al., 2007). Smit et al. (2005) found that more evolved morphological patterns adjust more slowly to changing offshore wave conditions than patterns that have just emerged.

Though an expansive set of hydrodynamic conditions was computed, we realise that only two profiles have been tested. Computations with other profiles (beyond the scope of this work) are required to fully test the applicability of $H_{rms}V_yW/H_t/Vol_a$ as a measure of the response time. It is anticipated however, that the trends and analysis of the behaviour of the two profiles also hold for other systems. Further, preliminary computations with larger grain sizes and corresponding fall velocities showed a slower response wih patterns similar to the ones originally computed. Other computations are required to fully investigate the role of the grain sizes on the rate of evolution.

2.5 Conclusions

Computations with a 2DH process-based model of the morphological response of a double nearshore bar system show that the emerging length scales on the outer bar are predicted to be larger than the length scales on the inner bar, comparing well with field studies (Van Enckevort et al., 2004). The computed length scales are proportional to the local longshore velocity over the bars. For similar longshore velocities, the length scale on the outer bar is still larger than on the inner bar. This difference is accounted for when multiplying the longshore velocity with the crest level, indicating the importance of the momentum associated with the longshore current. The length scales can be predicted when accounting for this momentum and the possible deceleration of the longshore current at the bar crest.

The response times of the modelled system increase with increasing local longshore velocities and wave heights. When the active volume of the bars, which depends on the breaker index, increases, the bar responds more rapidly. The response times are generally larger than storm durations. Our computations confirm the hypothesis of Van Enckevort et al. (2004) that bar systems with smaller bar volumes show a more rapid response than bar systems with larger volumes. This faster response is due to the steeper active volume of the bar with the smaller volume.

Different initial perturbations (order of cm) do not alter the overall trends in length scales and response times, however they do cause features to evolve at different locations, demonstrating the high level of sensitivity of the evolving bathymetry to the initial conditions. Accurate initial bathymetries are hard (expensive) to obtain in the field. It will therefore be very difficult to morphologically forecast exact rip locations for a field situation when starting from a seemingly reset morphology. Thus, we hypothesize that the stochastic nature of natural wave forcing and the slow response of sandbars under constant forcing prevents the generation of a typical wavelength corresponding to the concurrent offshore wave height in the field.

Acknowledgements

This work was made possible by the funding of the Dr. Ir. Cornelis Lely Foundation, The Netherlands. We thank WL Delft Hydraulics for the use of their Delft3D software. We highly appreciate the constructive discussions with Prof. Dr. M.J.F. Stive. A.R. acknowledges funding through the Dutch National Science Foundation (NWO) contract DCB.5856. B.G.R. acknowledges funding through Netherlands Organistation for Scientific Research Award 864.04.007.

Chapter 3

Role of morphological variability in the evolution of nearshore sandbars

M.W.J. Smit[1*], A.J.H.M. Reniers[2,3] and M.J.F. Stive[2]

This chapter is based on a paper submitted to Coastal Engineering.

1. Spatial Ecology Department, The Netherlands Institute of Ecology (NIOO-KNAW), PO Box 140, 4400 AC Yerseke, The Netherlands
2. Delft University of Technology, faculty of Civil Engineering and Geosciences, PO Box 5048, 2600 GA Delft, The Netherlands
3. Rosenstiel School of Marine and Atmospheric Science (RSMAS) University of Miami, 4600 Rickenbacker Causeway, FL 33149-1098, Miami, USA

*Corresponding author. Tel.: +31 113 577470; Fax: + 31 113 573616. E-mail address: M.Smit@nioo.knaw.nl (M.W.J. Smit).

Abstract

Computations using a depth-averaged morphological process-based model of a double nearshore bar system have been used to test the hypothesis that bathymetries with small variability adapt more easily to new hydrodynamic conditions than bathymetries with distinctly imprinted crescentic patterns. The computations are used to investigate the assumption that nearshore bathymetries tend to evolve toward a rip-channeled template matching concurrent constant hydrodynamic forcing, given these conditions prevail for an extended period of time. In each computation an initially alongshore uniform double barred bathymetry was forced by two subsequent piece-wise constant hydrodynamic conditions. For each set of conditions, four different computations showed the effect of a later transition moment -and thus more distinctly evolved patterns- on the level of adaptation to the second condition. After the transition to the second condition, different hydrodynamic patterns occur due to differences in the bathymetry at the transition moments. These patterns either reinforce the existing pattern or allow for adaptation to the newly expected rip channel distances, depending on how pronounced the existing features

were at the moment of transition. As hydrodynamic conditions generally change more rapidly than the adaptation time, which is in the order of days, it is highly unlikely that observed rip channel distances match length scales expected for concurrent hydrodynamic conditions, consistent with field observations (e.g. Holman et al., 2006). It is therefor concluded that nearshore patterns are formed by a combination of both the antecedent morphology -and thus antecedent hydrodynamics- and the current local hydrodynamic conditions, next to factors like sediment characteristics.

Keywords: nearshore bar system, process-based model, response time, length scale, rip channel, morphological processes, morphology, rhythmicity

3.1 Introduction

The morphology of nearshore sandbars is observed to vary in time, seemingly as a result of hydrodynamic conditions, the geometry and sediment characteristics. From field observations it is found that the lay-out of nearshore bars varies with the wave energy and runs through a cycle of beach states (Wright and Short, 1984; Lippmann and Holman, 1990; Ranasinghe et al., 2004). With highly energetic conditions, the beach-state has been observed to 'reset': the nearshore bar moves offshore and becomes alongshore uniform. In subsequent lower energy conditions, rip channels form and the bars move onshore, possibly even welding to the shore. Rip channels form due to the reinforcement of the hydrodynamic pattern over small alongshore variabilities. The rip channels seem to appear at quasi regular intervals, which have been hypothesized to be influenced by the cross-shore geometry and hydrodynamic conditions. However, field observations of rip channel distances did not give a clear relationship between hydrodynamic conditions and spacing (Holman et al., 2006; Turner et al., 2007). From numerical modelling efforts it was found that, with constant wave forcing, an initially alongshore uniform bathymetry does evolve toward a length scale which is related to the local conditions (e.g. Smit et al., 2008). Calvete et al. (2007) showed that the effect of different cross-shore profiles on the evolving rip channel distances can be of the same order of magnitude as the effect of different hydrodynamic conditions. This illustrates how sensitive the response of the nearshore system is to both the initial state of the system as well as the subsequent conditions. Changing the normal wave incidence angle after 12 days to 30 degrees Drønen and Deigaard (2007) observed an increase in the length scales of the bar crest similar to the case with 30 degrees wave conditions only. This change in length scale was attributed to the bar-generating mechanisms associated with the quasi-three-dimensional flow they used in their modeling efforts. However, the initially present short scale morphological variability inshore of the bar crest, resulting from the 12 day period of normally incident waves, showed a limited response to the changing wave conditions and was mostly maintained.

In earlier work we found that an initially alongshore uniform bar system has response times in the order of days. Hydrodynamic conditions might change even more rapidly, thus not allowing the system to evolve toward the preferred configuration. We therefor presume that observed geometries are a convolution of the effects of a sequence of past conditions. From earlier work, we conclude that both the duration (Smit et al., 2004) and sequence of conditions (Smit et al., 2005) as well as the initial beach state (Smit et al., tionb) is important for the final beach state.

Stive and Reniers (2003) state that sandbar behaviour is a combination of deterministic forced responses, deterministic chaotic responses and stochastic chaotic responses. In observations it is found that changing hydrodynamic conditions at times can have a large effect on the morphology and at other times, there is no effect. It is hypothesized that initial variability plays a role in this. Small initial variability will stimulate evolution as the small alongshore variabilities will more easily put sediment into suspension than with an alongshore uniform bathymetry. Large initial variability, like a pattern with deep rip channels intersecting the alongshore bars, will hardly change when new conditions force the system. We presume that a sandy coast has a preferred template corresponding to specific conditions, the mean cross-shore profile and the sediment characteristics. This template is influenced by the hydrodynamic conditions, cross-shore profile (e.g. Smit et al., 2008) and physical parameters like sand diameter. Hence, when the conditions change, the preferred template will be different. For the hydrodynamic conditions, several aspects are important: duration (Smit et al., 2004), angle of wave incidence, wave height, wave period and wave spreading (e.g. Reniers et al., 2004; Calvete et al., 2007; Smit et al., 2008).

In this study we investigate how the capacity of the system to adjust to new conditions depends on the morphological variability at the moment of changing conditions (transition moment $t = t_T$). We test the following hypothesis: low (high) morphological variability at the moment of changing hydrodynamic conditions will allow (inhibit) morphological adjustment to the new conditions.

The hypothesis will be tested by numerically computing the morphological evolution of an initially alongshore uniform double bar system as a response to two piece-wise constant sequential conditions. The first condition will be applied for four different durations, resulting in a different level of variability at the moment of transition to the second condition. We know the templates of the system for the individual conditions, in case these would be applied constantly to an initially alongshore uniform bar (Smit et al., 2008). Hence, to analyse whether a later transition moment will result in less adjustment, we compare the computed pattern with the expected pattern .

The applied model, computational set-up and parameters for analysis are described in Section 3.2, Section 3.3 describes the results. Subsequently, the work is discussed in Section 3.4 and conclusions are drawn in the final section.

3.2 Method

The modelling system Delft3D is used for the morphological computations (Roelvink and Van Banning, 1994; Lesser et al., 2004). It consists of several modules for simulating short waves, currents and sediment transport, which can be applied for coastal computations. The wave propagation, breaking and corresponding radiation stresses are computed with SWAN (Booij et al., 1999). The flow driven by radiation stress gradients is calculated with the depth-averaged non-linear shallow water equations. The corresponding sediment transport rates due to currents and short waves are determined using Bijker (1971). This formulation takes into account the effect of wave stirring and suspended sediment transport. No specific cross-shore effects, like undertow, are taken into account at this stage. For further details is referred to Smit et al. (2008).

The transport is calculated 'online'. This means that the transport and bottom changes are calculated for each flow time step, with a factor to speed up the computations, assuming that the flow field does not change significantly within that period (equal to the flow time step times the morphological factor) (Roelvink, 2006). For these calculations a morphological factor of 15 was used. This means that for every flow step of 6 s, the morphological adjustment over a period of 1.5 minutes is calculated. This loop is performed 60 times (which in this case corresponds to 1.5 hour morphologically), after which the waves are recomputed with the new bathymetry.

3.2.1 Initial bathymetry and grid

The initial bathymetry resembles a cross-section at Egmond aan Zee, The Netherlands (Figure 3.1). This measured cross-section is applied over a length of 6300 m, to obtain an alongshore-uniform stretch of coast. The model area has a cross-shore width of 1200 m. The grid cell size is 15 by 15 m. A small random perturbation (order of cm) is added over the whole model area reducing the time required to start the morphological evolution.

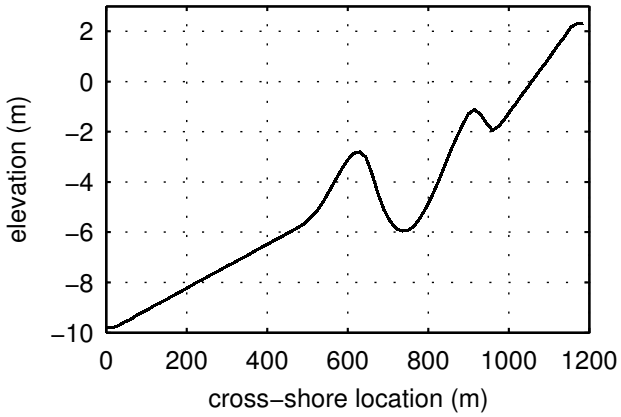

Figure 3.1: Elevation (relative to mean sea level) versus cross-shore location used in the simulations.

	H_s (m)	θ(°)	$\overline{\lambda}_{in}$ (m)	$\overline{\lambda}_{out}$ (m)
condition A	1.5	0	321	666
condition B	2.5	20	676	1604
condition C	1.5	10	570	1009
condition D	2.5	30	798	2032

Table 3.1: Overview of conditions and their end-state length scales (inner and outer bar) for constant hydrodynamic forcing.

3.2.2 Boundary conditions

The wave grid is larger than the flow grid to avoid shadow zones associated with the fact that waves are incident at the seaward boundary only. As a result the wave forcing applied in the flow domain is not affected by its lateral boundaries. The lateral hydrodynamic boundaries of the flow model are defined as zero water level gradients perpendicular to the shore normal. The seaward boundary is a zero water level boundary. The bottom boundaries are defined as zero depth gradients on the lateral boundaries.

3.2.3 Computational set-up - hydrodynamic conditions

An initially alongshore uniform double barred beach is forced with a set of two sequential wave conditions (referred to as condition I and II). Four individual conditions (A, B, C, D, Table 3.1) are selected to create in total 4 sets of sequential conditions. The four individual conditions were selected on the different end-states that resulted when each of these conditions was applied constantly on an initially alongshore uniform profile (Figure 3.2). This allows analysis of the adaptability of the bar system, scored on adaptability of length scales (rip channel distances). The conditions are chosen using earlier work in which 16 different constant wave conditions were applied to an initially alongshore uniform double bar system (Smit et al., 2008). The cross-profile of the bathymetry used in that study is identical to the cross-profile used in the current study as to avoid geometry-induced effects on the expected length scales. The four selected conditions (Table 3.1) are sequentially combined in two sets with increasing wave energy (AB and CD) and, reversing these two sequences, in two sets with decreasing wave energy (BA and DC, Table 3.2).

.

For each set of conditions I and II, four transition moments (t_T) were selected based on the amount of change of the bathymetrical evolution of condition I, resulting in four computations for each set. The amount of change (at each moment) is expressed by the root mean square of the difference of the depth at that moment minus the alongshore-averaged depth at that moment(RMS) (e.g. for Condition A: Figure 3.3). The moments of transition are based on the evolution of RMS of the inner bar (RMS_{in} e.g. for condition A: Figure 3.3). The first transition

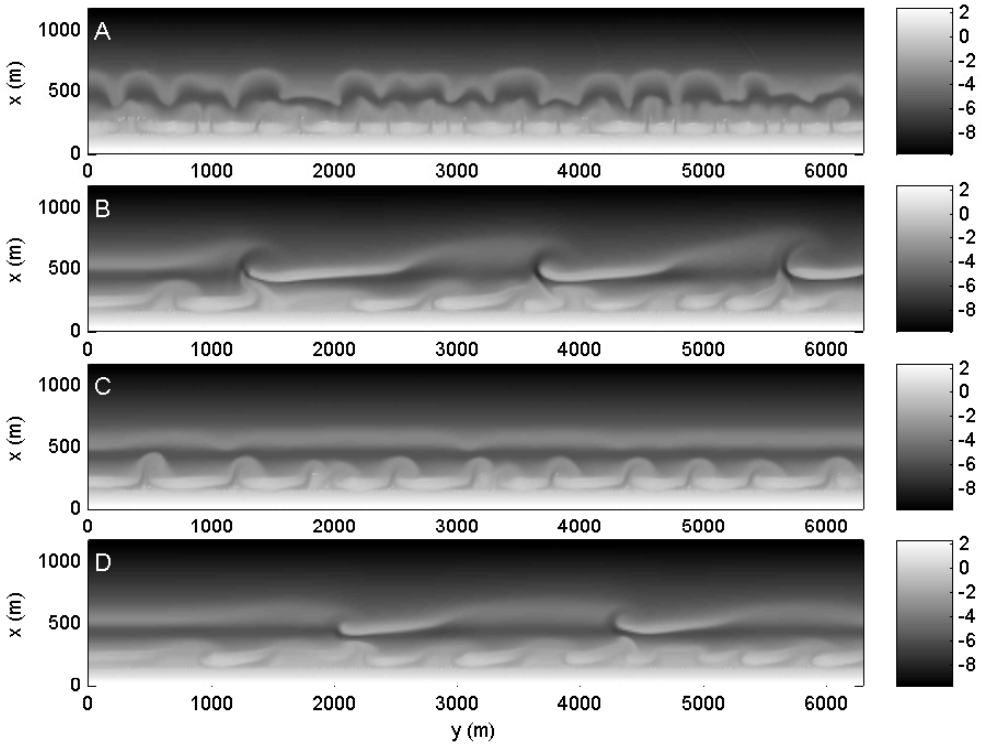

Figure 3.2: Bathymetries after 14 days of constant hydrodynamic conditions on an initially alongshore-uniform barred profile for condition A, B, C, D.

computation set	cond I	cond II	t_T 1	t_T 2	t_T 3	t_T 4	t_{end}
AB	1.5m 0^o	2.5m 20^o	1.5	4	6.5	7.5	20
BA	2.5m 20^o	1.5m 0^o	4	8.5	13	14	20
CD	1.5m 10^o	2.5m 30^o	3	5.5	8	9	20
DC	2.5m 30^o	1.5m 10^o	4	11	16	17	20

Table 3.2: Computational sequences, times are in days.

moment for the AB set is chosen at 1.5 days (when RMS_{in} just starts to evolve), the second at 4 days (at maximum slope), the third at 6.5 days (at about the maximum RMS_{in} value) and the fourth t_T one day later, after 7.5 days.

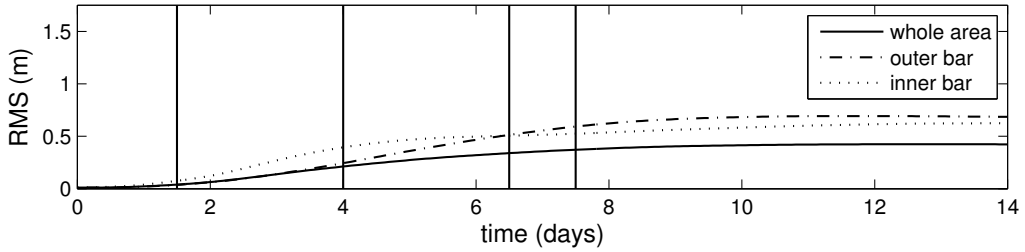

Figure 3.3: Evolution of the amount of variability (RMS) for a computation with constant hydrodynamic conditions: H_s of 1.5 m, normal wave incidence. The RMS for the whole area (solid line, the outer bar (dashed-dotted line) and the inner bar (dashed line) is indicated. The vertical lines represent the moments of transition, from 1(left) to 4 (right).

These choices correspond to different bathymetries to which the second condition is subsequently applied. The bathymetries range from hardly developed (first transition moment) to fully developed crescentic bars (fourth transition moment) with, in this case, small length scales, related to the shore normal wave conditions (condition A, Figure 3.4).

The second condition is then subsequently applied for a length of time that allows the bathymetry to evolve (RMS_{in} >0.1 m) and to have a total length of morphological evolution of 20 days (Table 3.2).

This computational set-up enables the investigation of the role of the antecedent morphology in the morphological evolution. It is expected that if a bathymetry is still close to a reset situation (i.e. alongshore uniform), it will easily adjust to the subsequently applied condition. In the case of a well-developed (i.e. deep channels) crescentic bar system, e.g. with small length scales, it is expected to have greater difficulties in developing into larger length scales by merging the smaller length scales into larger ones, as related to the second condition and vice versa for the cases with decreasing energy -and expected decreasing length scales.

3.2.4 Parameters for analysis

The patterns observed in the morphological evolution are described by their length scale. The length scales are defined by a Fourier analysis of the depth contour of each bar, resulting in a weighted length scale ($\overline{\lambda}$), which is determined at each time step. For the exact definition refer to Smit et al. (2008). However, due to the prolonged duration of the current computations, this method (based on contour lines of the bathymetries) shows irregularities in the evolution of the $\overline{\lambda}$ of the inner bar in the later stages of the computations. These irregularities in the $\overline{\lambda}_{in}$ are therefore smoothed using a triple running mean of almost one day (15 data points).

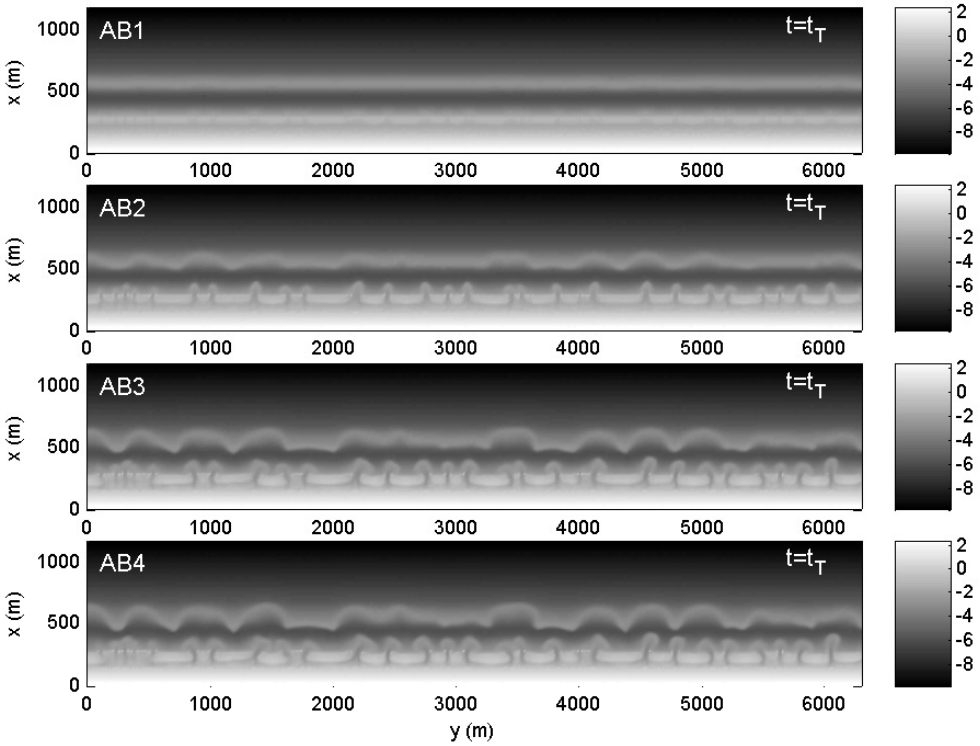

Figure 3.4: The bathymetries at t_T for AB1..4, i.e. after condition A. The most upper panel is at the first transition moment, after 1.5 days of condition A. The second panel is the bathymetry at the second moment (4 days), the third panel the third moment of transition (6.5 days) and the lowest panel the bathymetry at the fourth moment of transitions (7.5 days).

The scoring is computed for the evolution of $\overline{\lambda}(k,t)$ after the transition moment and is computed for both inner and outer bar separately and is defined as follows:

$$\overline{\lambda}Score_{bar}(k,t) = 1 - \left| \frac{\overline{\lambda}_{comp,bar}(k,t) - \overline{\lambda}_{II,bar}(k,t)}{\overline{\lambda}_{I,bar}(k,t_{end}) - \overline{\lambda}_{II,bar}(k,t_{end})} \right| \tag{3.1}$$

with *bar* referring to either inner (*in*) or outer bar (*out*), *comp* referring to the computed values of the computation under investigation, k specifies which computation is investigated (set,1..4; with set =AB, BA, CD or DC), t is time, t_T the moment of transition, t_{end} is the last moment of the computation, I refers to the computation with constant condition I, II refers to the computation with constant condition II.

The scoring shows how well the length scales in the system adjust to the expected length scale, when changing the conditions at increasingly later moments in time. The difference between the computed and expected value (numerator) is taken relative to the difference between the parameter values for condition I (at t_{end}) and condition II (at t_{end}) (denominator). Scores of 1 indicate a complete match of the computed and the expected parameter and show that the computed parameter has adjusted toward the expected value. When the difference between the computed $\overline{\lambda}$ and expected $\overline{\lambda}$ equals the difference between $\overline{\lambda}(t_{end})$ for condition I and II, the score is 0. When the difference between the computed $\overline{\lambda}$ and expected $\overline{\lambda}$ is even larger than the denominator, the score will be negative.

3.3 Results

3.3.1 Results for AB set of computations

The four different moments of transition have a distinct effect on the final bathymetries for the AB set (Figure 3.5). The final pattern of AB1 resembles the expected pattern for condition B best (compare Figure 3.5a to Figure 3.2b). This corresponds to the hypothesis that small initial variability facilitates the adaptation of the morphology to changing wave conditions. The evolution of the patterns is quantified by $\overline{\lambda}(t)$ and $\overline{\lambda}Score(t)$ (Figure 3.6). The evolution of $\overline{\lambda}(t)$ for the AB computations adapts increasingly better to the second condition for earlier t_T (illustrated for $\overline{\lambda}_{out}$ in Figure 3.6). For computations with later t_T (e.g. AB3, AB4), the score decreases.

3.3.2 Results for all computations

Also for the BA, CD and DC sets, the final bathymetries showed the impact of the moment of transition. The bathymetries at t_T and the final bathymetries are included in Appendix D, the

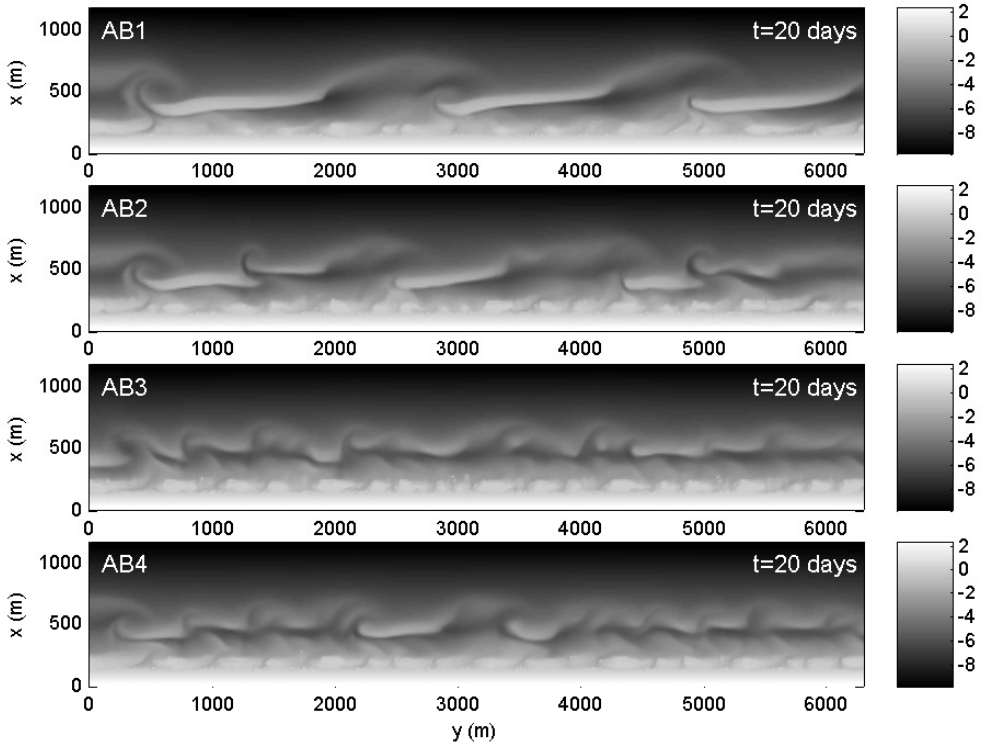

Figure 3.5: a-d: Final bathymetries for AB 1..4 computations. All after 20 days of morphological evolution. t_T of the upper panel was after 1.5 days of normal wave incidence (1.5 m height), of the second panel after 4 days, the third after 6.5 days and of the lowest panel after 7.5 days.

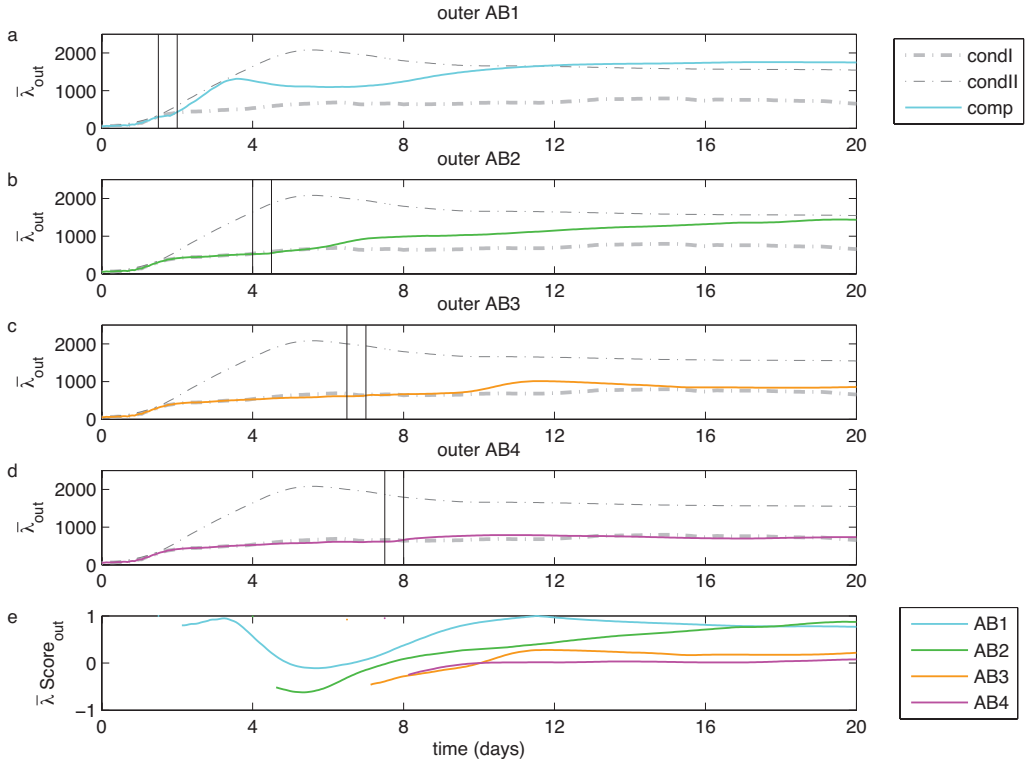

Figure 3.6: a-d: Outer bar $\overline{\lambda}(t)$ [m] for AB computations; e: $\overline{\lambda}Score(AB(k,t))$.

comp - in	t_{T1}	t_{T2}	t_{T3}	t_{T4}	comp - out	t_{T1}	t_{T2}	t_{T3}	t_{T4}
AB	0.98	0.69	0.48	0.18	AB	0.77	0.87	0.22	0.08
BA	0.73	0.73	0.31	0.28	BA	0.85	-0.38	-0.17	-0.21
CD	0.46	0.02	0.13	0.19	CD	0.72	0.86	0.58	0.99
DC	0.73	0.37	0.32	-0.08	DC	0.36	0.10	0.09	0.031

Table 3.3: $\overline{\lambda}Score(k, t_{end})$ as presented in Figure 3.7.

evolution of $\overline{\lambda}(t)$ for these computations is included in Appendix E. For all four sets of computations the scores at the end of the computation are presented as a function of the variability at the moment of transition ($RMS_{bar}(k, t_T)$) for both the inner and outer bar (Figure 3.7, Table 3.3). For both outer and inner bar most trends are decreasing, meaning that with a lower level of variability at t_T, the system adapts better than with a higher $RMS_{bar}(k, t_T)$, corresponding with our hypothesis.

After the transition, the evolving length scale generally starts to deviate from $\overline{\lambda}_I$ within one day, but reaching a new lay-out typically takes a considerable amount of time (order of days to 10 days, e.g. Figure 3.6). For almost all computations, condition II was applied for at least 5 days (20 days - t_T, see Tabel 3.2), allowing time to adjust with the exception of DC3 and DC4, which experienced only 4 and 3 days of condition II respectively. Analysing $\overline{\lambda}_{out}(k, t)$ for these computations shows minimal change of the length scale after the transition moment.

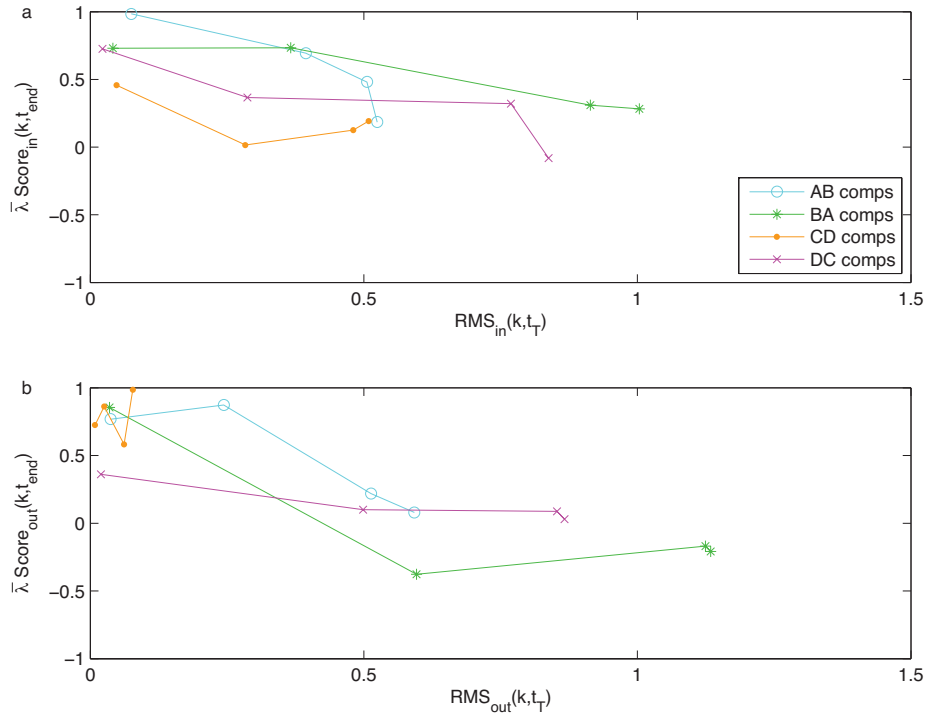

Figure 3.7: Score parameter $\overline{\lambda}Score(k, t_{end})$ as function of RMS_{t_T} for 4 sets of computations (legend) for a: inner bar and b: outer bar.

With the observed low rate of change it is expected that the found $\overline{\lambda}Score$s will remain the same even if the condition would have persisted for an extended period of time. In general hydrodynamic conditions do not last for long periods of time, which explains why observed rip channel distances are hard or impossible to match with the concurrent conditions.

There is no clear different scoring for outer or inner bar (like outer bar adaptation is performing worse). Although the intended length scales for outer and inner bar are generally different, as they are determined by, next to local velocities, the depth of the bar (Smit et al., 2008), the scoring for both bars show similar results. From this may be concluded that the initial depth of the bar and volume of the bar are not affecting the scoring significantly.

It could be argued that the magnitude of the length scales is an aspect why different sets of computations may give different results. Response times are larger for larger length scales (Smit et al., 2008) and it could therefore be expected that the adaptation is worse for computations with larger length scales. However, this analysis did not give an exclusive result (figure not included). This may be due to the fact that at earlier transition moments, the length scales have not fully developed yet, or because the scores per set are not sufficiently different.

Whether the trends between the different sets of computations are distinctly different, or whether the differences can be explained by the range in results due to different locations of features in the evolution, is analysed by performing extra computations. These computations, with different initial perturbations, investigate whether different patterns at the moment

of transition, but similar levels of variability, lead to different results in the scoring.

3.3.3 Role of initial random perturbation

The bathymetry in the first computation of each set is alongshore uniform with a small initial perturbation of order cm. This initial perturbation speeds up the morphological response. From earlier work it was found that different initial perturbations on alongshore uniform bars may result in different rip channel locations, but the length scales remain similar (Smit et al., 2008). In the current computations, the variability of the bathymetry at t_T is larger than the variability at $t = 0$ due to this initial perturbation and is therefore expected to have a larger impact on the evolution. To ensure that the observed trends in adaptability performance as a function of $RMS_{bar}(k, t_T)$ also holds for other initial perturbations, extra computations were performed. The set of BA computations was done with 4 extra, different initial perturbations, in order to have sets of totally five different initial perturbations. These perturbations were applied at the initially alongshore uniform bathymetry (t=0 days). Condition B was applied until the transition moment (which were again chosen as a function of the evolution of RMS_{in}). At each transition moment this resulted in a total of five slightly different bathymetries: the patterns and variability are similar, but the exact features and rip locations showed variability. Subsequently, condition A was applied to these bathymetries for the remainder of the computation. The resulting $\overline{\lambda}(t)$ evolution is then scored using the evolution of the computation with constant condition (condition A after the transition moment), with the corresponding initial perturbation. In this way 5 $\overline{\lambda}Score$s are computed for each group of five computations with the same transition moment. The mean and standard deviation of these scores as a function of the mean and standard deviation of the corresponding $RMS_{bar}(k, t_T)$ show a decreasing trend (Figure 3.8). This corresponds to the trend presented before for the BA set. This shows that the initial perturbations result in a range in scoring, but do not affect the hypothesized trend. Due to the range in scoring, the set of computations in the current work does not allow to differentiate between the effects of the different sets of conditions. Similar $RMS_{bar}(k, t_T)$ values (i.e. computations with the same transition moment) result in similar $\overline{\lambda}Score$s, reinforcing the hypothesis that the level of variability plays an important role in the adaptation capacity of the system. The present results suggest that if the initial RMS bathymetric variability at the moment of transition is larger than O (0.5) m the morphology does not adapt to the new wave conditions reflected by the zero model skill (Figure 3.8).

3.3.4 Role of energy flux

Above, the level of adaptation was analysed as a function of the variability at the moment of transition. In the field, however, the exact level of variability will generally be unknown due to the difficulty of measuring nearshore bathymetries. It would be beneficial if predicting whether a system in the field will adapt to new conditions can be based on parameters, which are more

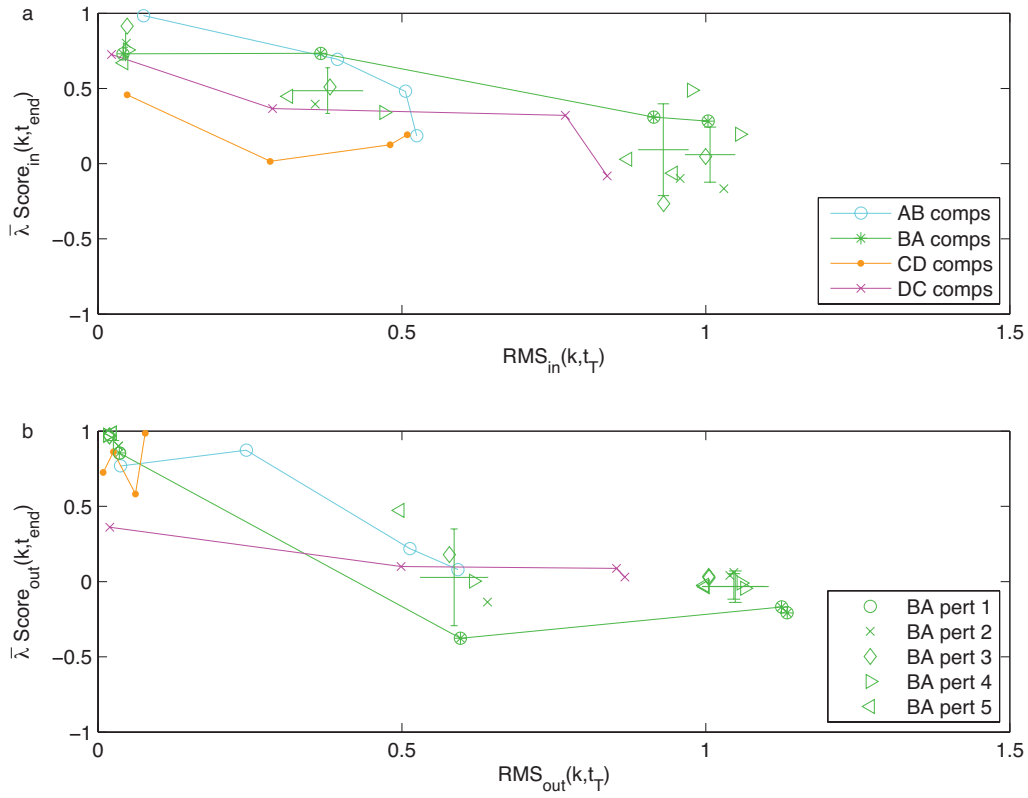

Figure 3.8: $\overline{\lambda}Score$ as a function of $RMS_{bar}(k, t_T)$ for the BA computations with different initial perturbations (green symbols) and the AB, BA, CD and DC sets of computations (all with identical initial perturbation 1) for inner (top) and outer bar (bottom).

readily available. Wave information is frequently available, either from a buoy or from a local wave model. The variability of the nearshore morphology is the result of the energy flux that has forced the system. To analyse the role of the energy flux in the adaptation level, $EC_{g,x}$ is computed on the offshore boundary of the domain, to analyse the scores for the outer bar.

$$EC_{g,x} = \frac{1}{8}\rho g H^2 C_g \cos\theta \tag{3.2}$$

with

$$C_g = nC$$

with

$$C = \frac{\omega}{k}$$

and

$$n = 0.5(1 + \frac{2kh}{\sinh(2kh)})$$

With ρ being density, H is the offshore wave height, C_g is the group velocity, θ is the angle with the shore normal, ω is the wave frequency, k is the wave number, h is the water depth.

$EC_{g,x}$ is integrated over the period that condition I was applied (resulting in $EC_{g,x}T_I$ (Figure 3.9)). It is expected that if little energy had forced the bathymetry, there would have been little morphological change (similar to low $RMS_{bar}(k, t_T)$ values) and therefore the adaptation score is expected to be higher. The figure indeed shows decreasing trends in a similar way to the trends as observed when $RMS_{bar}(k, t_T)$ was used as declaring variable.

In general, after a certain amount of energy has forced the initially alongshore uniform system, the bathymetry is not able to adapt anymore. This can be used in the field, when predicting whether a bathymetry is expected to change: if a reset-bathymetry is forced with a certain amount of energy, the length scales are most likely to be set and to remain at their existing value. This suggests that only in the case of an up-state transition (i.e. high energy event, resulting in a decrease of the alongshore variability), the bathymetry will again be able to change its length scales.

Antecedent morphology, hydrodynamics and morphological change

We hypothesized that large morphological variability does not adapt as easy to changed hydrodynamic conditions than small morphological variability. Morphological features affect the local hydrodynamic patterns, which, in turn, may reinforce existing features. When a different hydrodynamic condition forces the system (here condition II), the previous hydrodynamic pattern will change and thus subsequently change the antecedent morphological features. The new template of the hydrodynamic pattern will determine whether existing features will be reinforced (e.g. deepening of rip channels) or change (e.g. filling in of existing rip channels). With

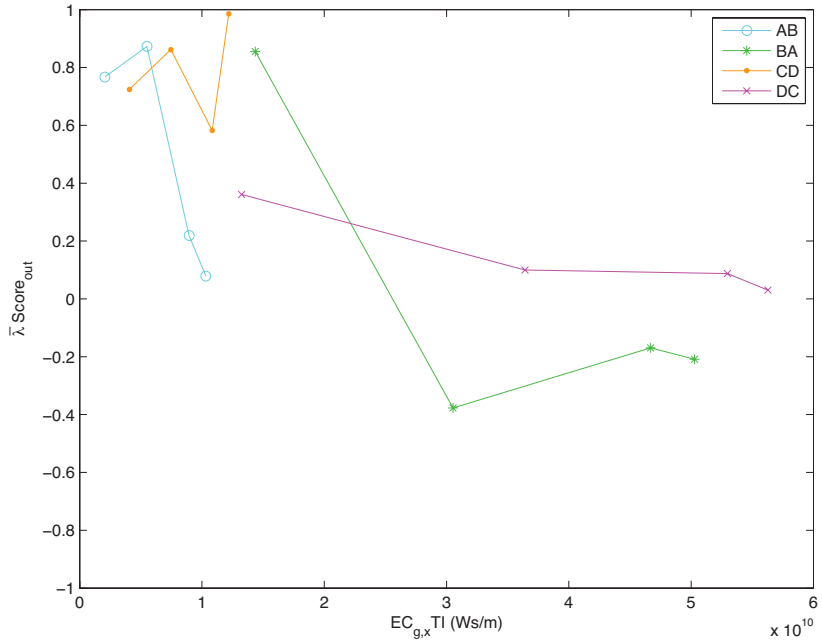

Figure 3.9: Score parameter $\overline{\lambda}Score$ for outer bar as function of $EC_{g,x}T_I$.

more evolved morphological features the hydrodynamic pattern changes less than with less evolved morphological features, thus hardly resulting in a changed bathymetry template and corresponding length scales. The following illustrates how the level of morphological evolution (due to condition I) affects the subsequent hydrodynamic patterns and response to condition II. We do this by investigating the morphological evolution and hydrodynamic patterns of computation AB2 and AB4 at t_T, t_T plus 1 day (to allow condition II to propagate throughout the domain) and at t_T plus 10 days. The two bathymetries at t_T differ in how distinct and well-developed the rip channels are (Figure 3.10a and 3.11a), although the location of evolved features is the same. After t_T, both morphologies are forced with the same offshore wave condition (condition B). The difference in both the hydrodynamic pattern at t_T plus 1 day as well as in the morphological evolution thereafter is due to the difference in morphology at the moment of transition and the subsequent different hydrodynamic pattern. At the moment of transition, the hydrodynamic forcing of the system changes, resulting in different current patterns over the evolved bathymetry. These new current patterns may either steer the bathymetry toward a new template by relocating sediment, or the currents may reinforce existing features by deepening existing channels. For computation AB2 (Figure 3.10), the existing rip channels at $y = 5500$ and 5650 m, formed after forcing with shore-normal waves of 1.5 m (condition A), disappear after condition II has been applied (condition B). Directly after the transition (t_T plus 1 day), the current patterns around the existing rip channel change. The main aspect is the appearance of an alongshore component in the flow circulation. When the rip currents have a large down-drift directed component (alongshore), existing rip channels seem to remain and migrate down drift in time (e.g. compare the rip channel at (950, 5200) and the one at (950, 5800) in

Figure 3.10b and c). For the other pre-transition rip channels the cross-shore currents are not strong enough to maintain the existing rip channels and the channels close as the shoals merge together, resulting in larger rip channel distances (compare the rip channel at (950, 5500) in Figure 3.10b and c).

For computation AB4, where the pre-transition rip channels remain after the transition and the length scales hardly adapt to condition II, we see that the hydrodynamic pattern on the inner bar directly after the transition stays almost unchanged throughout the remainder of the computation and so does the bathymetry (Figure 3.11). In this case, after the transition, all rips have large cross-shore as well as alongshore components, due to the more distinct rip channels in the morphology (e.g. compare the rip channel at (950, 5500) in Figure 3.10b and 3.11b). The patterns reinforce the existing rip channel locations, resulting in maintaining the pre-transition short length scales.

3.4 Discussion

3.4.1 Role of cross-shore profile at t_T

The hypothesis tested in this paper presumes that the system intends to go to a certain lay-out, which is governed by the initial profile, and the local hydrodynamic conditions. The bathymetries at t_T in the current work are partly evolved and therefore both the variability and the mean cross-shore profile may be different from the initial bathymetry (Figure 3.12 for AB set), indicating that the expected evolution might not be realistic (due to the sensitivity of the length scales to the initial cross-shore profile) as this was based on the evolution of a specific alongshore uniform profile (as it was at $t = 0$ days). This is due to the sensitivity of the length scales to the initial cross-shore profile. The main differences are that the crest height of the outer bar decreases with increasing t_T and that the inner bar moves onshore. The trough between inner and outer bar remains the same. These differences in the profile are however presumed to have only a small effect on the expected length scale and it is therefore not anticipated to qualitatively change the computed trends in scoring.

Calvete et al. (2007) tested how sensitive the length scales were to both the initial cross-shore profile and the wave heights for shore-normal wave conditions. They found that both parameters resulted in wavelength variations of about 13 %. For the cases in the current work, the differences between the expected length scales -related to the different conditions- are much larger and it is expected that the effect of hydrodynamic conditions is larger than the effect of the changed alongshore mean profile at t_T. This allows the use of $\overline{\lambda}_{II,bar}(k,t)$ (for $t > t_T$) as the expected values in determining the scoring of the adaptation level.

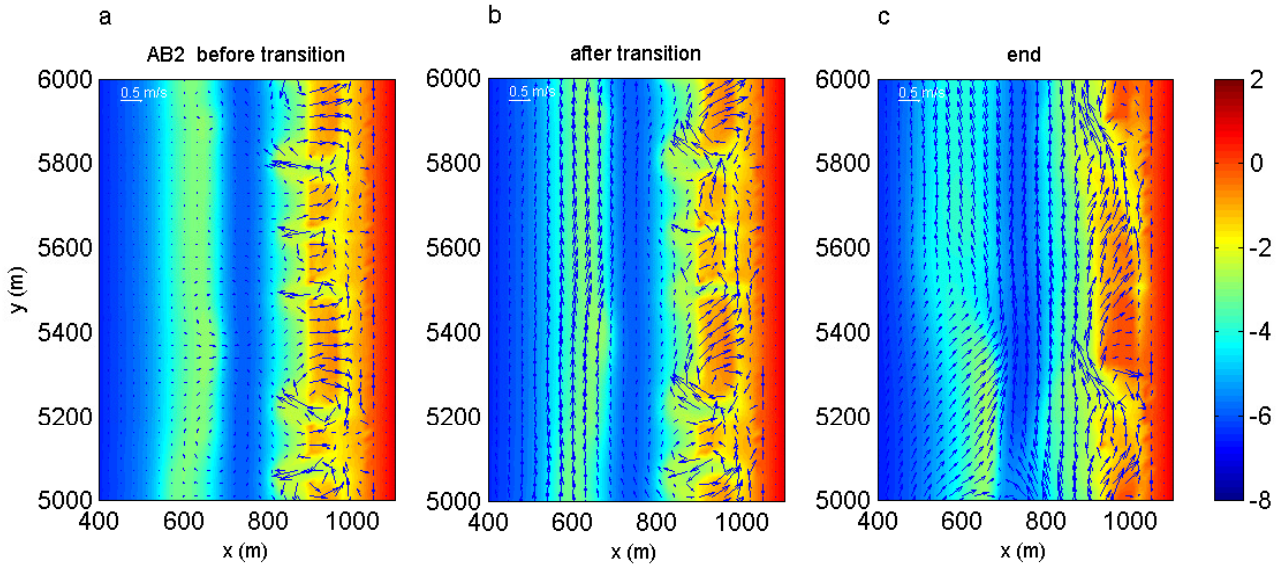

Figure 3.10: Bathymetry and velocities of computation AB2 at a: t_T (condition A still applies), b: after the transition (condition B applies), c: 10 days after t_T. The color indicates the elevation in a range from -8 to 2m; note that the velocities are plotted on a 30x30 m grid for clarity.

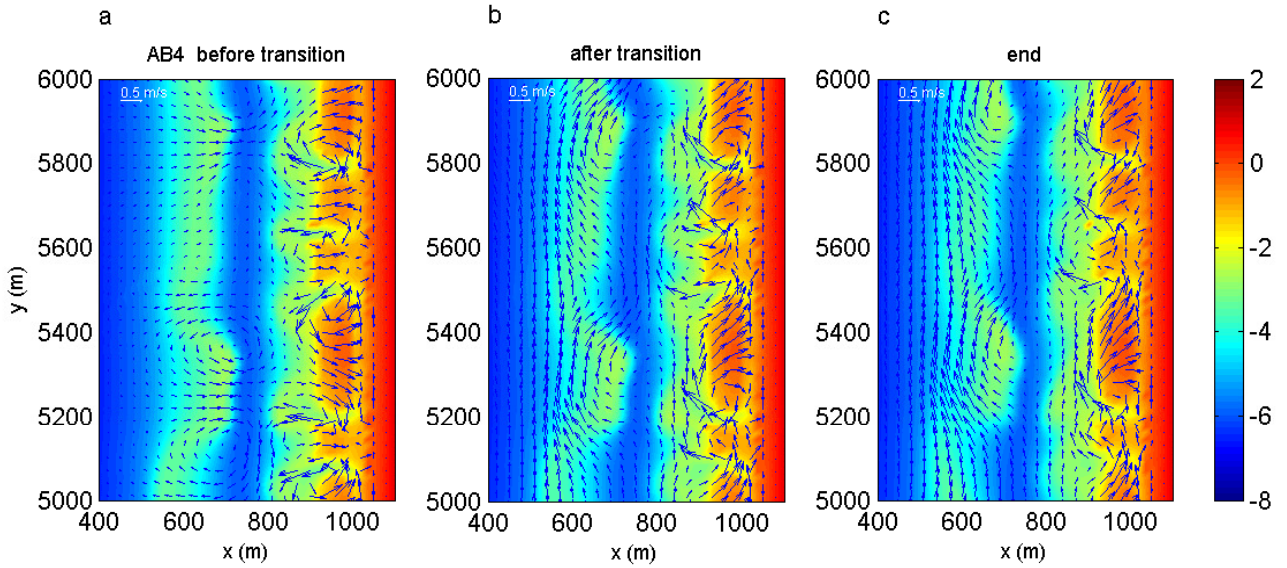

Figure 3.11: Bathymetry and velocities of computation AB4 at a: t_T (condition A still applies), b: after the transition (condition B applies), c: 10 days after t_T. The color indicates the elevation in a range from -8 to 2m; note that the velocities are plotted on a 30x30 m grid for clarity.

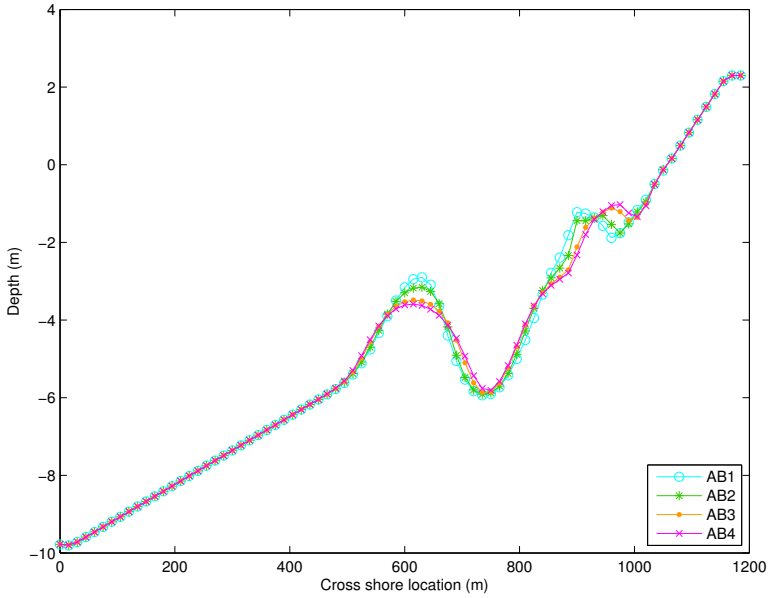

Figure 3.12: Mean cross profiles at t_T for the AB1..4 computations.

3.4.2 Effect of duration of condition

To illustrate the effect of the persistency of wave forcing, computations with continuously varying wave conditions were performed over a period of 14 days. All computations have identical initial alongshore uniform bathymetry with identical random perturbation (O cm), similar to the other computations in this paper. The significant wave height is 1.5 m and the average angle of wave incidence for each of these computations is 10°. The first computation has a constant angle of wave incidence of 10°. The wave angle of the second computation varies gradually with 1° every 1.5 hour, ranging from 0 to 20°. The angle of wave incidence of the third computations varies more abruptly, the angles change 5° every 1.5 hour where the extreme angles 0° and 20° persist for 24 hours (Figure 3.13).

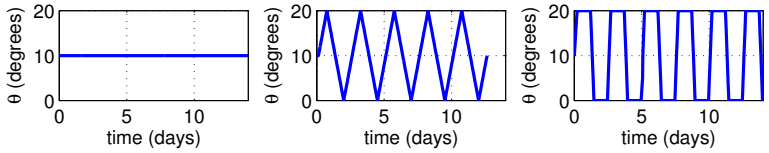

Figure 3.13: Offshore angle of wave incidence ($\theta(t)$) for three computations.

For all three computations, the morphological evolution of the inner bar is similar (Figure 3.14). For the outer bar, however, the time-varying forcing with longer persistency on the extreme values shows the strongest reaction of the outer bar. From computations with constant conditions (Smit et al., 2008) it was seen that, for $H_s = 1.5$ m, the outer bar reacted strongest on orthogonally incoming waves. For the other angles of wave incidence (and $H_s = 1.5$ m), the outer bar hardly evolved. It is expected that the persistency of the 0° angle of wave incidence causes

the stronger reaction on the outer bar. This indicates that persistency and re-occurrence of conditions play a role in the response of the system. These computations further illustrate that a system may respond differently to constant conditions than to time-varying conditions, even when the mean hydrodynamic conditions are identical. The latter is important in predicting expected behaviour of a nearshore bar system from field observations.

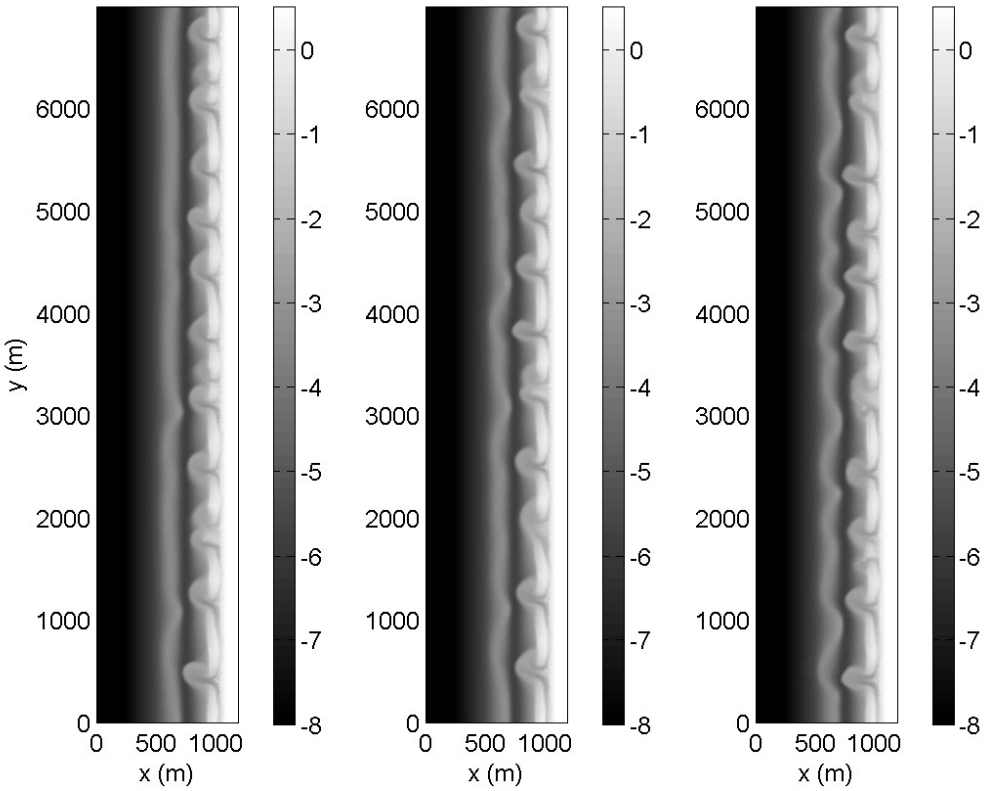

Figure 3.14: Final bathymetries for computations with (from left to right): constant conditions, smoothly varying conditions and abruptly varying conditions with longer persistency, grey levels indicate depth in m.

3.4.3 System behaviour

In the field, it has been observed that beaches seem to run through a cycle of 'beach-states' in response to offshore wave forcing (Wright and Short, 1984). An alongshore variable bathymetry, forced by higher energetic conditions may lead to an upstate transition: the alongshore variability decreases. Ultimately, the bathymetry may evolve into an alongshore uniform bathymetry: a reset-event. With subsequent smaller energy conditions, bathymetries have been observed to go through a down-state transition: rip currents evolve and crescentic patterns appear, the variability increases. This can prolong until another high energy event occurs and the system returns to a state with smaller alongshore variability. The current work presents down-state morphological evolution of a bathymetry from a reset-situation (alongshore uniform), followed

by a transition of hydrodynamic conditions, which may either aim to force the system in an up-state evolution (set AB and CD) or down-state evolution (BA and DC).

Plant et al. (2006) described the response of a nearshore bar system as a dynamical attractor. In their model, the morphology is described by the offshore bar location and the cross-shore amplitude of the crescentic features. The evolution in time of these is described by both interaction of these components and the offshore wave height. The parameter values describing the interactions were based on a 2 month video-based data set, describing a storm-event with a post-storm down-state evolution. For example, the system describes that shoreward migration must be coupled to a growth of alongshore variability. According to Plant et al. (2006), due to the large response time with respect to the duration of conditions, the system continually orbits through time-varying equilibrium points. Earlier work based on a computation with a constant condition showed that the behaviour of the system could be described with the proposed model (Plant et al., 2007).

The present results suggest that the dynamical attractor model would benefit from adding the wave incidence angle, as this is found to be equally important as the offshore wave height in understanding and predicting nearshore morphological evolution.

We found that in case of significant variability in the morphology at the moment of transition, no more adjustments are possible. This agrees with some field observations (Van Enckevort et al., 2004) where the variability first decreases before the morphology adjusts to the new length scale, though this has not been investigated specifically in detail yet.

Turner et al. (2007) analysed three years of video-based data of a nearshore bar system and found no correlation between the observed rip channel distances and the offshore wave height, period or energy (similar to Holman et al. (2006)). They stated that their analysis of observed rip channel locations cannot be 'reconciled with the majority of existing template and instability models for rip formation, that predict a relationship between incident wave conditions and regular spacing of rips alongshore'. We find that such relationships may still be valid, but should be perceived as the intention of the nearshore bar system in case the condition would prevail long enough and the antecedent morphology would facilitate adaptation. Turner et al. (2007) further state that it is moreover the morphology that governs rip channel distances and not so much offshore wave heights, period or energy. We would like to add that not only the morphology, which evolved in response to past hydrodynamic conditions, but also the response time to hydrodynamic conditions plays a significant role in the response of nearshore morphology. It is not so much the morphology at a single moment in time, which determines all, but it is the whole morphological process: the evolution in response to local hydrodynamic conditions, including morphological processes which damp or amplify the response.

3.5 Conclusions

This paper tested the hypothesis that small or no morphological variability on a nearshore bar system facilitates a better adaptation to changing hydrodynamic conditions than a morphology with distinct and deeply imprinted rip channels. Using a process-based model, computations were performed to simulate the morphological evolution of a nearshore double bar system in response to two successive piece-wise constant hydrodynamic conditions. Different moments of transition -resulting in different levels of morphological variability- indicated that a more distinctly developed bathymetry hardly adjusts to a new hydrodynamic condition. Due to more distinct morphology the current patterns would reinforce the existing pattern, thus preventing the system to change toward a new lay-out.

Next, sets of different successive hydrodynamic conditions show that the importance of the level of variability holds for both increasing and decreasing wave energy flux. This indicates that it is not so much the total energy flux, but the relation between cross-shore and alongshore components of the local velocities which determines whether existing channels will remain or disappear. Computations with different initial perturbations (all done for one set of hydrodynamic conditions) show a similar decreasing trend between the variability and the level of adaptation of the system, though with a small range due to the different initial perturbations. Similar variability at the moment of transition resulted in similar levels of adaptation, reinforcing the hypothesis that the variability plays a large role in the level of adaptation of the system.

In the field, wave conditions change significantly within the computed adaptation times, preventing the conditions to leave a remaining imprint. It can therefor be concluded that observed bathymetries are a result of antecedent morphology -and thus antecedent hydrodynamic conditions- and the current conditions.

The current work illustrates why observed rip channel distances in the field may not match with concurrent conditions. The main three reasons are: 1) the response time of the morphological system, 2) the relatively short duration of hydrodynamic forcings and 3) the level of existing morphological variability in the nearshore bar system. The forcing needs to prevail long enough, but it will change the length scales in the system only when the bathymetry has a low level of variability and the condition has sufficient energy to change the existing level of variability. It is therefore concluded that the response is governed by the change in hydrodynamic forcing, the morphology itself and the resulting local hydrodynamics and morphological processes combined with the duration of the hydrodynamic conditions.

Acknowledgements

The research was funded by the Dr. Ir. Lely foundation and the ONR-funded Beach Wizard project (N000140510266). AR was funded by NWO under contract DCB 5856. We thank Deltares (formerly known as WL Delft Hydraulics) for providing us with their Delft3D software.

Chapter 4

Hindcasting an up-state and down-state transition at a pocket beach

M.W.J. Smit[1*], A.J.H.M. Reniers[2,3], G. Symonds[4], B.G. Ruessink[5], M.J.F. Stive[2]

This chapter is based on a paper in preparation for Journal of Geophysical Research.

1. Spatial Ecology Department, The Netherlands Institute of Ecology (NIOO-KNAW), PO Box 140, 4400 AC Yerseke, The Netherlands
2. Delft University of Technology, faculty of Civil Engineering and Geosciences, PO Box 5048, 2600 GA Delft, The Netherlands
3. Rosenstiel School of Marine and Atmospheric Science (RSMAS) University of Miami, 4600 Rickenbacker Causeway, FL 33149-1098, Miami, USA
4. CSIRO, Institute for Marine and Atmospheric Research, Private Bag 5, Wembley, WA 6913, Australia
5. Utrecht University, Faculty of Geosciences, Department of Physical Geography, Institute of Marine and Atmospheric Research, Heidelberglaan 2, 3584 CS Utrecht, The Netherlands

*Corresponding author. Tel.: +31 113 577470; Fax: + 31 113 573616. E-mail address: M.Smit@nioo.knaw.nl (M.W.J. Smit).

Abstract

The geometry of nearshore bar systems is observed to vary in time, with an important role for offshore wave conditions and antecedent morphology (Wright and Short, 1984). The corresponding hydrodynamic and morphodynamic processes are not fully understood. In this study a hindcast is performed of an observed event at a pocket beach, located at Palm Beach in New South Wales, Australia, using a process-based depth-averaged morphodynamic model with sediment responding to the presence of wave groups, long waves, roller effects and corresponding wave breaking induced turbulence, wave asymmetry and return flow. The event consists of both an up-state (decrease in morphological variability during high wave energy) and a down-state transition (increase in variability during moderate or low energy conditions). The initial

bathymetries used in the computations are inferred from video-images. The model is capable of predicting the evolution in variability to some extent for both the up-state and down-state transition. The performance of the model is found to be highly sensitive to (1) the initial bathymetry (and variability therein), (2) the subsequent hydrodynamic conditions and (3) the description of the sediment transport processes in the model. The sensitivity of the model to these processes is illustrated with computations with different process and parameter settings compared with the base case. Excluding wave asymmetry results in a steeper profile near the shoreline and a lack of emergence of new features after the high energy event. Excluding long wave-induced sediment stirring leads to the evolution of distinct and pronounced shore-attached features, with significantly higher nearshore variability and shorter length scales. Excluding wave group effects leads to increased nearshore variability with shorter length scales located at the outer surf zone. Reduced wave breaking induced turbulence leads to significant nearshore variability in the inner surf zone with shorter length scales whereas increased turbulence inhibit the evolution of nearshore variability. Computations started at different moments in the observed morphological evolution show that the differences in the initial bathymetry and subsequent hydrodynamic conditions are as important as the inclusion of the physical processes.

Keywords: nearshore bar system, process-based model, hindcast, Argus, rip channel, morphological processes, reset event, length scale, response time, morphology, rhythmicity, prediction

4.1 Introduction

Nearshore bar systems are often described by bar position, alongshore variability and the presence of rip channels and shoals. These characteristics can be retrieved from in-situ field measurements and from video-images of dissipation patterns. The geometry of sandy coasts with nearshore bars have been observed to change in time (Lippmann and Holman, 1990). Understanding this behaviour will allow improved predictions of the nearshore morphological response to forecasted wave conditions, contributing to a better and safer use of the nearshore coastal zone.

Wright and Short (1984) characterized a sequence of beach states related to the incoming wave energy. They found that high wave energy generally leads to offshore movement and straightening of the bar (reset-event), resulting in a predominantly alongshore uniform bar profile. Subsequent down-state transitions during lower energy conditions, pass through a series of intermediate beach states, with higher alongshore variability, culminating in the low tide terrace morphology unless interrupted by another reset-event.

Down-state transitions from a reset-event can be explained by the presence of small alongshore variations in either the bathymetry or the hydrodynamic forcing. These result in small bathymetrical changes on an initially alongshore uniform profile, which are reinforced by morphological feedback and thus the system evolves toward crescentic patterns (down-state) (e.g.

Falqués et al., 1996, 2000; Garnier et al., 2006). The up-state transition and corresponding offshore movement of the bar and straightening of the rhythmicity during a reset-event is less well understood, although it is clear that high wave energy (Plant et al., 2006) and return flow (Ruessink et al., 2007) are important processes. The exact mechanisms and the relevant hydrodynamic and morphological processes for both types of transitions are, however, not yet fully understood.

Several modelling attempts have been performed aiming to understand the observed spacing between rip channels presuming that this is linked with either the offshore conditions or the nearshore geometry. Edge wave template models presume that infragravity waves, trapped in the nearshore zone due to refraction over the geometry, force their length scales onto the geometry (e.g. Bowen and Inman, 1971; Holman and Bowen, 1982). Using linear stability analyses and process-based modelling to analyse evolving length scales in down-state transitions, several relationships were found between the evolving morphology and either the hydrodynamics and/or the cross-shore profile.

However, comparison of model results with field observations are not conclusive. Holman et al. (2006) analysed 4 years of video data on occurrence and location of rip channels at Palm Beach, a 2 km long pocket beach in New South Wales, Australia. During this period they observed only 15 reset-events, indicating that reset-events occur infrequently and that beach state transitions not necessarily pass through the reset-morphology. In a similar study, the behaviour of a long straight beach was analysed on rip spacing, persistence and mobility (Turner et al., 2007). Their results complemented the findings by Holman et al. (2006) on rip spacing. In both studies the rip spacing was observed to be highly variable in time and irregular in space. Also, the rip location and spacing could not be related to offshore wave conditions, neither concurrent nor post-reset. The latter could be understood if rip locations are mainly geographically controlled, rather than hydrodynamically, by small bathymetrical variations still present after a reset-event.

It seems that both hydrodynamics as well as the antecedent morphology and the response time of the system play a role in the morphological evolution. Process-based model computations starting from a reset-event showed a relationship between resulting patterns (rip-channel distances) and local alongshore currents (which result from both the waves and the local geometry) (Smit et al., 2008). Further, larger depths over the bar lead to larger length scales, indicating the role of the cross-shore geometry. This agrees with the conclusions by Calvete et al. (2007), who analysed the behaviour of various reset bathymetries (alongshore uniform) with different initial cross-shore profiles in response to various shorenormal wave conditions. They concluded that the effect of the geometry can be larger than the effect of the hydrodynamics. At times, observed length scales will therefore be geometrically controlled and not so much hydrodynamically.

There may be two more reasons why Holman et al. (2006) and Turner et al. (2007) could not match the observed patterns with the concurrent conditions. First, the response time of the

system (Smit et al., 2008), which is usually in the order of days, and therefore longer than the duration of wave conditions, which generally vary more rapidly. Second: most modelling studies combined the evolution of a post-reset morphology (alongshore uniform) with the hydrodynamic conditions. From a process-based modelling study using bathymetries with increasing level of variability, it was found that when a nearshore bathymetry has reached a certain level of variability, it will no longer adjust to new length scales when it is forced with changing hydrodynamic conditions (Smit et al., tiona). As reset-events were found to occur infrequently, bathymetries with a higher level of variability are more likely to be found. The existing rip channels and resulting hydrodynamic pattern then prohibit the bathymetry to adjust to concurrent conditions. In that case, the observed morphological pattern is predominantly a result of the morphodynamic interaction of the previous period and not a result of the concurrent conditions.

The performance of a morphological prediction can be judged on three key elements of nearshore features: 1. the level of variability, 2. the length scales and 3. the exact rip channel locations. It is anticipated that it is most likely to achieve the best results for the first two. Rip channel locations are found to be highly sensitive to the initial bathymetry. For example, Smit et al. (2008) showed that different random seedings (order cm) on an initially alongshore double bar profile, forced with constant wave conditions, resulted in different rip channel locations, while not affecting the mean length scales. Model sensitivity to the initial bathymetry was also pointed out by Calvete et al. (2007) who showed that the rip spacing was a function of the initial cross-shore profile. As the bathymetry is usually not known at the required detail level, it is not expected that rip channel locations will occur in the same location as predicted.

It is not only the bathymetry which affects the rip channel locations. Even for a truly alongshore uniform bathymetry Reniers et al. (2004) suggested that the randomness of incident wave groups generating spatially inhomogeneous surf zone circulations results in highly variable rip current locations.

Up to date most modelling efforts have focussed on down-state transitions starting with an idealized alongshore uniform bathymetry. Only few attempts have been made to predict or hindcast observed morphological evolutions. To be able to hindcast an observed morphological evolution, the model needs to reproduce the morphological evolution at the correct pace as well as reproduce features with correct characteristics (e.g. spacings and locations). It is found that depth-averaged (2DH) process-based models can reproduce crescentic patterns in down-state transitions with spatial patterns, scales and variability similar to those observed in the field (e.g. Damgaard et al., 2002; Reniers et al., 2004; Drønen and Deigaard, 2007; Smit et al., 2008). Ranasinghe et al. (2004) used a depth-averaged process-based model to simulate two down-state transitions, starting with idealized observation-based bathymetries and comparing with observed video-images of wave breaking patterns. They forced the bathymetry with constant wave conditions toward a new state. They conclude that the transitions were governed by

the initial geometry and subsequent rip circulation of the changing hydrodynamic conditions. Castelle et al. (2006) used a 2DH process-based model including the effects of undertow to investigate crescentic pattern development of nearshore bars. Their results show that circulation eddies combined with (small) bathymetrical variability are a key component in the morphological evolution of crescentic patterns. They conclude that self organisation can lead to the development of such patterns. These studies focussed on understanding the morphodynamic response to hydrodynamic forcing by analysing the hydrodynamics and the geometrical features of the system. Klein and Schuttelaars (2005) analysed the role of the modelled process descriptions and found for bars evolving from an initially planar sloping beach, that both length scales and orientations of the developing bars were sensitive to the chosen transport formulation.

Very few modelling efforts concerning hindcasts of observed nearshore bar behaviour have been conducted. Grunnet et al. (2004) modelled the observed behaviour of a shoreface nourishment with a 3D model. They concluded that the model was capable of reproducing the observed profile development reasonably well for large spatio-temporal scales (kilometers and months). However, detailed morphodynamic predictions on the scale of sandbar behaviour did not perform as well. Predictions of the nearshore bar migration and development remained poor and bar flattening was found to be the general outcome. They suggest that including a phase lag between sediment transport and bathymetry (e.g. by adding a surface roller model) is essential for bar survival.

Reniers et al. (2004) used a more complex 2DH model (including wave groups, wave asymmetry, surface roller model and return flow) to investigate the role of wave groups and wave spreading in rip spacing for shore-normal incident waves. For an idealized case they found that rip channel distances decrease when the spreading increases. The same model was used to hindcast a downstate morphological evolution at Palm Beach, NSW (Smit et al., 2006) showing that a different choice for wave spreading and sediment transport equation leads to different outcomes. The findings stated above indicate that morphological modelling results are highly sensitive to the included processes, parameter settings and initial conditions.

To assess the importance of modelled processes and to constrain the corresponding model parameters, we perform a morphological hindcast of an observed up-state and down-state transition at Palm Beach, New South Wales, Australia. Model processes include wave groups, wave asymmetry, roller energy and wave breaking related turbulence, return flow and long waves. The hydrodynamic model parameters are calibrated by comparing with in-situ measurements of wave-height and velocity. Comparison with observed morphological changes is used to establish the dominant processes and their relevance during both up-state and down-state transitions. To assess the effects of the initial conditions on the predicted morphological evolution, computations are started at different moments in the observed morphological evolution. The initial bathymetries used in the computations are inferred from video-images.

Section 4.2 describes the observations of the hindcast event. The model approach, description and validation are described in Section 4.3. Section 4.4 discusses the model performance for

different process settings, the role of the initial morphological state of a bathymetry, the subsequent conditions and the impact of the balance of the morphological processes to damp and amplify new or existing features. A brief discussion on the comparison of the current work and work by others is included in Section 4.5. Conclusions are presented in the final section.

4.2 Hindcast observation

Holman et al. (2006) investigated four years of video data on the occurrence and location of rip channels at Palm Beach, during which they observed 15 reset-events. From this data set the sequence from 10 to 20 of July 1996 was selected for the hindcast model study. This sequence is captured by good-quality images, has wave data available and an acceptable duration from a computational point of view. The 10 day evolution (Figure 4.1) shows the rips that were initially present, partly disappear during the storm (July 15 and 16, $H_s \approx 3.5$ m), with new rips developing at different (than pre-storm) locations during the calmer post-storm conditions (H_s decreasing to 1 m).

Initial bathymetries for the morphological computations were obtained using the technique described by Van Dongeren et al. (2008), a 2D extension of the cross-shore profile approach of Aarninkhof et al. (2005). In this technique, roller dissipation patterns derived from daily averaged video images are compared with numerically predicted dissipation patterns. At locations where the computed dissipation is smaller than the video-based dissipation, the depth is decreased; in locations with too much dissipation, the depth is increased. We started with an initially alongshore uniform single bar bathymetry, computed dissipation patterns for the observed daily averaged offshore wave conditions and compared these with the daily averaged video images (Figure 4.1a). The mismatch between computed and observed dissipation was used to update the model bathymetry. Minimizing this mismatch then yields the video-estimated bathymetries (Figure 4.2). These bathymetries reflect our visual interpretations of the observed dissipation patterns (Figure 4.1a), with darker areas at rip channels and lighter areas corresponding to bars and shoals.

The following parameters are used to describe the observed evolution: $meanZ(x)$ (alongshore-mean cross-shore profile), $stdZ(x)$ (alongshore variability of the bathymetry with respect to this mean profile), $stdZmean$ (the cross-shore mean standard deviation over the main area of interest) and $\overline{\lambda}_y$ (the weighted alongshore length scale). Palm Beach is an embayed beach, having a natural curved shape, which introduces problems in longshore and cross-shore averaging if the bathymetry data would be used directly on a cartesian grid. To that end the data is adapted in a few steps to obtain the necessary parameters. At each day, the bathymetry below sea level is rectified parallel to the shoreline on a 5 by 5 m grid ($x5$, $y5$), resulting in Z_{obs} (stretched bathymetry, Figure 4.3a). The alongshore mean of this bathymetry results in $meanZ_{obs}$ (Figure 4.4). To remove remaining geometrically induced trends in Z_{obs} - due to the

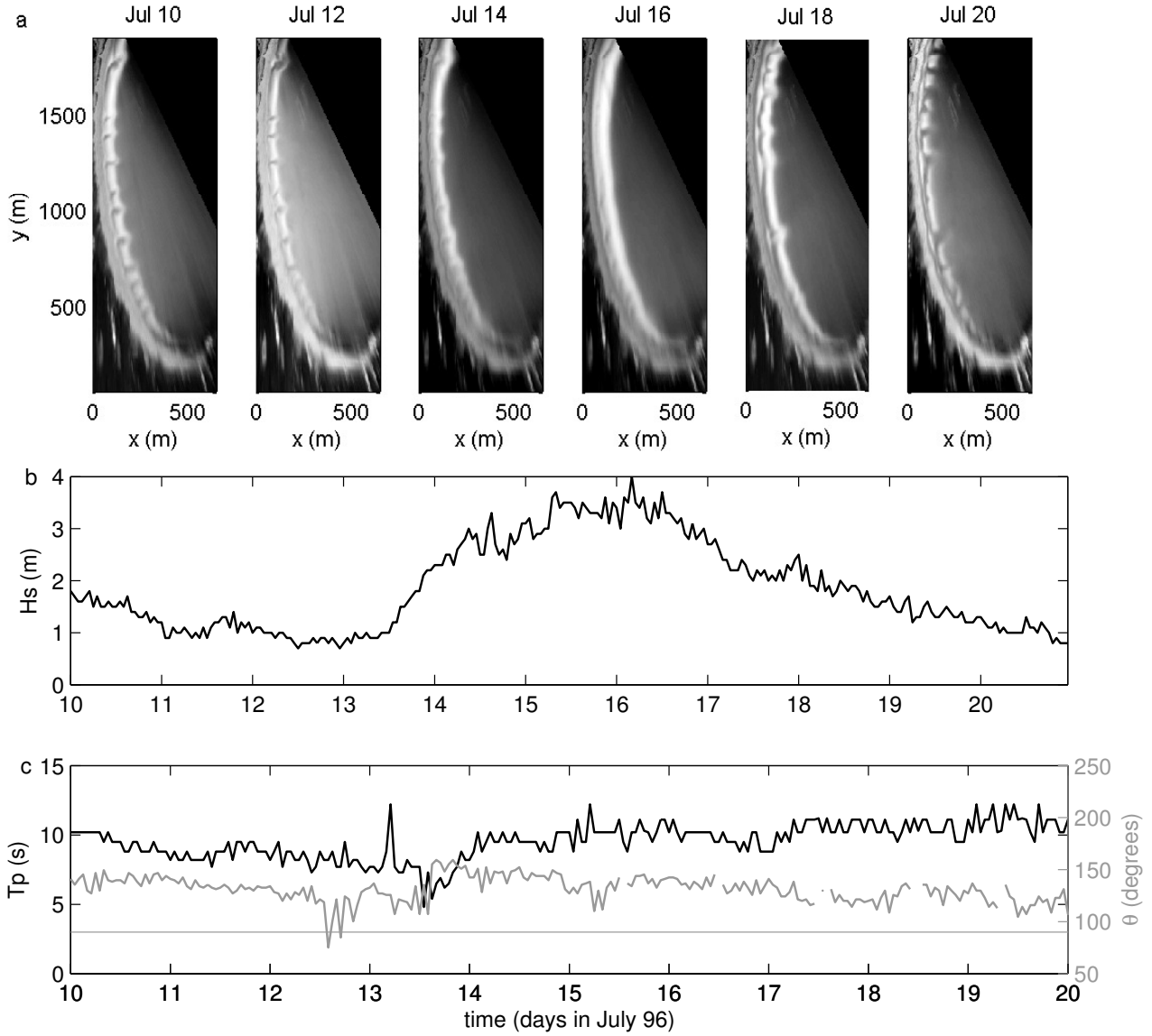

Figure 4.1: Selected event in July 1996. a: time-exposure video-images illustrating the dissipation patterns, with corresponding conditions measured by the offshore waverider: b: H_s (m), c: T_p (s) and θ (degrees), horizontal line indicates shore normal wave incidence.

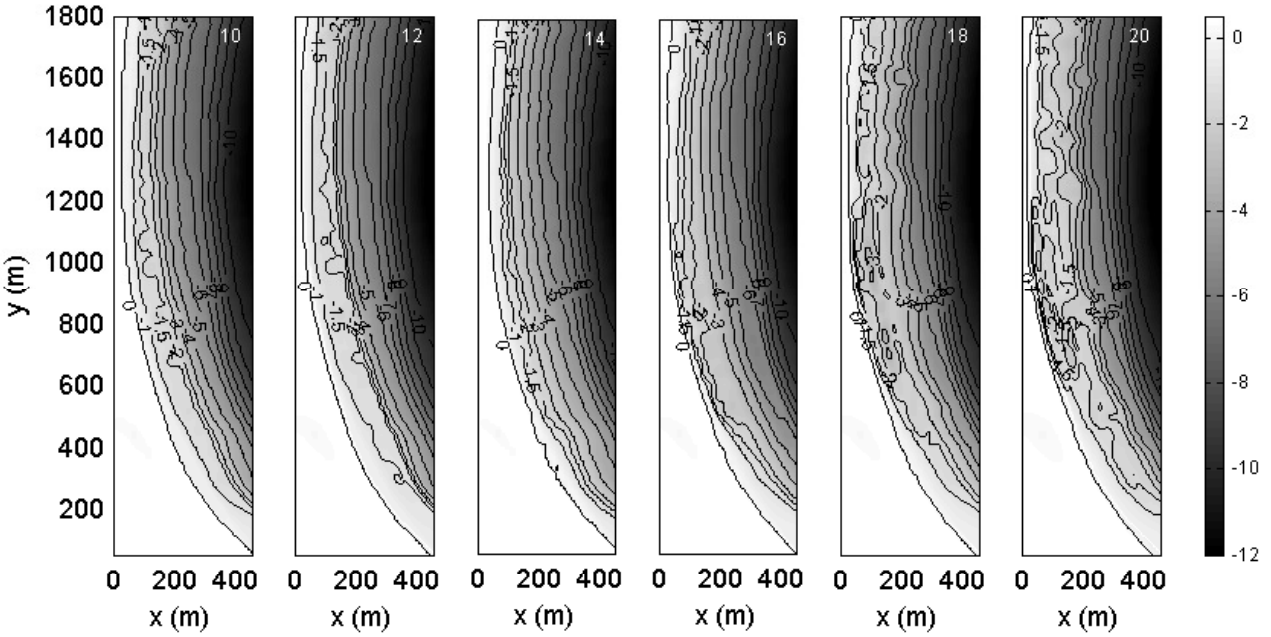

Figure 4.2: Video-based bathymetries on July 10, 12, 14, 16, 18, 20, 1996.

pocket beach geometry - a second order polynomial best fitting to Z_{obs} per cross-shore location was subtracted, resulting in $dZ2_{obs}$ (Figure 4.3b). This is used to compute the alongshore variability by taking the standard deviation ($stdZ_{obs}$) alongshore of $dZ2_{obs}$ (Figure 4.4). The averaged weighted length scale ($\overline{\lambda}_y$) is obtained at the cross-shore location with the highest $stdZ$ (X_{stdmax}), which are denoted by the black dots in Figure 4.4. These locations are determined manually by visual inspection of Figure 4.4. At these X_{stdmax}, the alongshore length scale is computed by taking a Fourier transform of $dZ2$ at this location and weighing this with the Fourier amplitudes (giving $\overline{\lambda}$). As the length scales were found to be sensitive to the selection of the alongshore section, the weighted length scale over 10 overlapping sections was computed and averaged, resulting in $\overline{\lambda}_y$.The sections are each 1400 m long, starting at $x5 = 200$ m and moving north with increments of 5 m. These parameters are all obtained for the main area of interest, ranging from 195 to 1600 m alongshore. The parameter $stdZmean_{obs}$ (Figure 4.6a) is the daily mean of these standard deviations over a cross-shore extent of 0 to 225 m, the main area of interest (the variability is largest in this area).

Figure 4.5 shows that the mean profile has an initial bar at about 100 m from the shoreline. In time, this bar increases in volume (July 11-12) and simultaneously the variability increases (Figure 4.4). This variability abruptly decreases during the high energy event on July 14 and 15 when the bathymetric features disappear (Figure 4.2 and 4.4). After the storm, the variability starts to increase both offshore and in the shallow nearshore starting from respectively July 16 and 17. The mean profile shows an offshore shift of the bar after the storm and a steepening of the nearshore profile. Figure 4.6a summarizes the observed initial increase, subsequent decrease and final increase of the variability. The length scales vary during the event, they are initially

187 m, increasing after the storm up to 270 m and decreasing to 235 m at July 20 (Figure 4.6b).

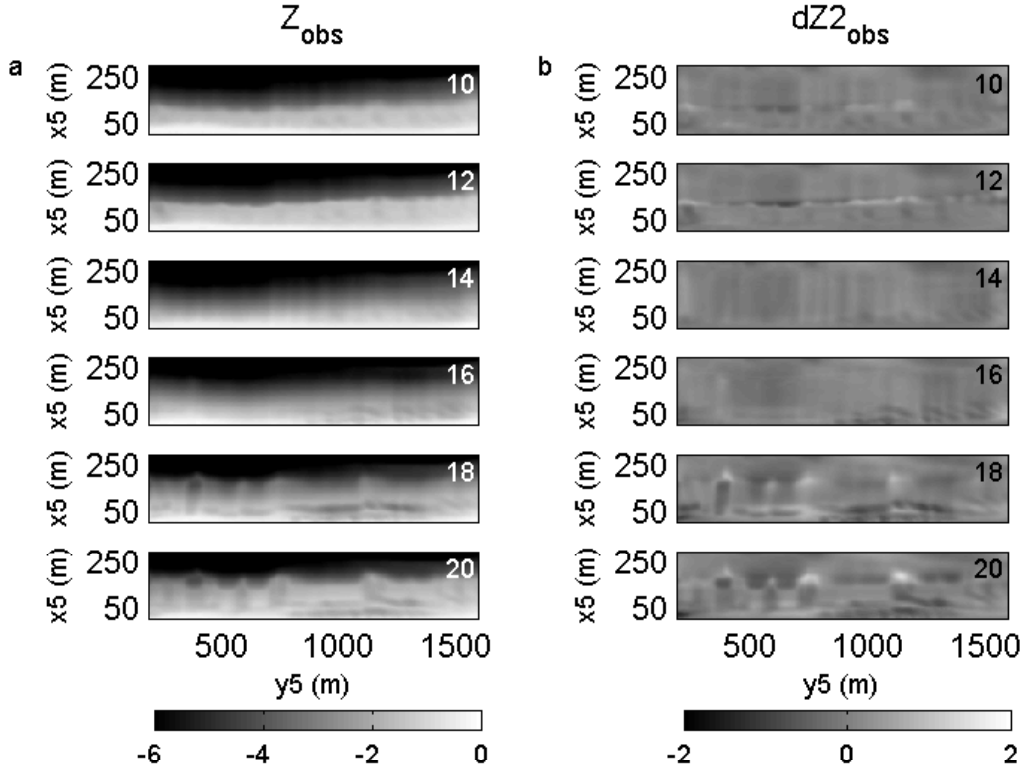

Figure 4.3: a: stretched bathymetry Z and b: stretched bathymetry minus geometrically induced trends $dZ2$ for observations at July 10, 12, 14, 16, 18, 20.

4.3 Model description

Roelvink and Stive (1989) tested the effects of several processes on the formation and evolution of a nearshore bar in a cross-shore flume experiment. They concluded from analyzing and hindcasting the observations, that including the effects of 1; wave asymmetry, 2; wave-group induced long waves, 3; the lag between the production and dissipation of breaking-induced turbulent energy and 4; turbulence stirring, resulted in the best match with the observed formation of an offshore bar. They state that 'deleting one of the mechanisms leads either to a less accurate prediction of the form or the position of the bar (usually too far seaward), to an overpronunciation of its form, or to deviations in the nearshore erosion area.' In summary: including spatio-temporal variability due to wave groups was found to improve the calculated bar formation. In a field case, the spatio-temporal variability does not only occur in the cross-shore, but also in the alongshore direction. Including wave group effects is therefor expected to have a significant impact on the morphological evolution (Reniers et al., 2004) and is therefor included and tested in the model used in the current work. Appendix F describes the differences in wave modelling when ex- (Chapter 2 and 3) or including wave group effects (this chapter).

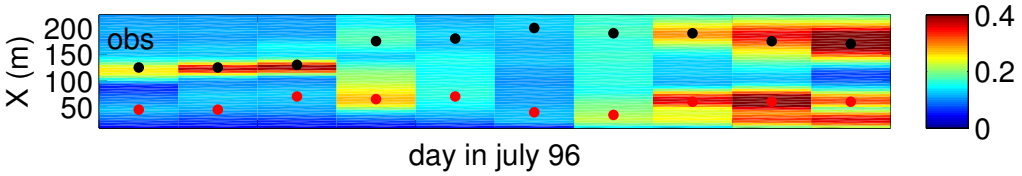

Figure 4.4: alongshore variability $stdZ_{obs}(x,t)$, with circles indicating the nearshore (red) and offshore (black) location with highest variability.

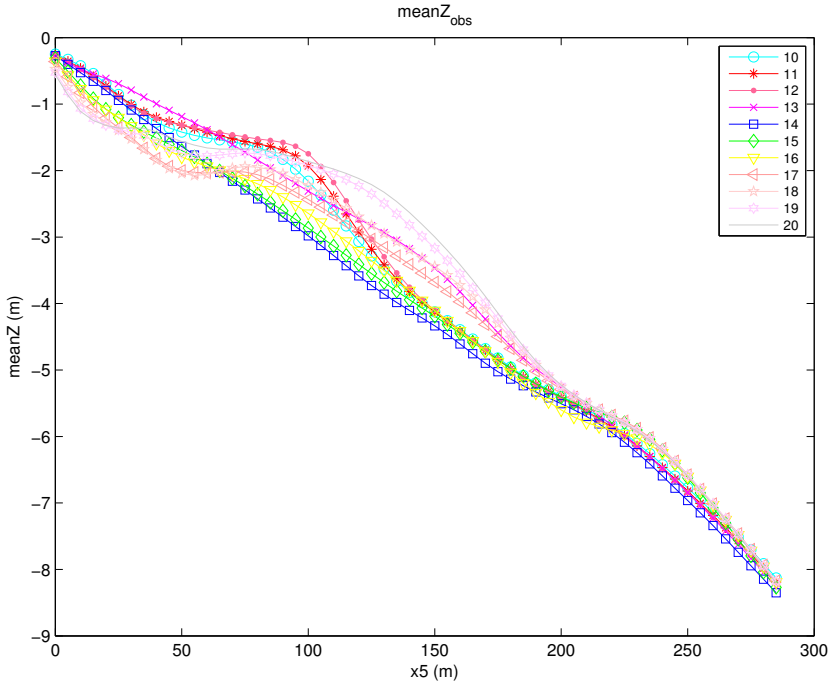

Figure 4.5: Mean cross shore profile, at days in July as presented in the legend.

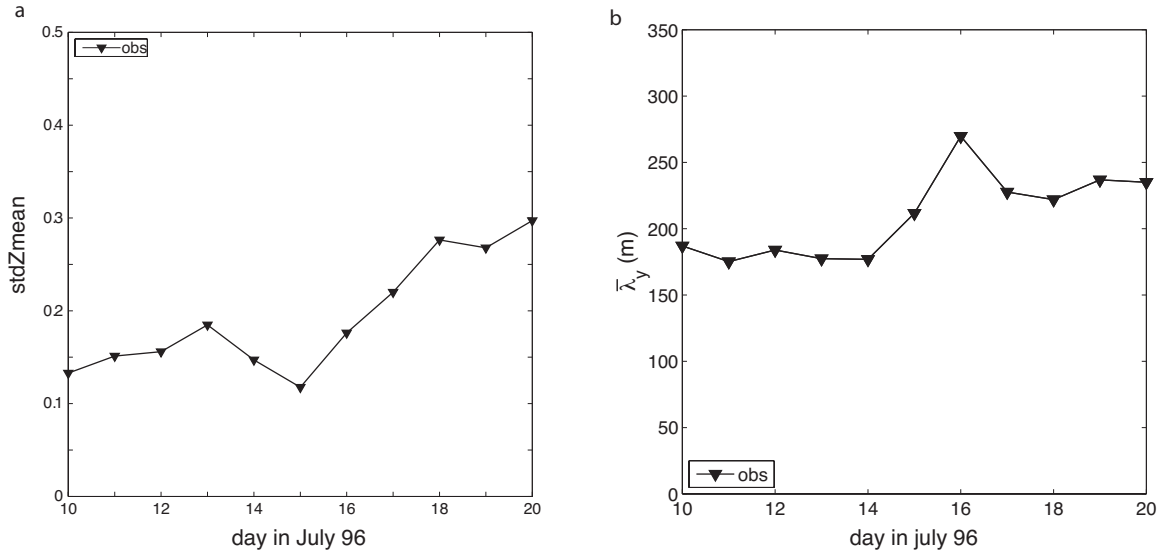

Figure 4.6: a: Mean alongshore variability $stdZmean_{obs}$ b: length scale $\overline{\lambda}_{y,obs}$.

Further, the effect of wave asymmetry on the evolution of nearshore morphology is examined. Due to the asymmetric shape of waves, the onshore orbital motion under the wave crest is larger than the offshore motion under the wave trough: this results in net onshore sediment transport. In addition, the effect of long wave induced stirring is tested by excluding this stirring in a separate set of computations. Lastly, the effect of turbulence in the diffusion is tested by linearly increasing this turbulence.

Modelling an observed morphological evolution means that both the amount of morphological change as well as the rate of morphological change needs to match the observed evolution throughout a series of hydrodynamic conditions. To investigate the role of the rate of change, computations with different adjustment rates have been tested.

In summary, in the current work we tested the effect of the following processes:

- wave asymmetry can be switched off (NA);
- long wave induced stirring can be excluded (NLW, then only stirring due to wave group averaged velocities and short wave orbital motions is accounted for);
- the wave groups can be switched off (NWG, in this case also the longwave induced sediment transport is switched off);
- diffusion, described as function of turbulence and water depth, and has a calibration parameter ($facvisc$) which enhances the turbulence;

In addition, we test the effect of one calibration parameter, which affects the rate of morphological evolution:

- the rate of change calibration parameter ($ACAL$).

4.3.1 Model set-up

A research version (Reniers et al., 2004) of the modelling system Delft3D (Lesser et al., 2004) is used for the morphological computations. It consists of several modules for simulating short waves, currents and sediment transport, which can be applied for coastal computations. Wave and roller modules describing wave propagation and breaking, operating on the timescale of wave groups (when activated), are coupled to a depth averaged nonlinear flow model to predict the time-dependent infragravity flow field. The mean wave direction in the wave and roller modules is obtained from the precomputed wave refraction using SWAN (Booij et al., 1999). Wave energy released at wave breaking is first transferred to roller energy prior to dissipation causing a spatial lag between the location of wave breaking and the actual dissipation. The temporal and spatial variation on the wave group scale of the wave and roller energy is used to calculate the radiation stresses. Nonlinear shallow water equations are used to solve the mean and wave group motions. The sediment transport is computed with an advection-diffusion model. The sediment transport module includes transport by the mean currents and optionally short and infragravity waves. Sediment is predominantly stirred by the wave orbital motion

and wave breaking-induced turbulence. The skewness of the short waves (wave asymmetry), responsible for onshore sediment transport, is parameterized on the time scale of the wave groups using a nonlinear Fourier representation.

4.3.2 Sediment transport formulations

In general, the same formulations have been used as in the model described in Reniers et al. (2004). In the computation of sediment transport and bottom changes, the following adaptations have been made.

The suspended sediment transport is modelled with a depth-averaged advection diffusion equation including horizontal diffusion terms (which were omitted in Reniers et al. (2004)):

$$\frac{\partial}{\partial t}hC + \frac{\partial}{\partial x}hCu^E + \frac{\partial}{\partial y}hCv^E - \frac{\partial}{\partial x}D\frac{\partial hC}{\partial x} - \frac{\partial}{\partial y}D\frac{\partial hC}{\partial y} = \frac{hC_{eq} - hC}{T_s} \tag{4.1}$$

in which h is the local water depth, C is the depth averaged sediment concentration, D is the horizontal diffusion coefficient, C_{eq} is the depth averaged equilibrium concentration, T_s is the adaptation time, representing the vertical diffusion of the sediment and u^E, v^E are the Eulerian velocities containing both wave-group averaged and long wave motions. The Gallapatti time scale T_s (Gallapatti, 1983) is given by:

$$T_s = max\left(0.05\frac{h}{w_s}, 1\right) \tag{4.2}$$

where w_s is the sediment fall velocity (here $w_s = 0.016$ m/s) and h is the water depth. The equilibrium concentration (C_{eq}) is a function of sediment stirring by the wave-group averaged, long wave and short wave orbital velocities:

$$C_{eq} = A_{ss}\left(\left(u_{tot}^2 + \frac{0.018u_{rms}^2}{C_d}\right)^{1/2} - u_{cr}\right)^{2.4} \tag{4.3}$$

Where A_{ss} is the suspended load coefficient, which is a function of the sediment grain size, relative density of the sediment and the local water depth (see Soulsby (1997) for details). C_d represents the drag coefficient, u_{cr} the threshold velocity, u_{rms} the short wave near bed orbital velocity including breaking induced turbulence (Equation 16, Reniers et al., 2004) and u_{tot} represents the combined wave-group averaged and long wave Eulerian velocity magnitude:

$$u_{tot} = \sqrt{(u^E)^2 + (v^E)^2} \tag{4.4}$$

where:

$$u^E = \bar{u}^E + u_L^E \tag{4.5}$$

In these expressions, $\bar{u}^E$ is the velocity averaged over many groups and u_L^E the long wave velocity. The Eulerian velocities (u^E and v^E) are obtained by subtracting the Stokes drift from the computed velocities, thus including the effect of undertow (Reniers et al., 2004).

The suspended sediment transport is then given by:

$$S_{s,x} = hCu^E - D\frac{\partial hC}{\partial x} \tag{4.6}$$

Bed load is computed locally using the transport formulation by Soulsby-van Rijn (Soulsby, 1997) (Equation 4.7):

$$S_{b,x} = A_{sb}u^E \left(\left(u_{tot}^2 + \frac{0.018{u_{rms}}^2}{C_d} \right)^{1/2} - u_{cr} \right)^{2.4} \tag{4.7}$$

Where A_{sb} is the bed load coefficient. The wave asymmetry sediment transport is represented by:

$$S_{a,x} = \frac{1}{T}\int [\alpha_w u_b' \left(A_{sb} + A_{ss}\right) \left(u_{tot}^2 + \frac{0.018{u_b'}^2}{2C_d} \right)^{2.4} \cos\theta] dt \tag{4.8}$$

where u_b' is the instantaneous near bed velocity obtained with Rienecker and Fenton (1981), the prime denotes intra-wave variables, T is the mean wave period, α_w is a calibration parameter, and θ is the mean wave direction with respect to the x-axis (i.e. cross-shore). Equivalent expressions are used for the alongshore transport components.

The bottom changes are obtained from continuity:

$$\left(1 - \varepsilon_{por}\right)\frac{\partial z_b}{\partial t} + ACAL\left(\frac{\partial S_x}{\partial x} + \frac{\partial S_y}{\partial y}\right) = 0 \tag{4.9}$$

in which z_b is bed level, $S_{x,y}$ are the combined suspended load ($S_{s,x}$ from Equation 4.6), bed load ($S_{b,x}$ from Equation 4.7) and wave asymmetry ($S_{a,x}$ from Equation 4.8) transport rates in x- and y-direction and $ACAL$ is a calibration coefficient (-) which is set to 1 unless stated otherwise (Section 4.4.3). For further details, refer to Lesser et al. (2004) and the Delft3D manual (www.deltares.nl).

The horizontal diffusion (D, Equation 4.1) is described as function of turbulence and depth.

$$D = facvisc \cdot \nu_t \frac{1}{e^{\frac{h}{4}} - 1} \tag{4.10}$$

With $facvisc$ a calibration parameter which is set to 2.5 unless stated otherwise, ν_t is the turbulent eddy viscosity (Battjes, 1975):

$$\nu_t = h(\frac{Dr}{\rho})^{1/3} \tag{4.11}$$

with Dr the roller energy dissipation obtained from the roller energy balance (Equation 4 in Reniers et al. , 2004) and ρ the water density.

Model adjustments for the different settings

When wave asymmetry effects are excluded (NA setting), S_x and S_y (as used in Equation 4.9) will consist only of suspended and bed load, ignoring the transport due to wave asymmetry (Equation 4.8). In the No Long Wave stirring (NLW) configuration the contribution of the long waves in u_{tot} used in Equation 4.3 and 4.7 is omitted. For the configuration without wave group effects (NWG), all wave group effects in all processes are excluded. For details see Appendix G.

4.3.3 Model Settings

Time steps

The transport and bottom changes are calculated for each flow time step, with a morphological factor to speed up the computations (Roelvink, 2006), assuming that the flow field does not change significantly within that period (equal to the flow time step times the morphological factor). For these calculations a morphological factor of 12 was used. This means that for every flow step of 2.4 s, the morphological adjustment over a period of 28.8 s is calculated. This loop is done 375 times (corresponding to 3 hours morphologically), after which the mean wave directions used in the wave and roller modules are recomputed with SWAN based on the new bathymetry.

Grid and settings

The offshore wave transformation for the hydrodynamic calibration is computed using 3 nested grids, the outer domain with a grid resolution of 100 m by 100 m with 2 inner nested grids, one with a 25 by 25 m resolution and the smallest with grid cells ranging from 6 by 10 to 18 by 10 m, identical to that used by Reniers et al. (2001) and Smit et al. (2006). For the morphological computations only the coarse and finest wave grids were used for the wave transformation as this was found to be sufficient to avoid boundary effects in wave transformation. The finest grid was used for the hydrodynamic computation and bed level update.

4.3.4 Hydrodynamic model calibration

The hydrodynamic module was calibrated using the data of the RDEX 1999 experiments and work by Reniers et al. (2001). The model was forced with wave conditions (significant wave height (H_s), peak period (T_p), angle of wave incidence (θ)) measured at 80 m water depth, 20 km South of Palm Beach and tidal elevation (Figure 4.7a), for the period of 10 to 22 October 1999. Wave refraction and shoaling is computed on the large wave grids applying a Jonswap

β	γ	$DSPR$
0.05	0.45	12.4^o

Table 4.1: Parameter settings for calibration.

spectrum with user-defined directional spreading ($DSPR$) with SWAN. For the local domain (where the finest grid is defined), the wave information on the boundaries is used as input to compute the flow transformation including wave groups and roller effects. In this area, the bottom roughness was computed using Manning, with the Manning coefficient set to 0.02. The wave dissipation due to wave breaking is computed using the dissipation formulation of Roelvink (1993). The computed results were optimized by calibrating the wave breaker parameter (γ), the roller dissipation coefficient (β) and $DSPR$ used in the wave module. Table 4.1 presents the optimal parameter values.

The modeled nearshore wave heights compare well with the measured wave heights at a Wave Gauge at 10 m water depth (RMSerror = 0.14 m, Figure 4.7b and Figure 4.8c). The wave heights do not match in detail, but the overall trend is covered by the model. Also the modelled hourly averaged velocity magnitudes in shallow water compare reasonably well to the measurements from 2 current meters (S4 North and S4 South with RMSerror = 0.19 m/s and 0.1 m/s respectively, in Figure 4.7b and Figure 4.8a and b). For example, the measured increase in velocities around 19 October was simulated well.

4.4 Model performance

4.4.1 Model settings

Morphological computations have been performed with six different settings: 1: the basic model settings ($base_n$, n = start date 11..20 July 1996); 2: without the effect of wave asymmetry on the sediment stirring (NA_n); 3: without long-wave induced stirring (NLW_n); 4: without wave groups (NWG_n); 5: with decreased turbulence ($diffFA_n$) and 6: with a higher adjustment rate ($diffAA_n$). The results of the latter two cases are presented in Section 4.4.3. For each of the settings, the morphological evolutions from the start date to July 20 were computed. For each of the ten start dates, the initial bathymetry was the bathymetry of one day prior to the start date; i.e. $base_{11}$ started with the bathymetry of July 10 and the hydrodynamic conditions of July 11. Tidal fluctuations have been omitted in the morphological computations. In explorative computations it was found that the tide (at Palm Beach the tidal range is less than 1 m) had no significant effect on the computed morphological evolution. The values mentioned in Table 4.1 are used for β, γ and $DSPR$.

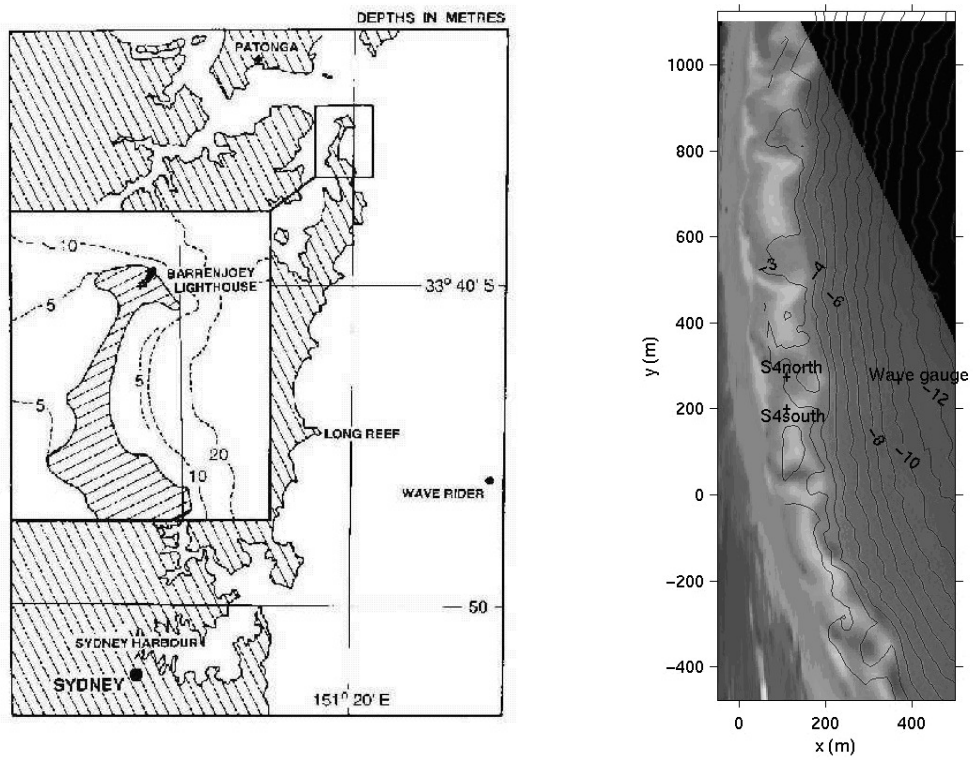

Figure 4.7: a: Palm Beach (enlarged area) is located north of Sydney. Directional wave rider is located approximately 20 km south of Palm Beach. b: Location of Wave Gauge and S4 current meters at Palm Beach, Sydney, with measured depth contours (m) superimposed on time exposure video image at the beginning of the RDEX experiment.

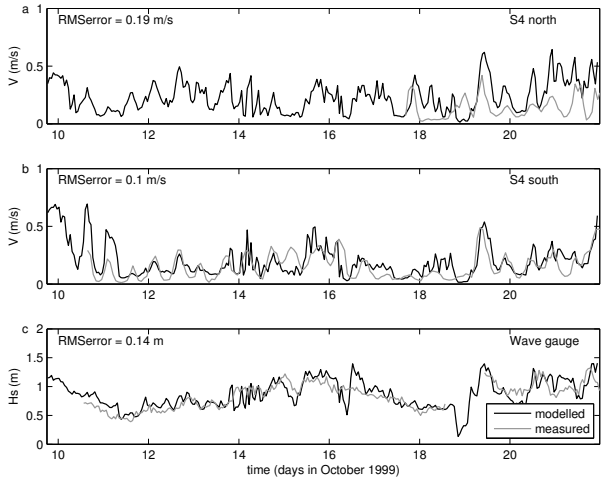

Figure 4.8: Modelled (black) and measured (grey) hourly averaged current magnitudes at a: S4 north, b: S4 south and c: H_s at Wave Gauge. Due to burial of the current meters, the measurements were not available continuously throughout the computed period. The RMS error is indicated in the top left corner of each plot.

4.4.2 Parameters for analysis

To quantify the performance of the model, a skill has been computed for three parameters: the overall bathymetry ($Sbathy_{i,n}(t)$, with i the computational setting, t = time), *meanZ* ($Smean_{i,n}(t)$) and *stdZ* ($Sstd_{i,n}(t)$) as follows:

$$Spar_{i,n}(t) = 1 - \frac{max(0, RMS(modelpar_{i,n}(t) - obspar(t)) - obserror)}{RMS(obspar_{t0} - obspar(t))} \tag{4.12}$$

with *par* either *bathy*, *meanZ* or *stdZ*, RMS = root mean square, *modelpar* is the parameter value as computed with the model, *obspar* refers to the observation based parameter value, $obspar_{t0}$ refers to the observed parameter value at the initial time of the computation. The RMS values were quantified over the cross shore area up to 225 m, which is the main region of interest as this is where the profiles vary most (Figure 4.4). An observation error (*obserror*=0.05 m) is subtracted from the model error (RMS($modelpar_{i,n}(t)$-$obspar(t)$)), accounting for the error in the observation-based bathymetries. All scores are initially 1, as the initial value of the parameter is identical to the observed value. A skill score of 1 means that the model predicts the observation parameter perfectly within the range of the observation error. A skill score smaller than 0 means that the model prediction is worse than presuming the parameter is constant in time.

4.4.3 Results

Effect of processes

The different process settings result in distinctly different computed evolutions of the bathymetry (Figure 4.9). All computational settings result in decreasing alongshore variability in the first days (Figure 4.10a), though *stdZmean* shows a slight increase in the observations. The variability decreases further during the storm (t = July 14, 15), except for NLW_{11}. During the subsequent lower energy conditions, the variability generally increases, with different magnitudes and locations for the different settings. These computed evolutions are described in detail below, using both the bathymetrical evolution and the skill parameters.

In the $base_{11}$ computation the alongshore variability of the bathymetry (Figure 4.9a, 4.11b and 4.10a) decreases slightly during the storm (July 14) and increases after the storm during the calmer hydrodynamic conditions. For the no wave asymmetry computation (NA_{11}), variability decreases in the first few days (Figure 4.9b, 4.11c, and 4.10a), then the bathymetry becomes steeper near the shoreline. Alongshore variability returns only to a limited extent. Including wave asymmetry effects in the sediment transport results in higher onshore transports and a higher rate of change in the nearshore. Excluding these onshore effects resulted in less pronounced features and onshore movement of the shoreline. Excluding wave asymmetry effects result in lower total transport and thus lower rate of change (Equation 4.9).

The computation without long wave induced stirring (NLW_{11}) shows a small decrease in variability during the first few days of the computation (Figure 4.9c and 4.10a). However, during the high energy conditions of the storm, the remaining features evolve further, instead of disappearing as in the observations. Their evolution continues after the storm, resulting in features that are more nearshore and more pronounced than the observed features, resulting in higher nearshore variability then was observed (compare Figure 4.11a and Figure 4.11d).

In the computation without wave groups (NWG_{11}), the initial alongshore variability decreases in the first few days (Figure 4.10a and 4.11e) and increases during the storm, where an offshore bar is formed (Figure 4.9d, day 14, 16 at $y = 1000$ m). However, formation of a distinct offshore bar was not observed until after the storm. After the storm, the variability increases further (Figure 4.11e). The length scales of NWG_{11} are smaller than the observed length scales and the length scales computed when wave group effects were included (e.g. $base_{11}$ in Figure 4.10b).

Comparing $stdZ_{base,11}$ and $meanZ_{base,11}$ (Figure 4.11b and 4.12) with respectively $stdZ_{obs}$ and $meanZ_{obs}$ (Figure 4.11a and 4.5) illustrates the similarities and differences of the computed and observed evolution. The observed heightening of the bar (up to day 12 in Figure 4.5) is not represented in the computation (Figure 4.12). Both the computation and the observations show offshore movement of the bar, however, in the computation this starts earlier (July 14) than observed. The main regions with high variability change in time from 100 m off-shore at the beginning of the computation to two areas (viz. 50 and 200 m off-shore, Figure 4.11b). Comparing this with the observed evolution (Figure 4.11a), we find that the model does not reproduce the initial increase in variability prior to the storm. Nor does it reproduce the correct post-storm magnitude of increase in variability. The post-storm cross-shore location of variability was matched to some extent.

The above interpretations from the bathymetrical evolutions are represented in the skill scores for *bathy*, *meanZ* and *stdZ* for the four different computations (Figure 4.13 and Figure 4.14). *Sbathy* has the same trend for all four computations: the skill decreases, with a minimum value during the storm (around July 15), increasing again during the lower energy conditions, until maximally a skill of 0. For all computations the scores are low, showing that a perfect bathymetrical match is hard to predict, especially with increasing prediction time and when passing through a reset-event. The negative scores indicate that the initial bathymetry matches the observed bathymetry at those days better than the model prediction of that day and thus it would have been better not to run the model. This is the case if one would pursue a perfect match of the observed and modelled bathymetry. However, due to the sensitivity to small bathymetrical variabilities in the initial bathymetry (e.g. Smit et al., 2008) and the observation-induced error in the used bathymetries, we can hardly expect to obtain perfect predictions.

We therefore analyse the performance of the model using two other parameters which describe the characteristics of the evolution: the mean profile (*Smean*) and the variability in the alongshore (*Sstd*). The scores decrease in the days after the storm as the model computes an increase

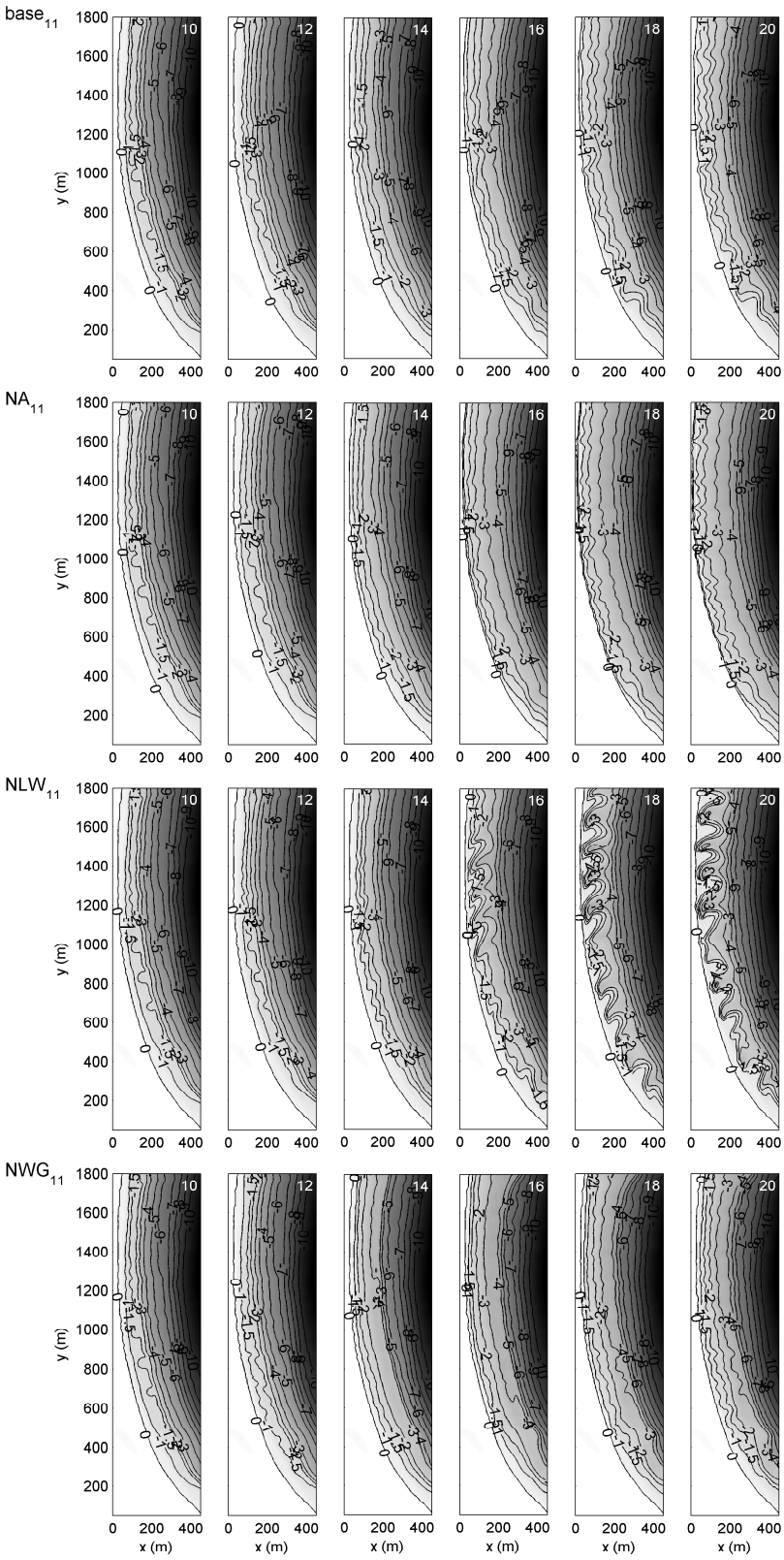

Figure 4.9: Bathymetries of computations starting with bathymetry of July 10 (initial), computed on July 12, 14, 16, 18, 20 1996, nr indicates day in July 1996 for 4 computations: a: $base_{11}$, b: NA_{11}, c: NLW_{11}, d: NWG_{11}.

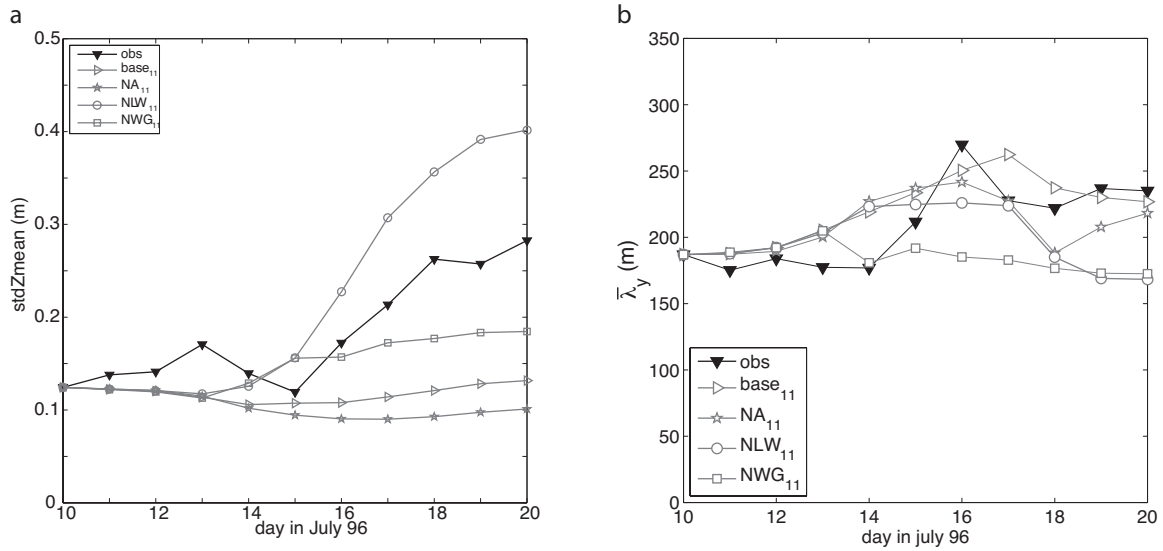

Figure 4.10: a: Mean alongshore variability $stdZmean_{obs}(t)$, $stdZmean_{base11}(t)$, $stdZmean_{NA11}(t)$, $stdZmean_{NLW11}(t)$, $stdZmean_{NWG11}(t)$, b: length scale $\overline{\lambda}_{y,obs}(t)$, $\overline{\lambda}_{y,base11}(t)$, $\overline{\lambda}_{y,NA11}(t)$, $\overline{\lambda}_{y,NLW11}(t)$, $\overline{\lambda}_{y,NWG11}(t)$.

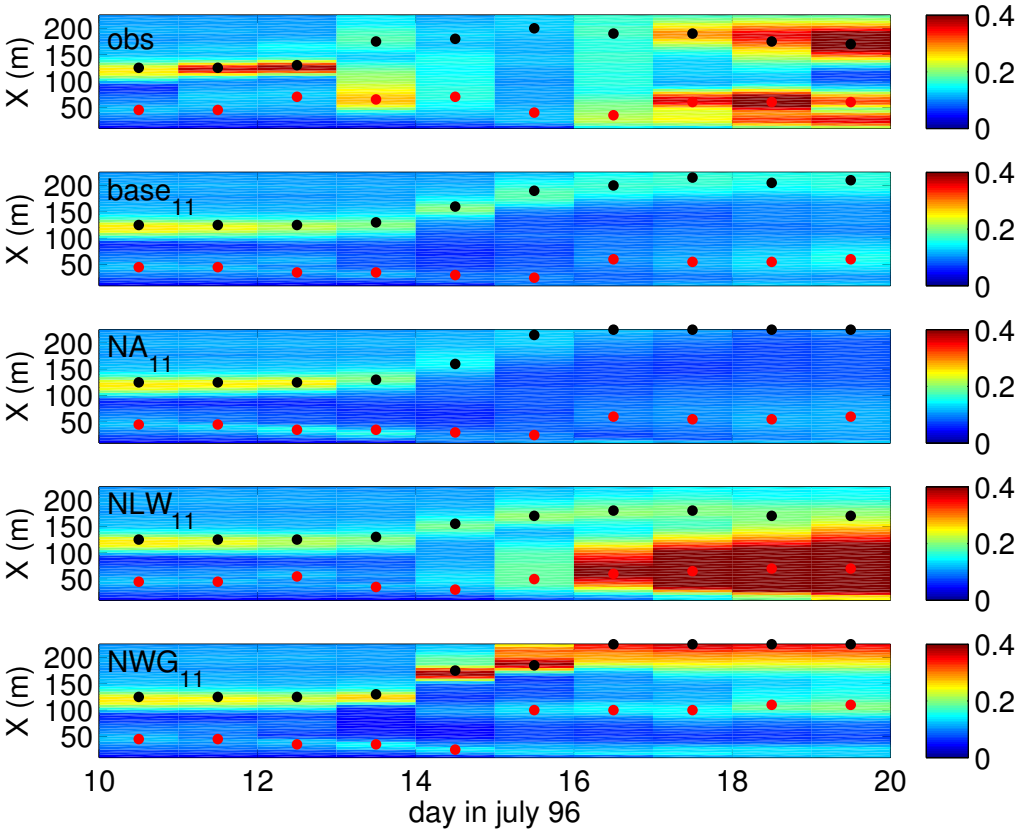

Figure 4.11: Alongshore variability a: $stdZ_{obs}(x,t)$, b: $stdZ_{base11}(x,t)$, c: $stdZ_{NA11}(x,t)$, d: $stdZ_{NLW11}(x,t)$, e: $stdZ_{NWG11}(x,t)$ with circles indicating the nearshore (red) and offshore (black) location with highest variability.

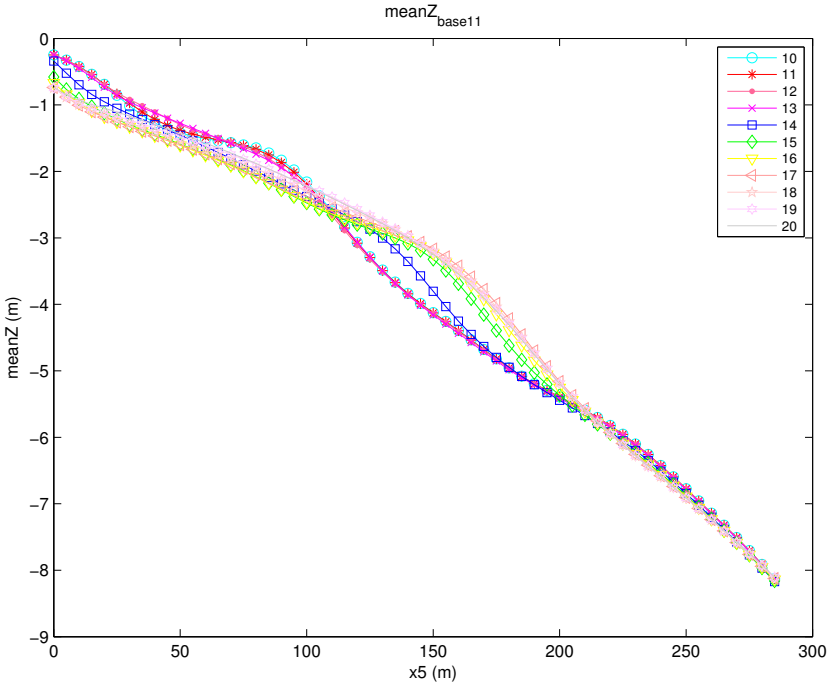

Figure 4.12: Mean cross shore profile $meanZ_{base,11}$ at days in July as presented in the legend.

in variability with a smaller magnitude and at different cross-shore locations than observed. *Smean* shows the same trend for all process settings: initially decreasing and increasing after the storm (Figure 4.14a). In the second half of the computation, *meanZ* is matched best by NLW_{11}, though the variability of this computation has a low score in this period due to the continuous evolution of pre-storm features. *Sstd* shows for all but the setting without wave groups the trend that the variability is matched well during the storm, and the skill score decreases again after the storm (Figure 4.14b).

Effect of initial conditions

Next to testing the effect of different processes, the effect of the antecedent morphology and the occurring hydrodynamic conditions is tested. This is done by starting computations at each day of the observed event and analysing the performance of the model for those different start dates. Different start dates of the morphological computation result in different computed evolutions (Figure 4.15). In general the post-storm computations starting only few days prior to July 20 give the best results on that day (see Figure 4.15 and $Sstd_{i,n}(20)$ in Figure 4.16). This can partly be attributed to the fact that the prediction time is short and in these 1-3 days the morphological evolution is small, therefore the computation has little chance to deviate from the correct prediction. For computations starting prior to the storm it was found to be impossible to quantitatively match the observed rate of change and the evolution in variability (Figure 4.17), indicating that the storm-event is modelled with limited skill with the tested and applied settings and processes. For the $base_n$ computations, the evolution of *stdZmean*

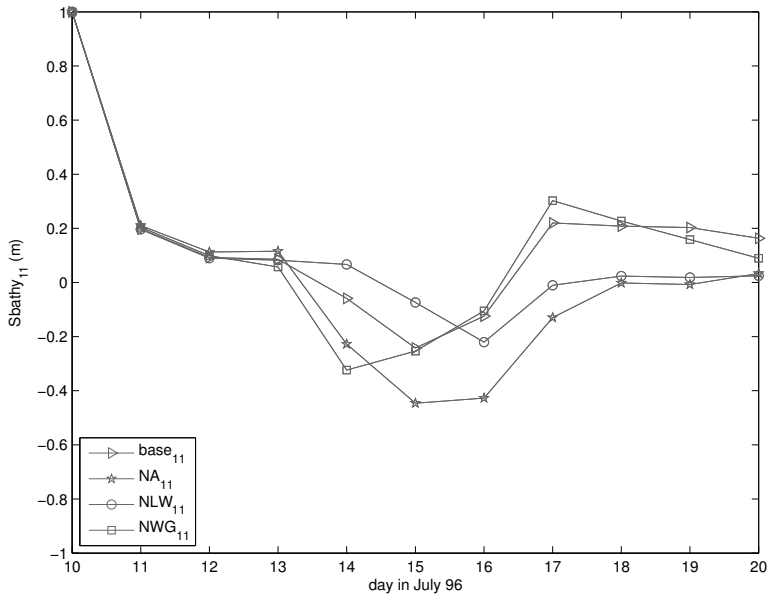

Figure 4.13: Skill scores for overall bathymetry: $Sbathy_{base,11}$, $Sbathy_{NA,11}$, $Sbathy_{NLW,11}$ and $Sbathy_{NWA,11}$ as a function of day in the morphological evolution.

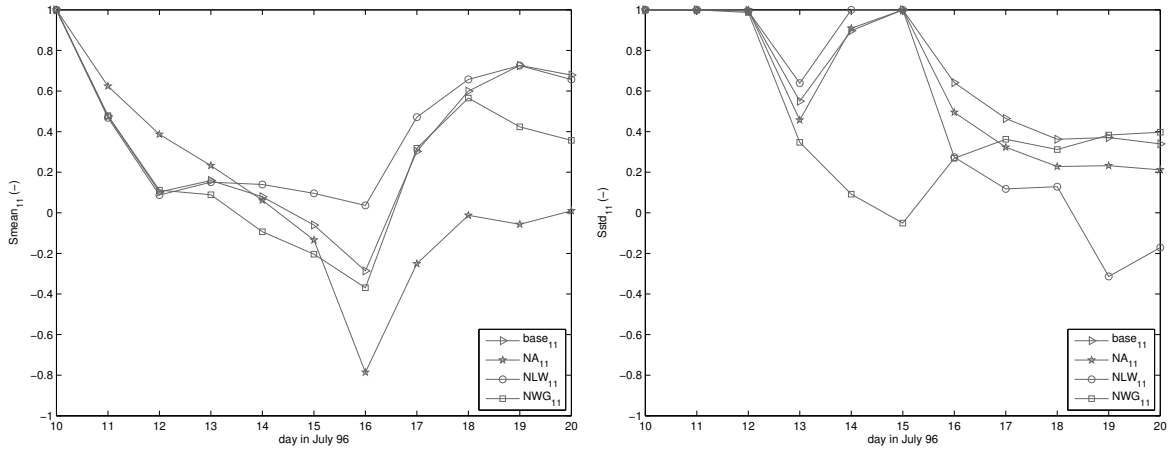

Figure 4.14: a: Skill scores for mean cross shore profile: $Smean_{base,11}$, $Smean_{NA,11}$, $Smean_{NLW,11}$ and $Smean_{NWA,11}$, b: Skill scores for alongshore variability: $Sstd_{base,11}$, $Sstd_{NA,11}$, $Sstd_{NLW,11}$ and $Sstd_{NWA,11}$ as a function of day in the morphological evolution.

of $base_{14}$ matches the observed evolution of variability best. It should however be noted that for this computation, the computed bathymetrical patterns (not shown) are different from the observed: the computed features are shore-connected with a cross-shore orientation, while the observed variability also occurs more offshore, with a predominantly alongshore orientation. Cross-shore averaged this results in near identical *stdZmean*, but the corresponding $Sstd$ of 0.5 reflects the differences in cross-shore location of variability. For the post-storm computations, all settings result in near equal final *stdZmean* and none of these computations quantitatively matched the observed increase in *stdZmean*.

In the first 1-3 days of any computation, the choice of included processes only results in different *stdZmean* when high initial variability is combined with high wave energy and with processes with small damping effects in the model (e.g. Figure 4.17 $comp_{14}$ for NLW). Damping refers to the disappearance of existing features due to diffusive effects of processes. Similar initial variability (Figure 4.17 $comp_{17}$ for NLW) but with subsequent calmer post-storm conditions resulted in an almost constant level of variability.

Conclusions on effect of processes and initial conditions

Morphological evolution is a result of interacting hydrodynamic and morphological processes. In time all these effects are cumulative which may lead to an evolution that deviates quickly from the observed evolution. Both magnitude and pace of the modelled morphological evolution therefore need to resemble the observed evolution in order to stay on track with the observations. The *base* settings of the morphological model include descriptions of processes which affect the pace and magnitude of the modelled morphological evolution. To quantify the effect of three key processes (wave asymmetry, long wave induced stirring, wave groups), computations excluding those were performed and compared to computations with the *base* settings. The nearshore morphological evolution is found to be highly sensitive to small differences in bathymetry and physical description of the processes.

Including wave asymmetry effects in the sediment transport results in higher onshore transports and a higher rate of change in the nearshore. Excluding these onshore effects (NA setting) resulted in less pronounced features and onshore movement of the shoreline.

Excluding long wave induced stirring (NLW setting) resulted in the evolution of more explicit features. This is a result of the long wave related diffusion in the model calculations. Normally the long wave induced velocities are especially large in the shallow areas. These are smaller in the NLW configuration, resulting in a smaller diffusive effect, which results in large, distinct features. This is visible in the computations which included the high energy event (starting before/on July 15). The variability then evolves similar to the other computations up to the storm, during the storm the variability increases (instead of the decrease observed at most other computations), this remaining variability then increases further in the calmer post-storm conditions (Figure 4.17), resulting in distinct features and high nearshore variability (Figure 4.11d).

Including wave groups seemed to contribute to the evolution of correct length scales. Excluding wave groups resulted in smaller length scales.

It was found that the modelled processes need to have the correct balance of amplifying and diffusive effects. Including wave groups in the model supported the computation of morphological evolution with decreasing variability during storm conditions and length scales that are matching the observed length scales better than the cases without wave groups (Figure 4.10b). However, when during these conditions the features are not removed sufficiently and there are few processes in the model with damping effects (as in NLW_{11}), the remaining features will continue to evolve and thus result in distinct features and a large level of nearshore variability in the final days of the evolution, that does not correspond with the observations (Figure 4.11a and d). When the model processes have too little amplifying effects, features will hardly evolve after the high-energy event (e.g. NA_{11}).

Other modelling studies mainly focussed on down-state transitions. The current work is, to the best of the authors' knowledge, the first hindcast study that includes both an up-state and a down-state transition. In the field, high energy events have been observed to reduce the alongshore variability. Subsequent moderate conditions result in an increase in variability. We found that the balance between processes is important to be able to hindcast this evolution. The difficulty is to match the morphological response both in magnitude and pace with the observed evolution during various energy levels. A model that is calibrated on a down-state evolution will not necessarily be able to hindcast an up-state evolution correctly as the balance between processes that result in increasing variability, will have to be different during an up-state transition in order to allow a decrease in variability. Hindcasting the current event requests that the model allows growth of features during lower wave energy conditions and diffusion or smearing of features during higher energy conditions. This requires the inclusion of process descriptions that depend on energy. In case the diffusive effects are too large, the high energy event may erode and diffuse all pre-existing features and no new rip channels will appear during subsequent lower energy conditions and the variability will remain low. In the opposite situation, if the diffusive effect is too small, pronounced features will appear, resulting in too much variability. With the subsequent higher energy conditions, these features will be reinforced by hydrodynamic feedback.

Our findings indicate the importance of the balance between processes with damping and amplifying effects, the initial bathymetry and the subsequent wave energy. We therefore tested the effect of damping and amplifying processes in the model (setting discussed below) by varying diffusion and amplification settings with respect to the *base*.

Effect of morphodynamic balance

The quality of a morphological hindcast is determined by how well the computed morphological evolution resembles the observed evolution. The computed morphological evolution therefore

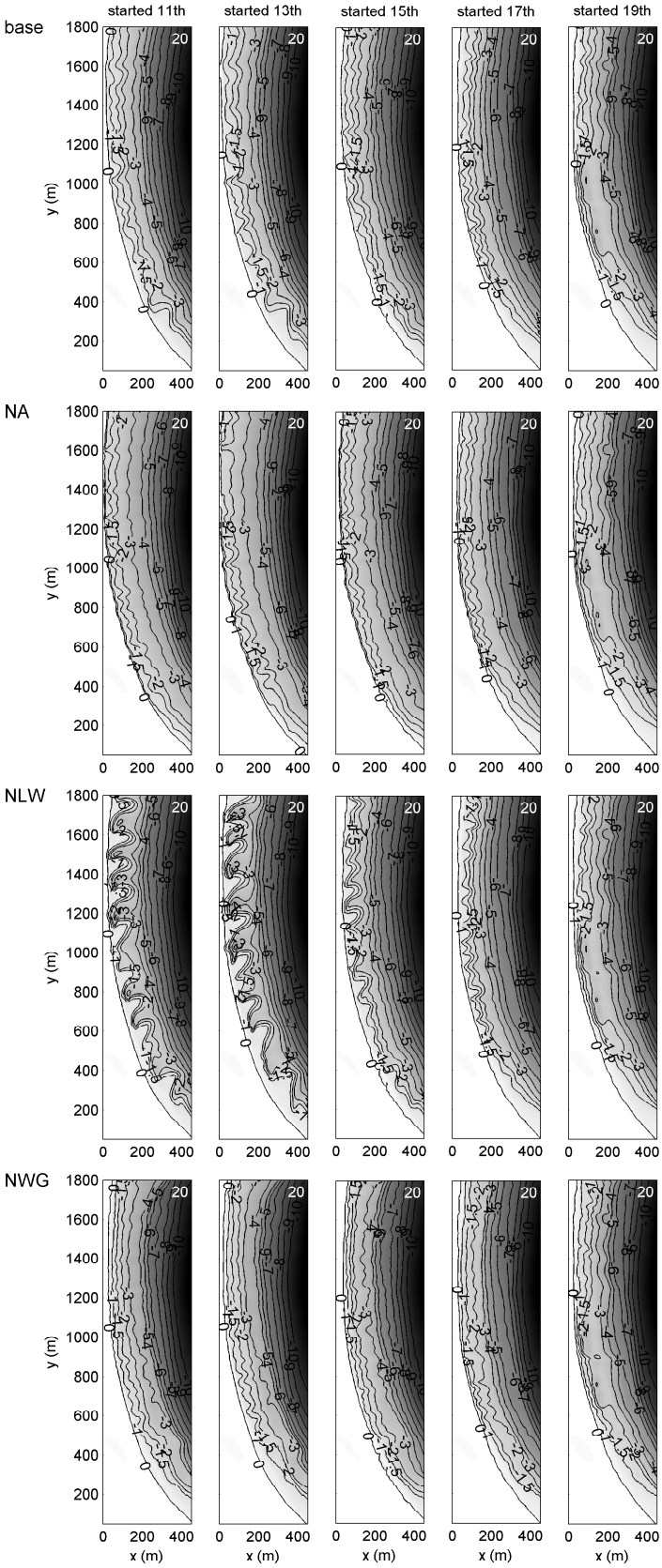

Figure 4.15: Bathymetries computed at July 20 1996, for 5 different morphological start dates (columns, indicated on top in days in July 1996) for 4 different settings (rows): *base*, NA, NLW, NWG.

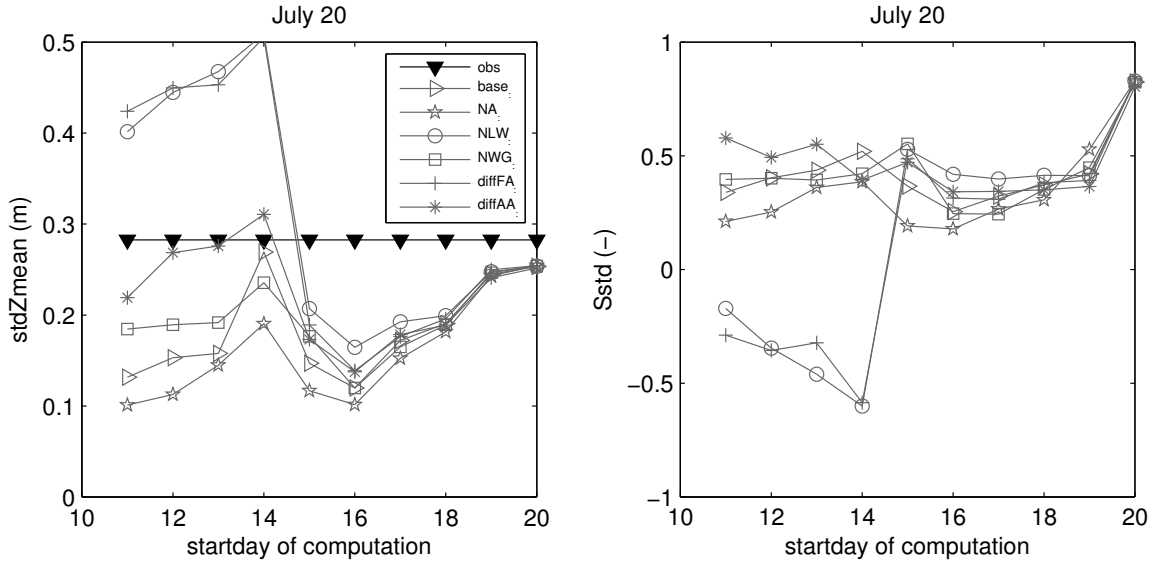

Figure 4.16: Mean alongshore variability *stdZmean* (left) and skill score for alongshore variability *Sstd* (right) at July 20 for *base*, NA, NLW, NWG, $diffFA$, $diffAA$ as a function of the startdate.

needs to be correct in both magnitude and pace of evolution. Specifically for an event with time-varying energy, this response needs to stay on track with the observed evolution in order to result in a best possible hindcast. It was found that the presence of and balance between processes with damping and amplifying effects (wave asymmetry, long wave induced stirring, wave groups) is crucial. These effects and the pace of evolution are also included in two parameters in the model, respectively $facvisc$ (Equation 4.10) and $ACAL$ (Equation 4.9). $facvisc$ linearly affects the amount of turbulent viscosity included in the modelled diffusion. Small $facvisc$ will result in smaller diffusion. $ACAL$ is a calibration parameter in the continuity equation which results in bed-level updating. The spatial sediment transport gradients are multiplied by the factor $ACAL$, thus directly affecting the bed level change due to continuity (i.e. no sediment will disappear). Large $ACAL$ will result in large changes. This section describes the effect of these two parameters on the morphological evolution, described in both the magnitude and pace of evolution.

Here we present the results of two settings used for computations for all start dates, varying either the $facvisc$ (computations $diffFA$) or the rate of change, $ACAL$ (computations $diffAA$) (Figure 4.18). $diffFA$ had lower $facvisc$ than in the *base* case (1 compared to 2.5), meaning there is less diffusion in the $diffFA$ computations. The $diffAA$ computations had a higher $ACAL$ setting (1.5 compared to 1 in the *base*-setting).

In the *base*, NA, NLW and NWG computations it was found that the observed increase of variability at the beginning and end of the morphological evolution was not reproduced by the model. When the diffusion is set 2.5 times lower than in the *base* computations, the computed evolutions vary significantly for different start dates (Figure 4.18a and 4.21). Com-

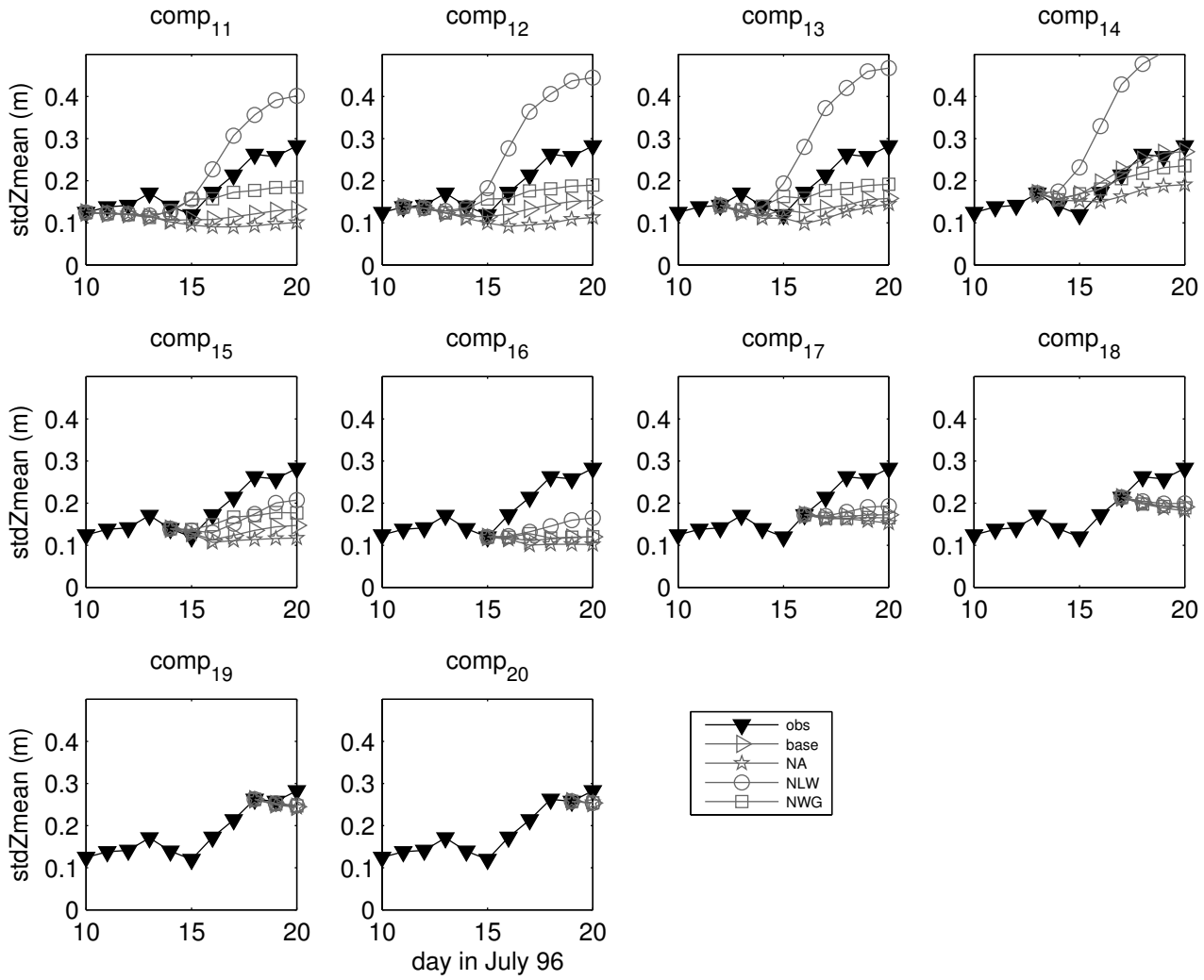

Figure 4.17: Evolution of the mean alongshore variability $stdZmean_{obs}$, $stdZmean_{base}$, $stdZmean_{NA}$, $stdZmean_{NLW}$, $stdZmean_{NWG}$ for different startdates ($\text{comp}_{11..20}$).

putations $diffFA$ develop large nearshore variability in the computations including the storm event (Figure 4.18a and 4.19a for $diffFA_{11}$). The computation starting July 11 still does not reproduce the observed initial increase in variability, though now it hardly decreases during the storm as seen in the previous computations. This results in a large increase in variability after the storm, seen as the evolution of distinct shore-attached features in the bathymetry (Figure 4.18a). When starting the computations just after the storm, the variability shows a small increase after a few days. The computations starting at July 18 and later show no change or even a decrease in variability. In these cases, smaller diffusion only seems to result in larger evolution of nearshore variability when the bathymetry already shows variability, combined with a high wave energy event.

$diffAA_{11}$ shows an initial decrease in variability and a post-storm increase in nearshore variability (Figure 4.19b). The bathymetrical patterns of the $diffAA$ and *base* computations with pre-storm start dates are similar, though for the $diffAA$ computations, the features are slightly further evolved (compare Figure 4.15a with Figure 4.18b), resulting in higher *stdZmean* values, matching better with the observations (Figure 4.21, panel 1-4). However, for both the *base* and $diffAA$ computations, the evolved patterns lack the observed nearshore trough (Figure 4.2, day 18-20).

For the $diffFA_{11}$ and $diffAA_{11}$ computation, $\overline{\lambda}_y(t)$ is similar to the evolution of the length scales of both the observations and $base_{11}$ during the pre-storm days, after the storm $\overline{\lambda}_y$ decreases rapidly (Figure 4.20).

For both cases we find computed variability to be higher than *stdZmean* in the *base*-case (Figure 4.21), especially for the computations including the high energy event. For the post-storm computations with lower energy, the different diffusion settings did not affect the *stdZmean* evolution, comparable to the results with different processes (Figure 4.17). These results indicate that a high energy event has large impact on *stdZmean*.

The response to the two different settings occurs at a different moment in time. With a lower $facvisc$, the $stdZmean_{diffFA,11}$ starts to increase on July 15. When $ACAL$ is increased, the evolution in $stdZmean_{diffAA,11}$ increases one day later: July 16 (Figure 4.21).

Various settings for $ACAL$ (0.25, 0.5, 0.75, 1, 1.25) and $facvisc$ (0, 1, 2, 2.5, 4, 5, 10) have been tested, aiming to obtain the correct balance in processes with amplifying and damping effects, matching with the concurrent hydrodynamic energy. Too high values for $ACAL$ (in combination with the concurrent energy) resulted in amplification of existing morphological features to for example shore-attached features that became more distinct than observed. Increasing values of $facvisc$ resulted in damping morphological processes, dissolving remaining features -especially during a high energy event- and prohibiting the appearance of new features during lower energy conditions. The settings of post-storm cases (not shown) where we calibrated the settings such that the computed post-storm evolution of the variability kept pace with the observed

evolution, resulted in a too distinct evolution with too high magnitudes when these settings were used for computations including the high-energy event. This indicates that either the currently used model does not incorporate all necessary processes to obtain the correct balance in amplifying and damping processes for both energetic and calm wave conditions or that the necessary processes are included, but that the correct balance was not within the tested range of parameter settings. Further the starting conditions and subsequent hydrodynamic conditions largely affect the computed evolution. When high energy conditions occur in the prediction period, different settings will then lead to largely different outcomes. Settings that work for a specific phase in the evolution, will not give the correct balance in a phase with other initial variability and other wave energy.

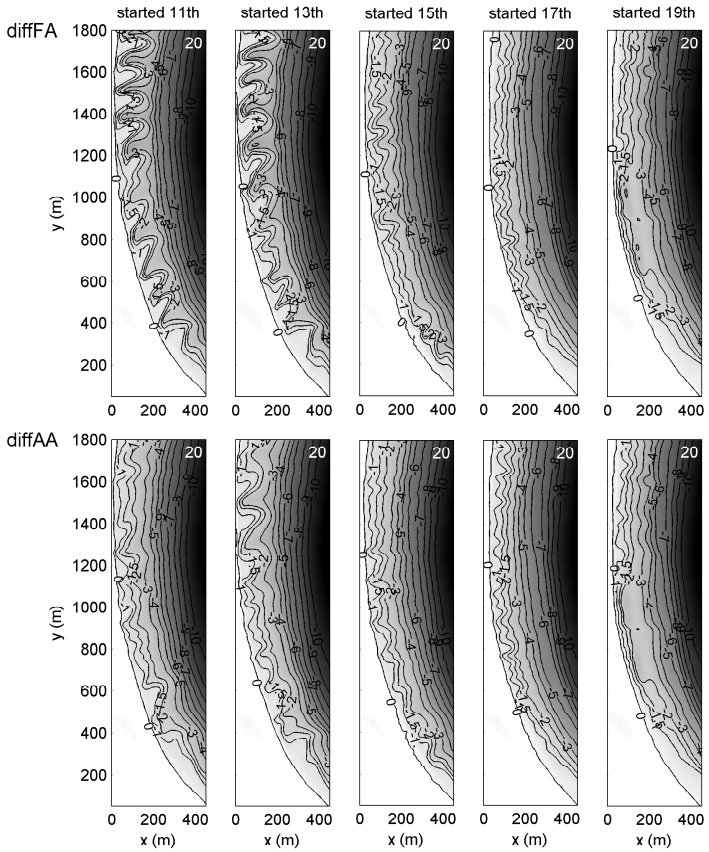

Figure 4.18: Each panel shows the bathymetry computed at July 20 1996, for 5 different computations, with each different morphological start dates (indicated on top in days in July 1996) for 2 different settings: a: $diffFA$, b: $diffAA$.

4.5 Discussion

Other morphodynamic modelling studies focussed on modelling idealized cases. Generally, the initial bathymetry would be alongshore uniform and downstate transitions would be analysed.

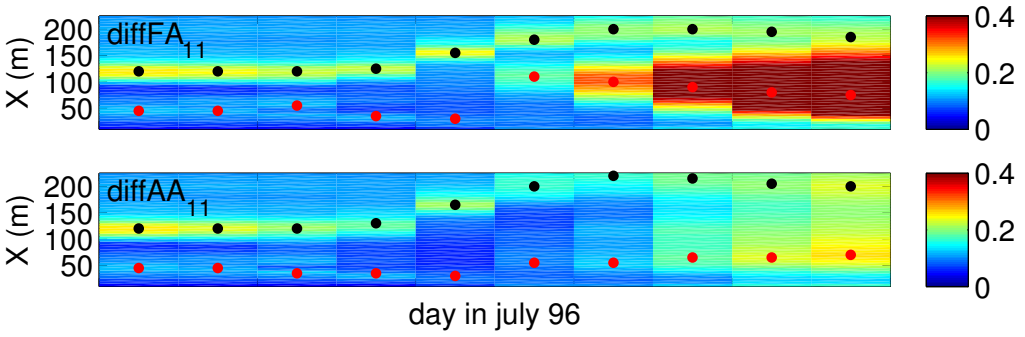

Figure 4.19: Alongshore variability a: $stdZ_{diffFA11}(x,t)$, b: $stdZ_{diffAA11}(x,t)$ with circles indicating the nearshore (red) and offshore (black) location with highest variability.

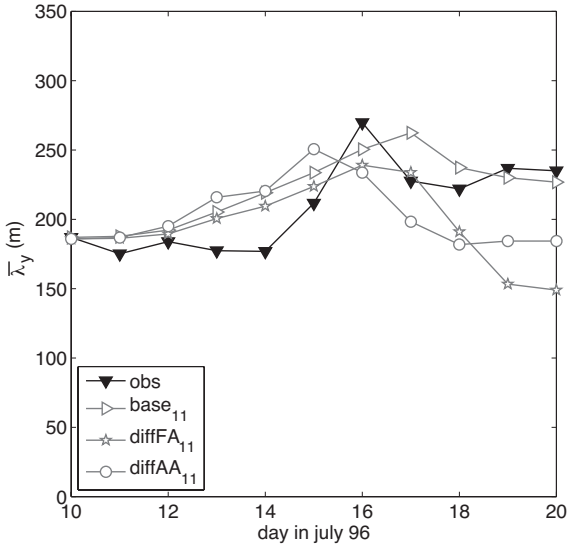

Figure 4.20: Evolution of length scales $\overline{\lambda}_{y,obs}(t)$, $\overline{\lambda}_{y,base11}(t)$, $\overline{\lambda}_{y,diffFA11}(t)$, $\overline{\lambda}_{y,diffAA11}(t)$.

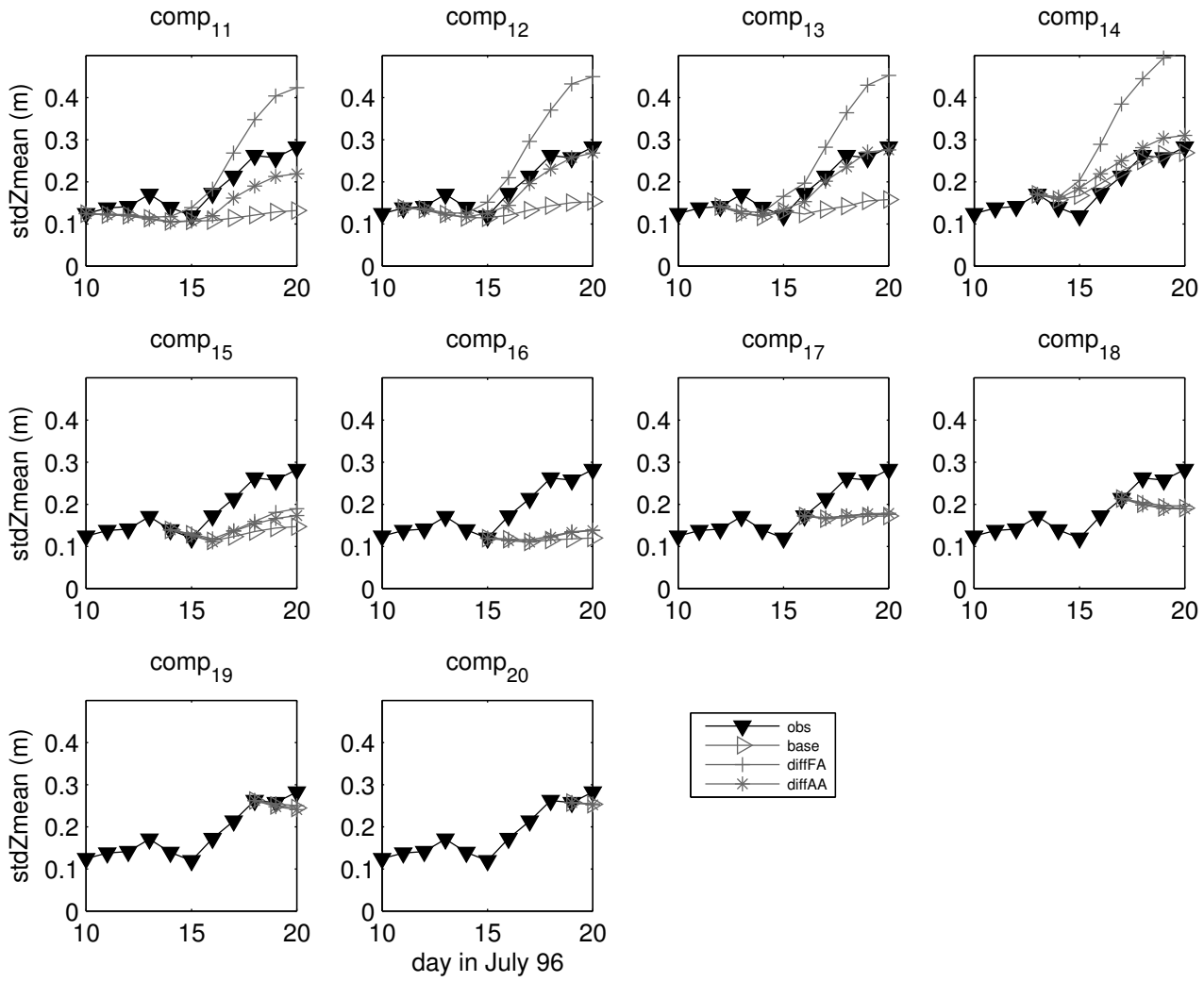

Figure 4.21: Evolution of mean alongshore variability $stdZmean_{obs}$, $stdZmean_{base}$, $stdZmean_{diffFA}$, $stdZmean_{diffAA}$ for different startdates ($\text{comp}_{11..20}$).

Some studies started with an idealized evolved bathymetry investigating the effect of antecedent morphology and the dominant morphological processes in the subsequent evolution (e.g. Ranasinghe et al., 2004; Castelle et al., 2005; Smit et al., 2005). In general, the applied conditions would be either constant or time-varying in an idealized way. In the current work, video-derived bathymetries have been used, forced with measured offshore wave conditions. The morphological results have been compared with observation-based bathymetries. Further, the chosen event encompassed both an upstate (reset-event) and downstate transition. The effect of the start date has been analysed by starting the computation at different moments in the evolution by using different initial bathymetries and the corresponding conditions. The aim was to find the required processes in the model to reproduce the observed behaviour, as well as to learn about the effect of the start configuration and the prediction horizon.

A concern in the analysis of our hindcasts is the error in the used data, specifically of the observation-based bathymetries. The data was used both as input for the model and for validation of the results. The exact magnitude of the error is unknown for this specific event and will be unknown in many cases due to the high costs associated with obtaining bathymetry data in the field. We accounted to the best of our knowledge for this problem by subtracting an observation error from the model error when computing the model skills. Hence, results that are within this error band are scored as perfect matches. Further, we focussed our analyses on the evolution of the variability as we expect the observation error of this parameter to be smaller than the error in parameters like $meanZ$. Another problem when quantifying the results of morphological model efforts is the often subjective parameters that are used, for example personal interpretations of dissipation patterns. We therefore defined objective parameters and used those for skill scores. We found that these parameters represent our subjective visual interpretations of the results in an objective way. We choose the mean cross shore profile, the alongshore length scales of the features and the variability of the bathymetry as the main parameters. In a prediction we would like to be able to forecast these parameters and accept that, due to the high sensitivity to small bathymetrical variations (which might be observation error induced) it will be hard to correctly predict locations of features evolving from a reset bathymetry.

The scores related to the mean profile decrease generally after the start of the computation. For the computations starting prior to the storm, the scores are minimal during the storm and increase after, indicating the model is not capable of reproducing the profile as observed during the storm. The best scores at the end of the evolution were for the computations without long wave induced stirring with pre-storm start dates, even though the variability scores for these computations were the lowest.

The *base* setting (including the effects of wave groups, wave asymmetry and long wave induced stirring), performed best on both the evolution of the length scale as well as the cross-shore location of the variability. Including all these effects resulted in evolution of variability which in

some cases matched the observations rather well, but in other cases rather poor, although not worse than the other settings when combined with the scoring on length scales and location of variability. The evolution of the length scales of alongshore features was best matched in the *base* case. When the effect of wave groups was excluded, the computed length scales dropped significantly, indicating the effect of the presence of wave groups. Reniers et al. (2004) indicated the importance of the spreading of the waves and the resulting length scales of the wave groups, affecting the length scales of the evolving morphology.

In general we found that the balance between the processes with damping and amplifying effects is crucial in reproducing the observed patterns. Sufficient diffusion is required during the high energy event to get rid of existing features and the diffusion needs to be small enough during the subsequent lower energy conditions to allow new features to evolve. The chosen definition relates the turbulence (and thus diffusion) with the roller energy. To allow for diffusion to adapt to the conditions, we improved the diffusion description by expressing it as a function of the local turbulence. During high energy events, there is more turbulence and thus more diffusion. With lower energy conditions, the turbulence reduces, hence the diffusion as well. However, with this description we could not reproduce the combination of same magnitude of observed increase in variability during the lower energy conditions (both prior and after the storm) and the decrease of variability during the storm. Trying different descriptions did not give a fully satisfying result. We hypothesize that the solution can be found in the description for the turbulence(/diffusion). However, more knowledge needs to be gained to be able to improve this description and relate it in the appropriate way to the local conditions. Other process-based model studies often opt for using a constant diffusion parameter (Smit et al., 2008, e.g.) or a depth-dependent value as in Drønen and Deigaard (2007) ($D = 100h^2$), which leads to much larger eddy diffusivity than in our model. The used values in our model for eddy diffusivity correspond quantitatively to the values suggested by Feddersen (2007).

We expect that improving the diffusion and turbulence description will enhance the capacity of the model to stay on track with the observed evolution throughout a reset-event, both the pace and the magnitude and thus increase the prediction horizon to match that of the wave conditions. A diffusion description which is stronger non-linearly related to the incoming wave energy is expected to give better results than the currently used description. With a more non-linear relationship, the diffusion will be more amplified during higher energy conditions and due to less diffusion during lower energy conditions, the growth of new features will be possible.

With the current model settings, data assimilation with observation-based bathymetries will force the model to keep pace with the observed morphological evolution. It would then be recommended to add observation based data at a frequency of around three days, depending on the conditions. In the first three days of the computations, the different settings only resulted in different evolutions if the storm was included in this period.

4.6 Conclusions

This paper investigated whether we could predict both up-state and down-state transitions on a natural beach. The used 2DH process-based model includes roller energy, wave asymmetry, long wave induced sediment stirring, wave groups and turbulence dependent diffusion affecting the total balance between damping and amplifying processes. We found that the model is capable of hindcasting the different transitions to a certain extent. The up-state transition (decreasing variability) is only possible when there is enough diffusion (damping processes) in the model. However, if there is too much diffusion during subsequent lower-energy conditions and the effect of amplifying processes too small, no new features will emerge and the downstate evolution will not be hindcasted properly. If there are not enough damping processes in the model and too many features remain during the high energy event, these will grow and cause larger variability than observed during the subsequent down-state transition.

The observed event showed an increase in variability in the first few days of the evolution. During the high energy conditions, the variability decreased. During the subsequent lower energy conditions, the variability increased in the nearshore area (smaller than 1 m deep) and the offshore area, just offshore of the new bar location. None of the computations reproduced the observed increasing variability in the first three days of the evolution. The observed decrease in alongshore variability during the high energy event was reproduced (resulting in increased $Sstd$ for those computations) by all but the computations without wave groups. After the storm event, the only computations where the variability was continuously increasing, were the computations without the effect of long wave induced stirring. However, this variability increased too far, resulting in too distinctly evolved nearshore attached features. For the other computations the nearshore variability remained the same or even decreased. In general, during the first three days of a computation, different settings only resulted in a different evolution if the storm was included in this period.

The evolution of the length scales of alongshore features was best matched in the case including all mentioned processes. When the effect of wave groups was excluded, the computed length scales dropped significantly, indicating the effect of the presence of wave groups on the evolution of nearshore features.

When there is small initial variability, the relative error in this bathymetry may be large. Combining this with the large sensitivity to small variations, it is likely that computations with larger initial variability will result in better matching of the observed evolution.

It is important to realize that if a model would have been morphologically calibrated for a certain transition, the same settings might not give as accurate results for a different type of transition.

With the current model we are not capable of following the pace and magnitude of evolution for different levels of hydrodynamic energy within one computation. Improving the balance

between amplifying and damping processes for both high and low wave energy is expected to improve the models capacities. It is expected that improving the diffusion and related turbulence description will improve this balance and thus increase the prediction horizon to match that of the wave conditions.

In general the hindcast results may be perceived as quite good. Users of morphological models should be aware that hydrodynamic calibration is no guarantee for morphologically correct predictions. A hydrodynamically calibrated model may give highly variable outcomes for morphological computations, depending on the chosen process settings and calibration parameter values. Morphological models should therefore always be calibrated morphologically as well as hydrodynamically. The used model is capable of modelling down-state transitions and one-state upstate transitions to some extent. As reset-events are found to occur infrequently, the model is expected to be capable of hindcasting most observations of several days length. Further, it has been found (Smit et al., tiona) that above a certain level of morphological variability, the bar system will not change pattern anymore unless a reset-event occurs. As nearshore bathymetries generally have a reasonable amount of variability, it is expected that downstate evolutions can be modelled and predicted reasonably well, certainly within a period of 3-5 days which generally equals the window of a reasonable level of certainty for wave predictions.

Acknowledgements

The research was funded by the Dr. Ir. Lely foundation and the ONR-funded Beach Wizard project (N000140510266). AR was funded by NWO under contract DCB 5856. We thank Deltares (formerly known as WL Delft Hydraulics) for providing us with their Delft3D software. We would like to thank CSIRO Marine and Atmospheric Research, Perth, WA, Australia for their hospitality. Devin Koepl from Oregon State University, thank you for providing us with the necessary Argus images.

Chapter 5

Synthesis

Text contains excerpts from Smit et al. (2007).

5.1 Introduction

Nearshore sandbar morphology has been observed to vary in time. Different morphologic patterns affect the way offshore waves will transform when approaching the coast and will thus affect local flows and subsequently, via a feedback mechanism, affect the local morphology and thus the spatial distribution and volume of sand in front of the coast. Different processes have been attributed a role in the formation of the observed templates/patterns (e.g. wave height, wave groups, antecedent morphology). Their formation and evolution is however not yet fully understood.

Knowledge of the coastal zone is important for coastal defense of the hinterland area as well as for a safe use of the nearshore zone (e.g. for recreational purposes). Beach and nearshore nourishments, for example, are often found to adapt to the longer-term profile shape in a matter of weeks but may show unexpected behaviour that could pose temporary local erosion problems (e.g. Wijnberg et al., 2006). Rip currents may even develop within days. Effective management of a variety of coastal functions thus demands a sound understanding of the complex morphological behaviour of coastal systems, long-term coastal monitoring strategies with high resolution in time and space and predictive skills to assess the future impact of coastal interventions.

When nearshore sandbars lose their alongshore uniformity, they often display crescent-(moon) like shapes. Nearshore bars discussed here occur in the surf zone: in water depths from 0 to about 6 m and offshore distances up to a few hundreds of meters. They are observed at both straight and pocket beaches, occurring as single or multiple bars. Crescentic bars show an alongshore sequence of shoals and cross-shore troughs. In these troughs, off-shore directed rip currents generally occur. Under high energy conditions, these shoals have been observed to connect, while rip channels disappear and the bar becomes alongshore uniform (a reset-event).

With subsequent lower energy conditions, rip channels reappear and the bar moves shoreward, ultimately welding to the shore through a number of beach states as defined by Wright and Short (1984), a downstate evolution. They based their analysis on the observed behaviour at various Australian beaches. Lippmann and Holman (1990) extended the work by Wright and Short (1984) by distinguishing two additional classes. They defined a sequence of eight beach states, based on four characteristics of the morphology (existence or absence of a bar, dominant bar scaling, longshore variability and trough). They based their analysis on a two year data-set of video images of Duck, North Carolina, USA. Sequences of beach states have been observed and analysed at other beaches like Palm Beach, New South Wales, Australia (Holman et al., 2006) (for example Figure 5.1), the Goldcoast, Queensland, Australia (Turner et al., 2007) and Miyazaki (e.g. Van Enckevort et al., 2004). At other sites the observed patterns are found to be more robust to changing hydrodynamic conditions, for example at Noordwijk, The Netherlands (Van Enckevort et al., 2004).

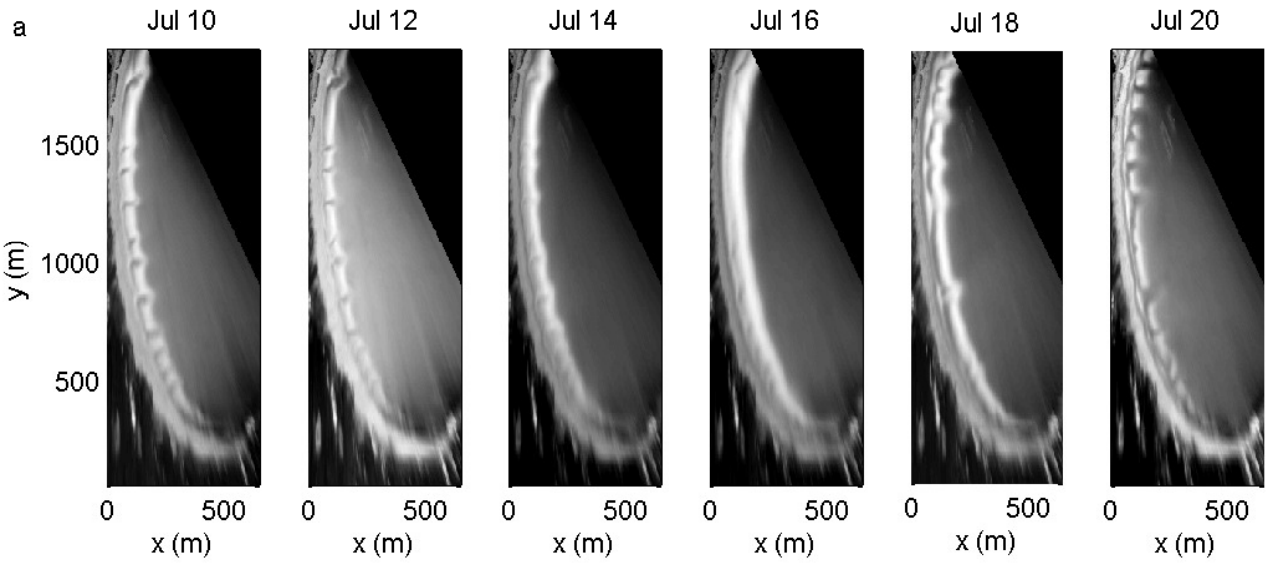

Figure 5.1: Example of observed morphological evolution in July 1996 at Palm Beach, New South Wales, Australia. Time-exposure video-images illustrating the dissipation patterns.

Understanding the observed behaviour has been approached in various ways. All approaches are based on the assumption that the system responds to hydrodynamic forcing. It has indeed been observed that when hydrodynamic conditions change, the crescentic bars respond. However, this response is not always instantaneously, meaning that the evolving length scales do not immediately or even after a long time span match the length scales of the forcing. Stive and Reniers (2003) distinguish three types of response. A main distinction is whether the system is deterministically forced (observed length scales correspond to length scales in the forcing) or whether the system is deterministically chaotic (i.e. the observed length scales correspond with the inherent length scales of the forcing processes and the length scales of the self-organisational processes are predictable). Another possibility would be that the system is

stochastically chaotic. Stochastic refers to the stochastic nature of the **history** of forcing conditions. If a system would respond in a stochastic chaotic manner, the response is determined by a mix of the antecedent and concurrent conditions (which are chaotic by nature) and properties of the system. In case a system would be deterministically forced by the incident waves, the arising length scales would be in the order of 25-100 m, corresponding to length scales of incident waves in shallow water. Though short rip channel distances have been observed, crescentic bars generally have spacings in the order of hundreds of meters, indicating that the response is not deterministically forced and that a chaotic type of response is having a dominant effect in the nearshore evolution. One explanation of rip channel spacings being deterministically forced would be the forcing due to edge waves (e.g. Bowen and Inman, 1971; Holman and Bowen, 1982). However, later work could not verify these relationships (e.g. Caballeria et al., 2002; Reniers et al., 2004).

However, from existing literature it is undecided whether the responses are actually deterministic chaotic or stochastic chaotic. Different views on the type of response have led to a variety of hypotheses explaining nearshore bar behaviour. One approach is attempting to directly link observed spacing with the concurrent conditions, presuming the system responds either deterministically forced or deterministically chaotic to the offshore wave conditions.

This Synthesis first further elaborates on the different views on understanding nearshore bar behaviour, followed by the research questions addressed in this thesis. The answers found are summarized, the 4th section describes the conclusions, followed by a discussion and recommendations.

5.2 Observation and model based explanations of nearshore bar behaviour

Wright and Short (1984) combine incoming energy with the type of coast (reflective to dissipative), to explain whether the response will be slow (low energy, reflective) or fast (high energy, dissipative coast) and whether erosion or accretion will occur. Further, they define a down-state sequence of six beach states ranging from dissipative to reflective passing through alongshore bar-trough, rhythmic bar and beach, transverse bar and rip, ridge runnel or low tide terrace states. They found that beaches reshape into the next down-state template under moderate conditions. With a high energy event, the system may be pushed up-state, possibly jumping up more than one state at once. The work by Wright and Short (1984) was extended by Lippmann and Holman (1990) by adding two classes. They distinguished eight classes, using four characterizations of the morphology. They analysed a two year video-based dataset using the beach class model. Lippmann and Holman (1990) came to similar conclusions on nearshore behaviour as Wright and Short (1984). Further, they added that down-state transitions seem more morphologically controlled and up-state transitions seem more hydrodynamically controlled.

5.2.1 Observation based analysis of rip locations and hydrodynamic conditions

The appearing rip channel distances have a high level of rhythmicity, though distances seem to vary at different beaches. Van Enckevort et al. (2004) analyzed video observations collected at four barred sites (two single barred and two double barred sites). Their analysis shows that crescentic sandbar wavelength and cross-shore amplitude variations over space and time are very common. Wavelengths of the shortest and longest crescent at any moment in time could differ by a factor of two. The crescents showed to merge and split, resulting in length scales that vary in time. They observed different response times at the different sites, leading to the hypothesis that the volume of the bars plays a role in the response times of the system.

Holman et al. (2006) analysed four years of high resolution (both in time and space) video data from Palm Beach, New South Wales, Australia. Palm Beach is a pocket beach of around 2 km length, with a single bar, which template is highly variable in time. They used the video-based dissipation patterns as an estimate for the bar location and indicated rip locations on these images. Analysing these rip locations over time allowed an analysis of spacings, persistence and location preferences of these rip channels and an analysis of combining these with hydrodynamic conditions. The rip spacing had a lognormal distribution with a mean spacing of 178 m. However, due to the high alongshore variability of the spacing, time mean of the standard deviation/longshore mean of rip spacing was 39 %, therefore possibly disqualifying this variable as an appropriate and reliable variable to compare observed with predicted length scales. Their main conclusion was that the length scales could not be matched with concurrent conditions. Further, according to Holman et al. (2006), occurrence statistics 'showed no evidence of the preferred location pattern associated with standing edge waves trapped in an embayed beach'. Next, throughout this four year observation period around 15 reset-events (the system returning to a longshore uniform bar-trough configuration under the influence of high wave energy) were observed, spanning around 8 % of the observation period. In many model approaches (both 2DH and linear stability analysis (LSA)), the behaviour of nearshore systems starting from a reset-situation is analysed. It is therefore necessary to bear in mind that these events occur rarely and that on average the nearshore bar template is often an evolved beach state. We therefore need to understand the role of the antecedent morphology and how a nearshore bar system subsequently evolves in response to new hydrodynamic conditions while already having an evolved beach state (as a result of responding to antecedent hydrodynamic conditions).

Turner et al. (2007) analysed the behaviour of a 2km stretch of a long, straight beach at the Goldcoast, Queensland, Australia in a way similar to Holman et al. (2006), using three years of video-based data. Their findings were similar, though the mean rip spacings were slightly different. They also found no tendency for preferred rip locations alongshore following storm reset events. The alongshore spacing varied similarly. Further, they found no clear relationship between 'the number of rips and prevailing offshore wave conditions, including significant wave height, peak wave period and incident wave power'. Based on these findings they state that 'rips

may become rapidly topographically controlled soon after a reset event, and their location is then primarily determined by the evolving nearshore morphology, rather than the hydrodynamic forcing.' Their findings reinforce the need to investigate the role of the antecedent bathymetry in the response to hydrodynamic conditions.

5.2.2 Analysis of trends in length scales and responses using LSA and other models

Several efforts have been made to link bar behaviour with either hydrodynamic conditions or bar geometry using both linear stability analyses (LSA) and depth-averaged (2DH) process-based models. Studies of single barred systems based on linear stability analyses showed for example that for obliquely incident waves, the length scales increase with increasing trough area and increasing alongshore current velocities (Deigaard et al., 1999). For shore normal incident waves Damgaard et al. (2002) found that the length scales remained unchanged with increasing wave height, only the growth rate increased, whereas Calvete et al. (2007) found increasing length scales for increasing wave heights. In addition, Calvete et al. (2007) point out that slight variations in the characteristics of cross-shore depth profiles, such as water depth above the crest, rather than the offshore wave conditions can be more important for rip channel spacing.

An advantage of 2DH morphodynamic models over linear stability analysis is that they allow for temporal and alongshore variations in crescent lengths and for finite amplitude effects (e.g. Damgaard et al., 2002; Reniers et al., 2004; Smit et al., 2004). This is consistent with Van Enckevort et al. (2004) who observed variations in the field up to a factor 2 in the wavelength and amplitude of individual crescents at any moment in time. The modelling study by Reniers et al. (2004) for example, predicts a variation which agrees with the measurements presented by Holman et al. (2006). Klein and Schuttelaars (2006), who investigated the morphodynamic evolution of double barred beaches for both the linear and non-linear regime, found that the spacings predicted with the linear stability analysis are only observed during the exponential growth phase of the non-linear experiments. In the dynamic phase, multiple modes span the bed features.

LSA only allows the exploration of the initial growth of features, it does allow the analysis of trends in the initial growth phase in a very time efficient manner as computations with process-based models are usually time-expensive.

When modelling nearshore bar behaviour on a longer term, process-based modelling may lead to an accumulation of small errors and thus the prediction will quickly deviate from the reality. For understanding longer term behaviour, more aggregated models are often used. Pape et al. (subm) predicted cross-shore bar migration using a more aggregated model based on wave heights. They conclude from their model hindcasts, that the main aspect of long-term cross-shore sandbar behaviour can be described by migration toward a wave height dependent

equilibrium location. Further, they conjecture that 'the development of alongshore variability is not limited to moderate wave height conditions, but is the result of out-of-equilibrium cross-shore states that are most common during those conditions'. Furthermore, alongshore variability could not be predicted as well as cross-shore bar location with an aggregated model (Splinter, 2009).

5.2.3 Findings on the role of wave groups and edge waves on length scales

Wind-driven short waves travel in wave trains creating a bound a long wave. This results in water level set-down at the location of the highest short waves. In the nearshore zone this water level set-down, under the wave group crest, results in offshore directed currents. The high short waves at these locations stir up the sediment, which is then transported offshore due to the bound infragravity wave induced current, resulting in net offshore transport. In the nearshore zone the long waves refract due to the morphology and as a result may become trapped in the nearshore region, thereby creating standing edge waves. It has been hypothesized that these standing edge waves are the mechanism that leads to crescentic bar patterns and that determine their length scales (e.g. Bowen and Inman, 1971; Holman and Bowen, 1982). However, the drift velocities due to these standing edge waves are rarely expected to have a significant impact as 1: the drift velocities are small compared to the velocities associated with the wave orbital motions and mean currents; 2: the infragravity wave spectrum would be required to be narrow, which is rarely found in nature; 3: this theory presumes a deterministic forced response of the nearshore system to the hydrodynamic forcing, whereas feedback between hydrodynamic and morphological processes is much more likely because of the role of bathymetrical features in hydrodynamic patterns. In the process-based modelling work by Damgaard et al. (e.g. 2002), crescentic patterns evolved, even though wave groups were not included in the model. Crescentic patterns are found to evolve as a result of morphological feedback between small alongshore variations in either the hydrodynamics or the bathymetry and the hydrodynamics. In the case of process-based modelling, the variations can also be triggered by unavoidable numerical inaccuracies. Reniers et al. (2004) included wave groups in their 2DH process-based model and analysed the evolution of an initially alongshore uniform barred beach and the formation of crescents on a single barred beach. They found that without directional spreading, evolution of the nearshore bathymetry into quasi-rhythmic patterns occurs, indicating a self-organised response due to morphodynamic feedback. This corresponds with the findings by Caballeria et al. (e.g. 2002) who stated that edge waves were not necessary to generate growing features. Next, Reniers et al. (2004) found that infragravity waves play a role in the transport of sediment and the main contribution in the analysed cases was smoothing of the resulting bathymetrical features. Next, the spreading of the waves (when included), affects the spacing of the rips, indicating a quasi-forced response as the spreading was not necessary in order to obtain crescentic patterns. Further they conclude that the observed coupling between edge waves and the final complex beach topography is a result of the underlying bathymetry and not the other

way round. In contrast, Aagaard and Greenwood (2008) found standing edge waves playing a role in the morphological evolution by acting as a mechanism to advect the sediment that was stirred up by the wave orbital motions of the incident short waves.

5.2.4 State of numerical morphodynamic modelling

In order to use a numerical model to improve our understanding of the nearshore zone, a model that allows morphological feedback is required. Linear stability analyses only allow the analysis of the initial formation of nearshore patterns and their length scales and growth rates and do not allow to explore the continued morphological evolution. To model and analyse this evolution in all its aspects therefore requires a process-based model. Several studies have used various numerical models which included/excluded certain processes.

To be able to hindcast an observed morphological evolution, the model needs to reproduce the morphological evolution at the correct pace as well as reproduce features with correct characteristics (e.g. spacings and locations). It is found that depth-averaged (2DH) process-based models can reproduce crescentic patterns in down-state transitions with spatial patterns, scales and variability similar to those observed in the field (e.g. Damgaard et al., 2002; Drønen and Deigaard, 2007; Smit et al., 2008). Ranasinghe et al. (2004) used a depth-averaged process-based model to simulate two down-state transitions, starting with idealized observation-based initial bathymetries and comparing with observed video-images of dissipation. They forced the bathymetry with constant wave conditions toward a new state. They conclude that the transitions were governed by the initial geometry and subsequent rip circulation of the changing hydrodynamic conditions. Castelle et al. (2006) used a 2DH process-based model including the effects of undertow to investigate crescentic pattern development of nearshore bars. Their results show that circulation eddies combined with (small) bathymetrical variability are a key component in the morphological evolution of crescentic patterns. They conclude that self-organisation can lead to the development of such patterns. These studies focussed on understanding the morphodynamic response to hydrodynamic forcing by analysing the hydrodynamics and the geometrical features of the system. Only few studies analysed the role of the modeled process descriptions. Klein and Schuttelaars (2005) found for bars evolving from an initially planar sloping beach, that both length scales and orientations of the developing bars were sensitive to the chosen transport formulation. Very few modelling efforts concern hindcasts of observed nearshore bar behaviour. Grunnet et al. (2004) modelled the observed behaviour of a shoreface nourishment with a 3D model. They concluded that the model was capable of reproducing the observed profile development reasonably well for large spatio-temporal scales (kilometers and months). However, detailed morphodynamic predictions on the scale of sandbar behaviour did not perform as well. Predictions of the nearshore bar migration and development remained poor and bar flattening was found to be the general outcome. They suggest that including a phase lag between sediment transport and bathymetry (e.g. by adding a surface roller model)

is essential for bar survival. Reniers et al. (2004) found that the spreading of the wave groups affected the length scales evolving at a nearshore bathymetry. Including both these processes (roller effects and wave groups) will therefore lead to process descriptions that better represent the processes in the field and are therefore expected to have a positive contribution toward the quality of the hindcast.

5.3 Research questions

The main research question addressed in this thesis is:

Why does an observed nearshore bar pattern look the way it does?

We hypothesized that the response of a nearshore bar system is a function of both the hydrodynamics and the concurrent morphology. In fact we would like to know when precisely the observed pattern is a function of the concurrent hydrodynamic conditions or the antecedent bathymetry or a mix thereof.

The main question is split into three subquestions:

- How would a nearshore bar system evolve if it would have a constant forcing and an initially alongshore uniform profile?
  - what is the role of the concurrent hydrodynamic conditions?
  - what is the role of the geometry?
- What is the role of the antecedent morphology?
- Which processes are dominant in creating the observed patterns?

The following describes the findings in this thesis, related to the questions stated above.

5.4 This thesis

Numerical computations of the morphologial evolution of nearshore bar systems were performed using a depth-averaged process-based model. The morphological response -or lack thereof- to various constant wave conditions and time-varying wave conditions were tested using various initial bathymetries. Another set of computations aimed to hindcast an observed morphological evolution. In this case, the effect of various processes and the effect of the duration of the hindcast were tested. The results were analysed using the evolving variability of the bathymetry, the alongshore length scales of the features and the response time of the evolution.

5.4.1 System's intention

The intention of the system is the response the system would show if it would have a constant forcing and no morphologically induced restrictions, other than those due to the initially alongshore uniform profile. The current work finds that an initially alongshore uniform double barred beach responds distinctly different to different hydrodynamic conditions. This leads to the conclusion that a system responds to hydrodynamic conditions and that its response can not be purely attributed to the systems initial geometry. We used a process-based model to compute the morphological evolution as a response to two weeks of constant wave conditions. The evolution showed alongshore variable distances between rip channels, similar to observations in the field (e.g. Van Enckevort et al., 2004). The weighted length scale as a result of different forcings showed clear trends of increasing length scales for increasing alongshore currents (either due to more oblique waves or due to higher waves) and increasing depths. The length scales ranged from 300-700 m for the inner bar, and from 600-2000 m for the outer bar. The length scales are thus a function of both the geometry and the hydrodynamic conditions.

The initial bathymetry was perturbed with a random seed (order cm). Analysing computations with 5 different random seedings showed that the different seedings do not alter the mean length scales, but they do alter the location of the rip channels and evolving features. The rip channel location seems therefore to be determined by the antecedent morphology.

The response time of the system was in the order of days and found to depend linearly on the local wave height, the alongshore current, the steepness of the bar and inversely on the active volume of the bar. The results of the model computations agreed with the hypothesis that smaller bar volumes respond more rapid (Van Enckevort et al., 2004). The response time of the system is determined by both the nearshore geometry and the local hydrodynamics. The latter are a function of both the offshore wave conditions, geometry and the nearshore hydrodynamic processes. A nearshore bar system may not always evolve toward new conditions as conditions may not last long enough to allow the system to change (related to the response time of the system).

Similar types of analyses on trends in length scales as a function of wave height, or geometry, have been done by others using LSA or process-based models. Generally, these encompassed only oblique waves, only shore normal waves, or single barred beaches. Due to the sensitivity of the quantitative values to the local geometry, it is hard to compare the works quantitatively as the used cross profiles used are different. The current work adds analysis of a series of conditions ranging from shore normal to oblique and from small offshore wave heights to larger wave heights.

5.4.2 Role of antecedent bathymetry

To investigate the role of the antecedent morphology, the effect of the initial level of variability in the morphology was tested. Different bathymetries with increasing levels of morphological variability were tested with identical offshore wave forcing. The resulting nearshore hydrodynamic patterns prohibited adaptation toward the new wave conditions of bathymetries with a high level of initial variability, due to the differences in nearshore morphology (e.g. deeper rips). Computations with increasing level of initial morphological variability showed decreasing levels of adaptability when different hydrodynamic conditions forced the system.

This shows that, even if the new conditions would remain for an extended period of time, the bathymetry may not adjust toward these new conditions. Whether a system responds to a new condition, turns out not only to depend on the response time, but also on the antecedent morphology.

A morphology with a deeply imprinted pattern turns out to have a lasting effect on the hydrodynamic patterns, the circulation cells will remain even if offshore wave conditions change significantly and thus the morphology will remain unchanged. If the morphology has more shallow variations, different hydrodynamic conditions may lead to a changed hydrodynamic pattern, allowing the morphology to change.

This may explain why in the work of both Holman et al. (2006) and Turner et al. (2007) observed patterns could not be matched with hydrodynamic conditions for long time periods. There are in fact three reasons. First, in case the level of nearshore variability is high, it prohibits the adaptation to new hydrodynamic conditions. Second, for the post-storm events (in cases that the variability was in fact low enough), the response time and short duration of post-storm conditions may prevent the observed pattern to match the expected pattern. Third, whether the bathymetrical variability is actually really low enough may not always be completely visible during higher energy events (due to wide band of breaking waves) and the overly calm post-storm conditions when no dissipation patterns are visible. Our findings agree with work by Huntley and Coco (2009), who investigated the behaviour of patterns in small bedforms using abstracted models. They found that the initial state of the seabed has a profound influence on the rate at which the bed responds to new conditions. Also they found that new bedforms can only grow after existing variability has decreased.

5.4.3 Role of different processes

Work by others showed that accounting for short waves only, does not fully represent the nearshore hydrodynamics and including wave group effects had been found to affect the length scales. To test how well we could hindcast an observed reset-event, we therefore used a process-based model that could include the effects of wave groups. Further, the model included a surface roller model which accounts for the phase lag between sediment transport and bathymetry. Next,

wave asymmetry and long wave induced stirring was included and their effects investigated. Finally, the effect of smaller diffusion and of larger adaptation rates was tested.

A hindcast was performed of a ten day morphological evolution including both up-state and down-state transitions.

All of the included processes showed to affect the total balance between damping and amplifying processes and therefore the pace and magnitude of morphological evolution.

Excluding wave asymmetry results in a steeper profile near the shoreline and a lack of emergence of new features after the high energy event. Excluding long wave-induced sediment stirring leads to the evolution of distinct and pronounced shore-attached features, with significantly higher nearshore variability and shorter length scales. Excluding wave group effects, leads to increased nearshore variability with shorter length scales located at the outer surf zone. Reduced wave breaking induced turbulence effects, leads to significant nearshore variability in the inner surf zone with shorter length scales, whereas increased turbulence effects inhibit the evolution of nearshore variability.

We found that the used model is capable of hindcasting the different transitions to a certain extent. The up-state transition (decreasing variability) is only possible when there is enough diffusion (processes with damping effects) in the model. However, if there is too much diffusion during subsequent lower-energy conditions and the effect of amplifying processes too small, no new features will emerge and the downstate evolution will not be hindcasted properly. If there are not enough damping processes in the model and too many features remain during the high energy event, these will grow and cause larger variability than observed during the subsequent down-state transition.

When there is small initial variability, the relative error in this bathymetry may be large. Combining this with the large sensitivity to small variations, it is likely that computations with larger initial variability will result in better matching of the observed evolution.

It is important to realize that if a model would have been morphologically calibrated for a certain transition, the same settings might not give as accurate results for a different type of transition.

With the current model we are not capable of following the pace and magnitude of evolution for different levels of hydrodynamic energy within one computation. Improving the balance between amplifying and damping processes for both high and low wave energy is expected to improve the model's prediction capacities. It is expected that improving the diffusion and related turbulence description will improve this balance, thus enhancing the capability of the model to stay on track with the observed evolution throughout a reset-event, both the pace and the magnitude of evolution. This will increase the prediction horizon to match that of the wave conditions.

However, more knowledge needs to be gained to be able to improve this description and relate it in the appropriate way to the local conditions. Other process-based model studies often opt for using a constant diffusion parameter (as used in Chapter 2 and 3 e.g. Smit et al., 2008) or a depth-dependent value as in (Drønen and Deigaard, 2007) ($D = 100h^2$), which leads to much larger eddy diffusivity than in our model. The used values in our model for eddy diffusivity correspond quantitatively to the values suggested by Feddersen (2007).

A diffusion description which is stronger non-linearly related to the incoming wave energy is expected to give better results than the currently used description. With a more non-linear relationship, the diffusion will be more amplified during higher energy conditions and due to less diffusion during lower energy conditions, enabling the growth of new post-reset features.

Conclusions on hindcast quality i.e. model performance

In general the hindcast results may be perceived as quite good. Users of morphological models should be aware that hydrodynamic calibration is no guarantee for a morphologically correct prediction. A hydrodynamically calibrated model may give highly variable outcomes for morphological computations, depending on the chosen process settings and calibration parameter values. Morphological models should therefore always be calibrated morphologically as well as hydrodynamically. The used model is capable of modelling down-state transitions and one-state upstate transitions to some extent. As reset-events are found to occur infrequently, the model is expected to be capable of hindcasting most observations of several days length. Further, it was found that above a certain level of morphological variability, the bar system will not change pattern anymore unless a reset-event occurs. As nearshore bathymetries generally have a reasonable amount of variability, it is expected that downstate evolutions can be modelled and predicted reasonably well, certainly within a period of 3-5 days -and longer for nearshore systems with a large response time- which generally equals the window of a reasonable level of certainty for wave predictions.

5.5 Conclusions

5.5.1 Research answers

The main research question was: Why does an observed nearshore bar pattern look the way it does? This question was split into three subquestions, which are answered below, followed by answering the main question.

What is the intention of the system?

The intention of the system -when evolving from a reset-morphology- is a function of the local alongshore current and the depth, the latter related to the momentum associated with the

alongshore current. The response times of the modeled system decrease with increasing local alongshore velocities and wave heights (i.e. faster response). When the active volume of the bars, which depends on the breaker index, increases, the bar responds more rapidly. The response times are generally larger than storm durations. Our computations confirm the hypothesis of Van Enckevort et al. (2004) that bar systems with smaller bar volumes show a more rapid response than bar systems with larger volumes. This faster response is due to the steeper active volume of the bar with the smaller volume.

What is the role of the antecedent morphology?

Different initial perturbations (order of cm) do not alter the overall trends in length scales and response times, however they do cause features to evolve at different locations, demonstrating the high level of sensitivity of the evolving bathymetry to the initial conditions. Computations with bathymetries with different levels of variability showed that small or no morphological variability on a nearshore bar system facilitates a better adaptation to changing hydrodynamic conditions than a morphology with distinct and deeply imprinted rip channels. Due to more distinct evolution the current patterns would reinforce the existing pattern, thus preventing the system to change toward a new lay-out. Next, sets of different successive hydrodynamic conditions show that the importance of the level of variability holds for both increasing and decreasing wave energy flux. This indicates that it is not so much the total energy flux, but the relation between cross-shore and alongshore components of the local velocities which determines whether existing channels will remain or disappear.

Which processes are dominant in creating the observed patterns?

The process-based model used to hindcast a morphological evolution including both up-state and down-state transitions, included the effects of roller energy, wave asymmetry, long wave induced sediment stirring, wave groups and turbulence dependent diffusion. All of these processes affected the total balance between damping and amplifying processes and therefore the pace and magnitude of morphological evolution. It is found that processes need to be included in such a way that the balance in damping and amplifying effects leads to an evolution that matches the observed pace and magnitude of evolution.

Why does an observed nearshore bar pattern look the way it does?

The main research question aimed to explain why observed patterns have the observed lay-out. From work by others is known that crescentic patterns initially form due to morphological feedback of small perturbations (either on the morphology or in the wave pattern) and the hydrodynamic forcing. Once patterns are being formed, the remaining questions are why these patterns seem to have certain length scales, certain levels of variability and when and how

property/parameter/process	affects
hydro + geo	length scale and response time
perturbation	location of rips
variability	level of adaptation
WA	shore-line position, amplifying effect
LW	diffusive effect
WG	length scale, diffusive effect in shallow zone
diffFA	diffusive effect
diffAA	amplifying effect (rate of change)

Table 5.1: System properties, processes and their effects, hydro = hydrodynamic conditions, geo = geometry, variability = level of morphological variability, WA = wave asymmetry, LW = long wave induced stirring, WG = wave groups, diffFA = the effect of diffusion, diffAA = the effect of the adaptation rate.

these patterns change. These have been addressed in the current work and are summarized in Table 5.1.

To conclude: observed nearshore patterns are formed by a combination of the initial bathymetry (the location of features and cross-shore profile: depth of the bar crest and volume of the bar), the level of variability therein (affects the adaptability of the system), the level of wave energy forcing the system and the balance between damping and amplifying processes in the system (Figure 5.2). The performance of the modelling of the evolution of the nearshore morphology is determined by the above, by the accuracy of the morphology and by the quality of the description of the processes. Upto a certain level of morphological variability, the patterns will change in response to the local hydrodynamics and the length scales will adjust accordingly when the conditions prevail long enough. After a certain level of morphological variability has been reached, the occurring length scales will remain, until a reset-event occurs, resulting in a decrease of the variability as the bar becomes alongshore uniform and thus infinite length scale. In case the model includes too little diffusive effects, the nearshore variability will continue to increase. In case the model includes too large diffusive effects, all existing variability will be removed.

In general it can be stated that nearshore morphology is sensitive to

- bathymetry (location of perturbations and features and level of variability),
- local conditions,
- prolonged conditions.

The **modelling** of nearshore morphology is sensitive to

- the above and
- chosen process settings,
- chosen calibration parameter values.

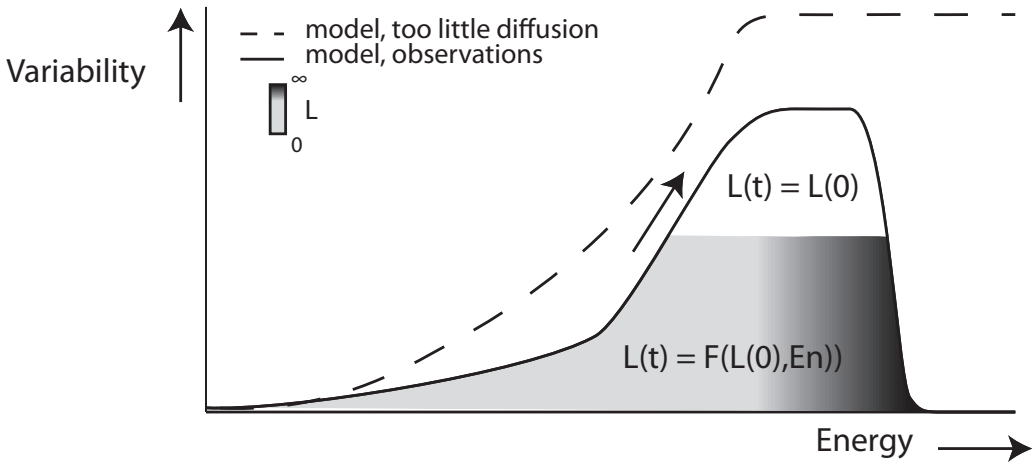

Figure 5.2: The variability of a nearshore bathymetry depends on the initial level of variability, the hydrodynamic conditions, the occurring diffusion and the chosen processes settings in the model (the first three items indicate whether change will occur in the field, the latter is how it is dealt with in the model). With a high level of variability, no changes will occur (length scale (L) stays constant), except if the process settings result in a large role for the diffusion. If the hydrodynamic energy is very high, it will force the variability to decrease rapidly, leading to a reset-event.

5.5.2 Conclusion on modelling and behaviour

Place and time are crucial, also in morphological modelling. The location of features and their size will affect where new features may emerge (if starting from a low level of variability, order cm) or whether the nearshore bar system will remain unchanged (if initial bathymetry has larger level of variability). In the latter case, only extreme conditions will be able to affect the system and result in a changing bathymetry. Time is important in the modelling as the computed morphological evolution needs to occur at the same rate as the observed, otherwise the level of variability (how far features are evolved) will not match the observations and then the model may for example allow the bathymetry to adapt to new conditions, while in the field the features are too deeply imprinted to allow changes. Further in time, the duration of conditions and order of conditions will affect the morphological evolution.

5.6 Discussion and recommendations

5.6.1 Type of response

To what extent are observed patterns created by chaotic or by forced behaviour? And for the parts of the behaviour that are chaotic, is this deterministically chaotic, or stochastic chaotic response -i.e. antecedent conditions play a role- (Stive and Reniers, 2003)? The effect of five processes on the nearshore evolution has been tested: wave asymmetry, long wave induced stirring, wave groups, the effect of diffusion, the effect of the adaptation rate. Per process, the

type of response which affects the morphological evolution can be distinguished. The evolving length scales did not correspond with length scales of the individual processes, the response is thus chaotic. The tested processes on their own have a chaotic response. However, the total balance of the different processes may result in a stochastic chaotic response. Whether the response depends on the antecedent conditions (i.e. stochastic) is determined by both the level of energy of the incoming waves and the level of morphological variability.

If the incoming energy is extreme, the antecedent morphology plays no role: all pre-existing features will be erased (a reset-event). The response is deterministic chaotic in this case. However, such events are rare (Holman et al., 2006). If the energy level is lower than extreme and the antecedent level of morphological variability is large enough, the antecedent morphological patterns will determine the morphological evolution and possibly will remain: a stochastic chaotic response. As bathymetries generally have a reasonable level of variability, the evolution will generally be stochastic chaotic: length scales that are not identical to the length scales of the forcing and with a role of the antecedent morphology. The antecedent hydrodynamic conditions are only important if they have left an imprint in the morphology. The morphological evolution is therefor determined by the antecedent morphology and the current forcing conditions as was hypothesized.

5.6.2 Matching demand and model

For different aims of hindcasts or predictions, different processes and descriptions need to be included in a model (Table 5.2). If one wants to model exact rip locations, a depth averaged (2DH) process-based model will be required, which includes all processes, investigated in the current work. With the current knowledge, predictions of rip channel locations of about 3 days in advance can be made. If no large changes in wave conditions are to be expected and the model is morphologically calibrated well, it is expected that forecasts of 5 to 7 days should be possible. At times, in the field, expert judgement will be of equal or higher quality than a model forecast, for example the knowledge of an experienced lifeguard, overlooking the ocean in the morning.

The current work relates to the prediction of bar behaviour on scales of days to weeks and spatial scales upto a few kilometers. Using detailed process-based models may lead to an accumulation of errors and therefore a quick deviation of the correct outcome when modelling over longer time scales. For those types of predictions, models on a more aggregated level may be more appropriate. Especially for predictions concerning cross-shore bar behaviour this can be approached reasonably well (e.g. Pape et al., subm). Predicting alongshore variablity was attempted by Plant et al. (e.g. 2006), however this approach was recently found not to be universely applicable for other sites and events.

aim of prediction	required method
trends (e.g. incr. $\overline{\lambda}$)	LSA
	2DH model, basic processes
length scales	LSA
	2DH model, incl proc
exact rip locations	2DH model, incl proc, expert

Table 5.2: LSA = linear stability analysis, 2DH = depth averaged, process based model, basic processes refers to the processes included in the model used in Chapter 2,3, incl proc refers to the processes included in the advanced model as used in Chapter 4.

5.6.3 Potential of data modelling integration

Due to the high level of sensitivity to bathymetrical features and at the same time the high level of uncertainty of the bathymetry, there is large potential for data-model integration to obtain for example an updated bathymetry and use that for a prediction of the subsequent morphological evolution. Such types of modelling systems are now in their testing phase and are expected to have high potential. The technique used in this research to derive initial bathymetries for the morphological computation of the hindcast, is based on work by Van Dongeren et al. (2008), a 2D extension of the cross-shore profile approach of Aarninkhof et al. (2005). In this technique, roller dissipation patterns derived from daily averaged video images are compared with numerically predicted dissipation patterns. At locations where the computed dissipation is smaller than the video-based dissipation, the depth is decreased; in locations with too much dissipation, the depth is increased.

5.6.4 Recommendations

Suggestions for model tests

The quality of the model can be tested more extensively by modelling various events in order to obtain a statistical overview of rip channel distances, locations and the concurrent conditions. This will allow comparison with the statistical analysis in Holman et al. (e.g. 2006). If the statistics of the modelled evolution compare well to the statistics of the observations, the model is doing a good job in producing correct patterns. However, to predict the possible dangers of expected rips, the channel depth and shoal elevation need to be predicted correctly too, as these are important for the rip current strength. Currently, bathymetries inferred from video images were used to test the model performance. Obtaining these bathymetries depends on the availability of video data and dissipation of waves over the bars. If there are no dissipation patterns due to a lack of waves, there may still be morphological features, but they can then not be inferred from video images. Next, these video-inferred bathymetries may still include errors. The best comparison could be made if in situ-measured bathymetries would be available.

However, these datasets are very costly and near impossible to obtain during a reset-event due to the harsh conditions in the field during such an event. However, it is recommended to aim for the collection of both field data (before and after a reset or severe storm event) as well as collecting video-images and pixel time series. This information can then be used to hindcast this sequence, either based on the field measurements, or based on the video-inferred bathymetries. This will allow a full comparison of the value of the used model input and further develop the modelling capacities.

Suggestion for model improvement -part 1: Empirical parameters and process descriptions

As many of the processes playing a role in nearshore morphological evolution are not fully understood, the used formulations describing these processes, include empirical parameters. It would be wise to check the used values for these parameters. These parameters are usually set, using for example laboratory measurements or fieldwork and a description incorporating other effects which are at that moment either unknown or not described specifically. In the currently used model (in Chapter 4), several processes have been incorporated explicitly, like wave groups. It may then lead to errors in the balance if an empirical parameter in e.g. the sediment transport equation is used, which originally was derived for a situation which included all transport effects in one equation, without differentiating for the contribution by either short or long waves. If the long wave effects are now explicitly added, this may lead to for example an overestimation of the transport or diffusion in certain cases. Reviewing the several empirical parameters in the description of morphological evolution and redefining those, may lead to an improved balance of the processes throughout forcings with different energy levels.

Suggestion for model improvement -part 2: Turbulence description

With the current model we are not capable of following the pace and magnitude of evolution for different levels of hydrodynamic energy within one evolution with varying levels of energy. Improving the balance between amplifying and damping processes for both high and low wave energy is expected to improve the models capacities. It is expected that improving the diffusion and related turbulence knowledge and thus their description will improve this balance and thus increasing the prediction horizon to match that of the wave conditions.

References

Aagaard, T. and Greenwood, B. (2008). Infragravity wave contribution to surf zone sediment transport - the role of advection. *Marine Geology*, 251.

Aarninkhof, S., Ruessink, B., and Roelvink, J. (2005). Nearshore subtidal bathymetry from time-exposure video images. *Journal of Geophysical Research*, 110(C06011).

Bagnold, R. (1966). An approach to the sediment transport problem from general physics. *Geol. Surv. Prof. Paper*, 422-I.

Bailard, J. (1981). An energetics total load sediment transport model for a plane sloping beach. *Journal of Geophysical Research*, 86 (C11):1093810954.

Battjes, J. A. (1975). Modelling of turbulence in the surfzone. In *Symposium on Modeling Techniques, Am. Soc. of Civ. Eng.*, volume 2, pages 1050–1062, San Francisco, California.

Bijker, E. (1971). Longshore transport computations. *Journal of Waterways, Harbours and Coastal Engineering Division*, 97(No. WW4).

Booij, N., Ris, R., and Holthuijsen, L. (1999). A third-generation wave model for coastal regions, part i, model description and validation. *Journal of Geophysical Research*, 104:7649–7666.

Bowen, A. and Inman, D. (1971). Edge waves and crescentic bars. *Journal of Geophysical Research*, 76(36):8663–8671.

Caballeria, M., Coco, G., Falqués, A., and Huntley, D. (2002). Self-organisation mechanisms for the formation of nearshore crescentic and transverse sandbars. *Journal of Fluid Mechanics*, 465:379–410.

Calvete, D., Coco, G., Falqués, A., and Dodd, N. (2007). (un)predictability in rip channel systems. *Geophysical Research letters*, 34(L05605).

Castelle, B., Bonneton, P., and Butel, R. (2006). Modélisation du festonnage des barres sableuses d'avant-côte: application à la côte aquitaine, france. *C.R. Geoscience*, 338 (11):795–801.

Castelle, B., Bonneton, P., Butel, R., and Dupuis, H. (2005). Morphodynamic modelling of nearshore crescentic bar dissymetry on an open coast: Aquitanian coast, france. In *Coastal Dynamics*, Barcelona, Spain.

Damgaard, J., Dodd, N., Hall, L., and Chasher, T. (2002). Morphodynamic modelling of rip channel growth. *Coastal Engineering*, 45((3-4)):199–221.

Deigaard, R., Drønen, N., Fredsøe, J., Hjelmager, J., and Jørgensen, M. (1999). A morphological stability analysis for a long straight barred coast. *Coastal Engineering*, 36:171–195.

Drønen, N. and Deigaard, R. (2007). Quasi-three-dimensional modelling of the morphology of longshore bars. *Coastal Engineering*, 54:197–215.

Falqués, A., Coco, G., and Huntley, D. (2000). A mechanism for the generation of wave-driven rhythmic patterns in the surf zone. *Journal of Geophysical Research*, 105(C10):24,071–24,087.

Falqués, A., Montoto, A., and Iranzo, V. (1996). Bed-flow instability of the longshore current. *Continental Shelf Research*, 16(15):1927–1964.

Feddersen, F. (2007). Breaking wave induced cross-shore tracer dispersion in the surfzone: model results and scalings. *Journal of Geophysical Research*, 112(C09012).

Gallapatti, R. (1983). A depth integrated model for suspended transport. Technical report, Delft University of Technolgy.

Garnier, R., Calvete, D., Falqués, A., and Caballeria, M. (2006). Generation and nonlinear evolution of shore oblique/transverse bars. *Journal of Fluid Mechanics*, 567:327–360.

Grunnet, N., Walstra, D., and Ruessink, B. (2004). Process-based modeling of a shoreface nourishment. *Coastal Engineering*, 51:581–607.

Holman, R. and Bowen, A. (1982). Bars, bumps and holes: models for the generation of complex beach topography. *Journal of Geophysical Research*, 87(C1):457–468.

Holman, R. and Stanley, J. (2007). The history and technical capabilities of argus. *Coastal Engineering*, 54:477–491.

Holman, R., Symonds, G., Thornton, E., and Ranasinghe, R. (2006). Rip spacing and persistence on an embayed beach. *Journal of Geophysical Research*, 111(C01006).

Huntley, D. and Coco, G. (2009). How do bedforms respond to changing conditions? a study using abstracted models. In *Coastal Dynamics*, page Keynote, Japan.

Ikeda, S. (1982). Lateral bed-load transport on side slopes. *ASCE Journal of the Hydraulic Division*, 108 (11):1369–1373.

Johnson, D. and Pattiaratchi, C. (2004). Transient rip currents and nearshore circulation on a swell-dominated beach. *Journal of Geophysical Research*, 109(C02026).

Klein, M. and Schuttelaars, H. (2005). Morphodynamic instabilities of planar beaches: sensitivity to parameter values and processes. *Journal of Geophysical Research*, 110(F04S18).

Klein, M. and Schuttelaars, H. (2006). Morphodynamic evolution of double-barred beaches. *Journal of Geophysical Research*, 111(C06017).

Lesser, G., Roelvink, J., Van Kester, J., and Stelling, G. (2004). Development and validation of a three-dimensional morphological model. *Coastal Engineering*, 51(8-9):883–915.

Lippmann, T. and Holman, R. (1990). The spatial and temporal variability of sand bar morphology. *Journal of Geophysical Research*, 95(C7):11575–11590.

MacMahan, J., Thornton, E., and Reniers, A. (2006). Rip current review. *Coastal Engineering*, 53:191–208.

Nairn, R., Roelvink, J., and Southgate, H. (1990). Transitione zone width and implications for modelling surfzone hydrodynamics. In Edge, B., editor, *Coastal Engineering COnference,*

1990: Proceedings of the International Conference, pages 68–81, Am. Soc. of Civ. Eng., Reston, Va.

Pape, L., Plant, N., and Ruessink, B. (subm). On cross-shore sandbar behaviour and equilibrium states. *Journal of Geophysical Research*.

Plant, N., Holland, K., and Holman, R. (2006). A dynamical attractor governs beach response to storms. *Geophysical Research Letters*, 33(L17607).

Plant, N., Holland, K., Holman, R., Splinter, K., Reniers, A., and Smit, M. (2007). A dynamical systems approach to analyzing morphodynamic states. In *5th IAHR Symposium River, Coastal and Estuarine Morphodynamics: RCEM 2007*, pages 217–221, Enschede, The Netherlands.

Ranasinghe, R., Symonds, G., Black, K., and Holman, R. (2004). Morphodynamics of intermediate beaches: a video imaging and numerical modelling study. *Coastal Engineering*, 51:629–655.

Reniers, A., MacMahan, J., Thornton, E., and Stanton, T. (2006). Modelling infragravity motions on a rip-channel beach. *Coastal Engineering*, 53:209–222.

Reniers, A., Roelvink, J., and Thornton, E. (2004). Morphodynamic modelling of an embayed beach under wave group forcing. *Journal of Geophysical Research*, 109(C01030).

Reniers, A., Symonds, G., and Thornton, E. (2001). Modelling rip currents during rdex. In *Coastal Dynamics*, pages 493–499, Lund, Sweden.

Reniers, A., Van Dongeren, A., Battjes, J., and Thornton, E. (2002). Linear modelling of infragravity waves during delilah. *Journal of Geophysical Research*, 107(C10).

Rienecker, M. and Fenton, J. (1981). A fourier approximation method for steady water waves. *Journal of Fluid Mechanics*, 105:119–137.

Ris, R., Holthuijsen, L., and Booij, N. (1999). A third-generation wave model for coastal regions, part ii, verification. *Journal of Geophysical Research*, 104:7667–7681.

Roelvink, J. (1993). Dissipation in random wave groups incident on a beach. *Coastal Engineering*, 19:127–150.

Roelvink, J. (2006). Coastal morphodynamic evolution techniques. *Coastal Engineering*, 53:277–287.

Roelvink, J. and Stive, M. (1989). Bar-generating cross-shore flow mechanisms on a beach. *Journal of Geophysical Research*, 94(C4):4785–4800.

Roelvink, J. and Van Banning, G. (1994). Design and development of delft3d and application to coastal morphodynamics. In *Hydroinformatics 1994*.

Ruessink, B., Kuriyama, Y., Reniers, A., Roelvink, J., and Walstra, D. (2007). Modeling cross-shore sandbar behavior on the timescale of weeks. *Journal of Geophysical Research*, 112(F03010).

Smit, M., Aarninkhof, S., Wijnberg, K., Gonzlez, M., Kingston, K., Southgate, H., Ruessink, B., Holman, R., Siegle, E., Davidson, M., and Medina, R. (2007). The role of video imagery in predicting daily to monthly coastal evolution. *Coastal Engineering*, 54(6-7):539–553.

Smit, M., Reniers, A., Ruessink, B., and Roelvink, J. (2008). The morphological response of a nearshore double sandbar system to constant wave forcing. *Coastal Engineering*, 55(10):761–770.

Smit, M., Reniers, A., and Stive, M. (2005). Nearshore bar response to time varying conditions. In *Coastal Dynamics*, Barcelona, Spain.

Smit, M., Reniers, A., and Stive, M. (In preparationa). Role of morphological variability in the evolution of nearshore sandbars. *Coastal Engineering*.

Smit, M., Reniers, A., Stive, M., and Roelvink, J. (2004). Non-linear behaviour of a double nearshore bar system. In *International Conference on Coastal Engineering*, Lisbon, Portugal.

Smit, M., Reniers, A., Symonds, G., and Ruessink, B. (2006). Modelling non-linear nearshore dynamics of a barred coast: Palm beach, sydney, australia. In *International Conference on Coastal Engineering*, San Diego, USA.

Smit, M., Reniers, A., Symonds, G., Ruessink, B., and Stive, M. (in preparationb). Hindcasting up-state and down-state transition at palm beach, nsw, australia. *Journal of Geophysical Research*.

Soulsby, R. (1997). *Dynamics of marine sands*. Thomas Telford, London.

Soulsby, R., Hamm, H. Klopman, G., Myrhaug, D., Simons, R., and Thomas, G. (1993). Wave-current interaction within and outside the bottom boundary layer. *Coastal Engineering*, 21:41–69.

Splinter, K. (2009). Development of 2d models to estimate nearshore bathymetry and sediment transport.

Stive, M. and De Vriend, H. (1994). Shear stresses and mean flow in shoaling and breaking waves. In Edge, B., editor, *Proceedings of the twenty-fourth international conference*, pages 594–608, Am. Soc. of Civ. Eng., Reston, Va.

Stive, M. and Reniers, A. (2003). Sandbars in motion. *Science*, 299:1855–1856.

Stokes, G. (1847). On the theory of oscillatory waves. *Trans. Cambridge Philos. Soc.*, 8:441–455.

Svendsen, I. (1984). Mass flux and undertow in the surf zone. *Coastal Engineering*, 8(4):347–365.

Symonds, G. and Ranasinghe, R. (2000). On the formation of rip currents on a plane beach. In *International Conference on Coastal Engineering*, pages 468–481, Sydney, Australia.

Traykovski, P. (2007). Observations of wave orbital scale ripples and a nonequilibrium time-dependent model. *Journal of Geophysical Research*, 112(C06026).

Turner, I., Whyte, D., Ruessink, B., and Ranasinghe, R. (2007). Observations of rip spacing, persistence and mobility at a long, straight coastline. *Marine Geology*, 236:209–221.

Van Dongeren, A., Plant, N., Cohen, A., Roelvink, J., Haller, M., and Catalan, P. (2008). Beach wizard: Nearshore bathymetry estimation through assimilation of model computations and remote observations. *Coastal Engineering*, 55:1016–1027.

Van Dongeren, A., Reniers, A., , Battjes, J., and Svendsen, I. (2003). Numerical modelling of infragravity wave response during delilah. *Journal of Geophysical Research*, 108(C9).

Van Enckevort, I., Ruessink, B., Coco, G., Suzuki, K., Turner, I., Plant, N., and Holman, R. (2004). Observations of nearshore crescentic sandbars. *Journal of Geophysical Research*, 109(C06028).

Wijnberg, K., Aarninkhof, S., and Spanhoff, R. (2006). Response of a shoreline sand wave to beach nourishment. In *International Conference on Coastal Engineering*, pages 4205–4217, San Diego, USA.

Wright, L. and Short, A. (1984). Morphodynamic variability of surf zones and beaches: a synthesis. *Marine Geology*, 56:93–118.

Appendix A

Rip current awareness

The following image has been downloaded from www.ripcurrents.noaa.gov. Like many other organisations, the government of the united states developed this image and an information campaign to warn and educate beach goers. It should be noted that from recent rip current experiments is found that swimming away from the rip current -'break the grip of the rip'- may not always be the best solution and a larger focus should possibly be on drifting with the current before attempting to head back to shore. Rip currents are often not symmetrical and may be oblique to the coast. Swimming shore-parallel, aiming to get out of the rip may then still lead to exhaustion and worse, panicking and possibly worse consequences. In such a case it is better to drift with the current -while waving for attention from life guards or beach goers. Once in deeper water, the rip current will be less strong or non-existent and it will be easier to swim away from the line of the rip. It is important to keep track of one's location in sea by checking one's position with respect to a landmark, this will give information on the direction of the rip current. One should then swim toward the area where, shoreward from the swimmer, the waves are breaking. Returning to the shore is then possible by swimming and rolling with the waves toward the coast. In short this would be: drift off and roll back.

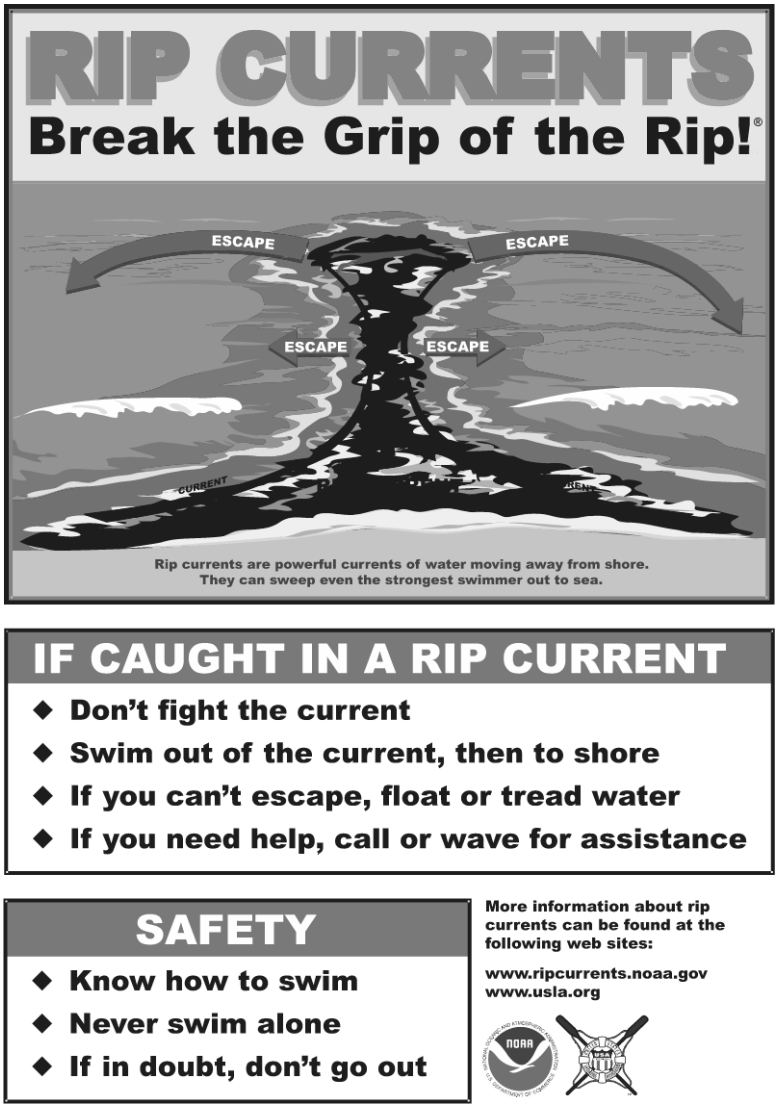

Figure A.1: How to deal with rip currents, poster downloaded from www.ripcurrents.noaa.gov

Appendix B

Addition to Chapter 2: Bathymetrical evolution for 16 hydrodynamic conditions

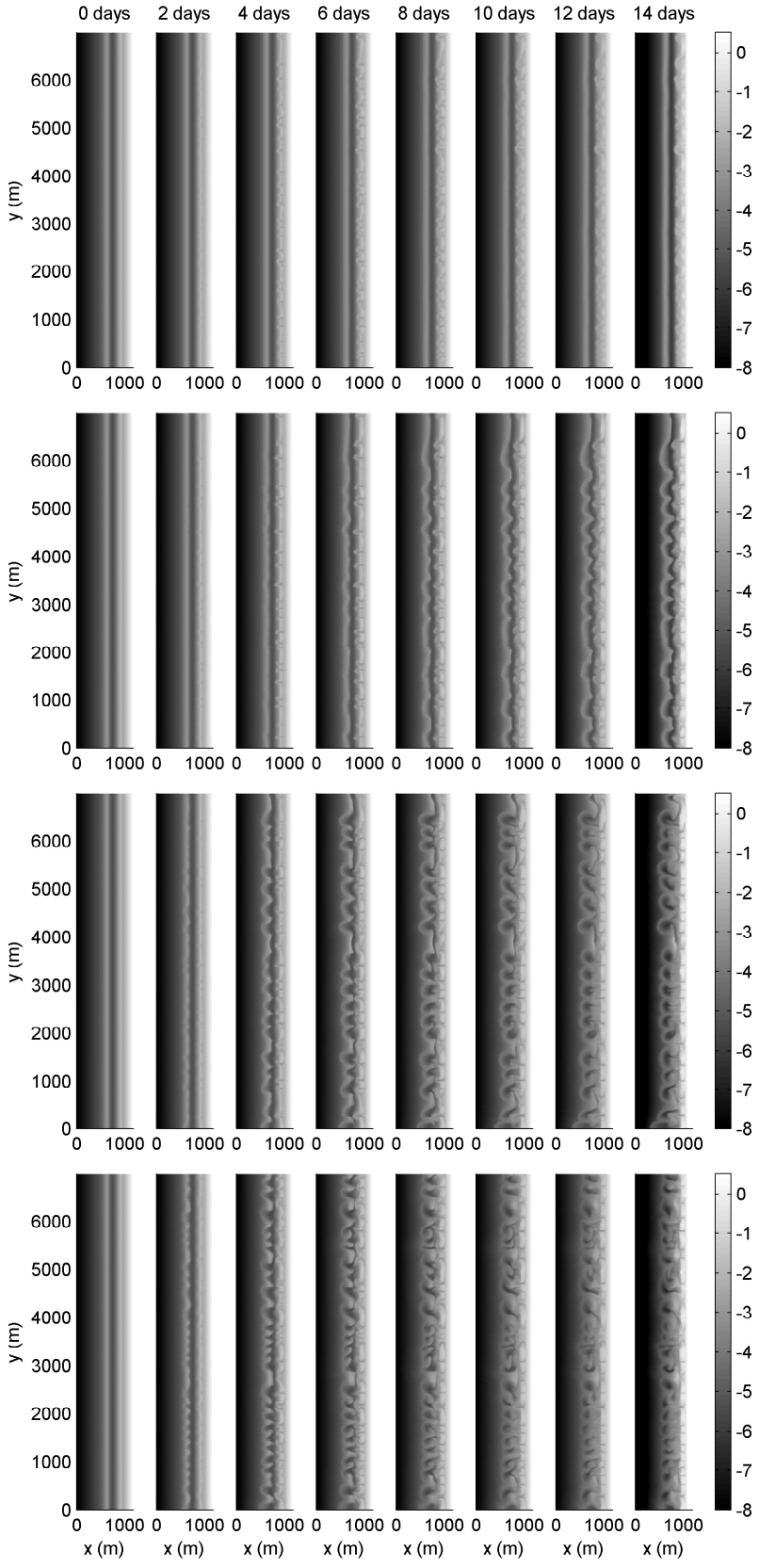

Figure B.1: Morphological evolution of initially alongshore uniform bathymetry with random initial perturbation 1 (O cm), forced with wave conditions with $\theta = 0^{o}$ (shore normal), $H_s = 1$, 1.5, 2, 2.5 m respectively (top to bottom panel), colorbar indicates elevation in m (light is shallow, dark is deep).

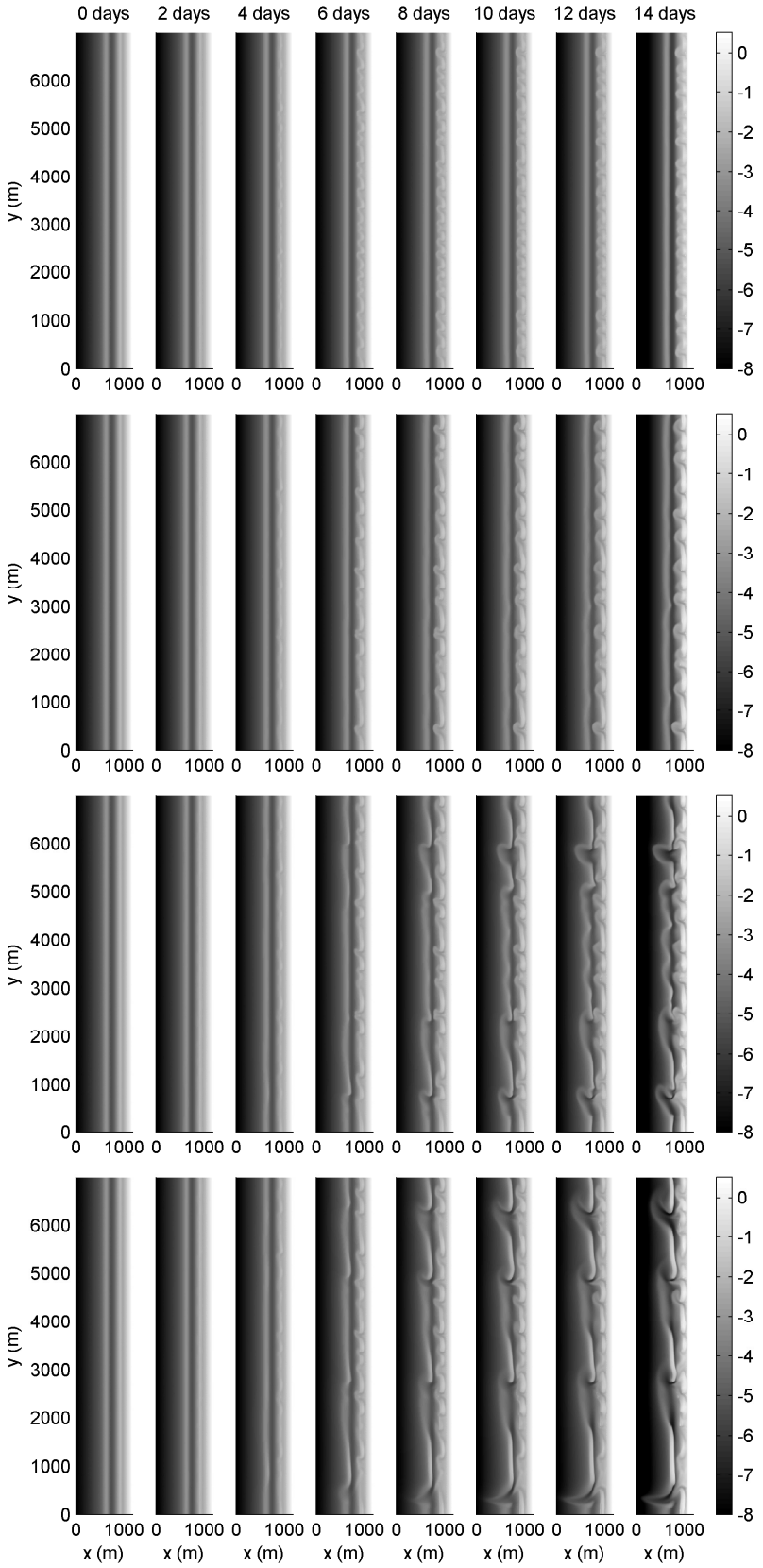

Figure B.2: Morphological evolution of initially alongshore uniform bathymetry with random initial perturbation 1 (O cm), forced with wave conditions with $\theta = 10^{o}$, $H_s = 1$, 1.5, 2, 2.5 m respectively (top to bottom panel), colorbar indicates elevation in m (light is shallow, dark is deep).

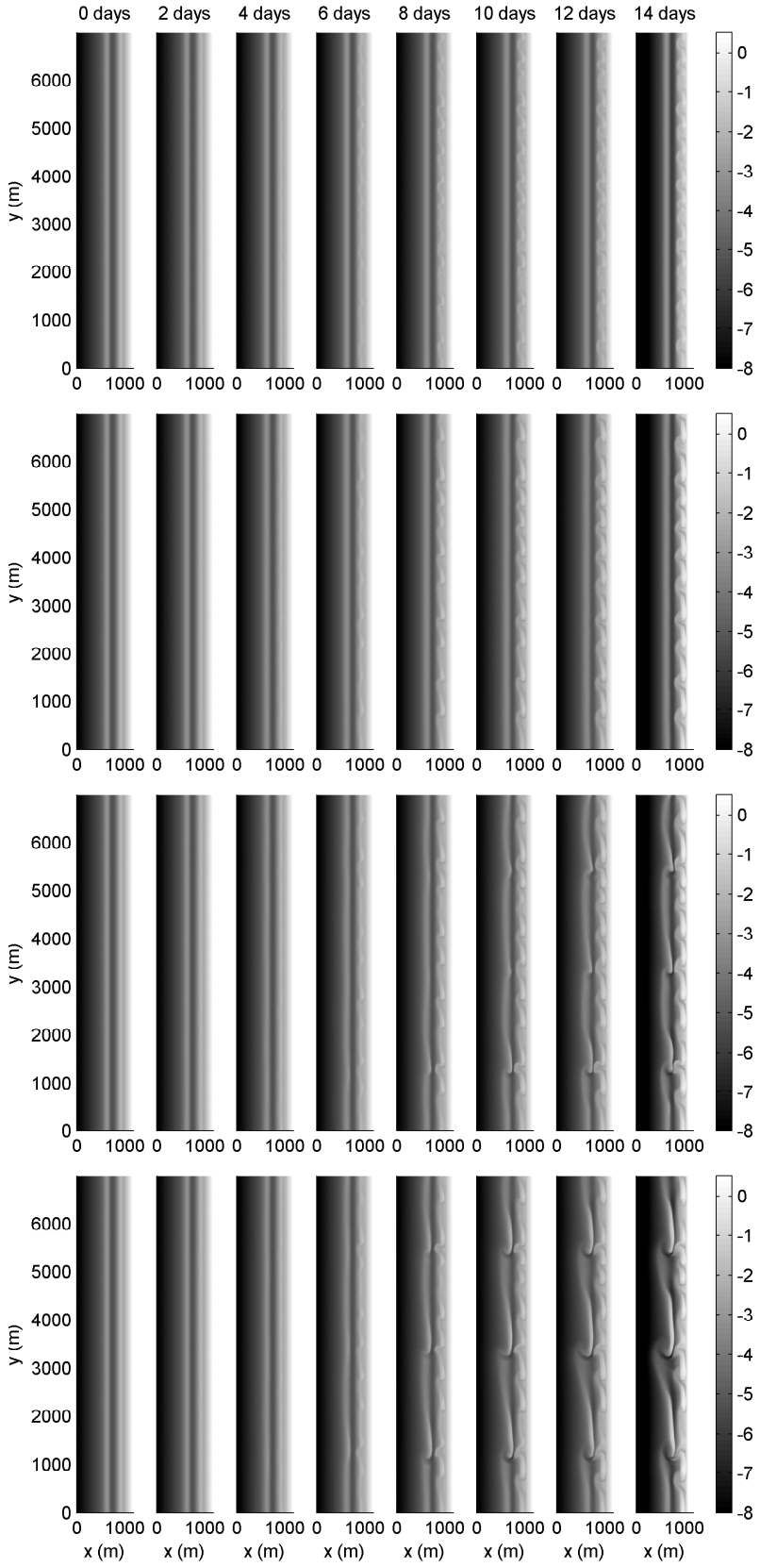

Figure B.3: Morphological evolution of initially alongshore uniform bathymetry with random initial perturbation 1 (O cm), forced with wave conditions with $\theta = 20^{o}$, $H_s = 1$, 1.5, 2, 2.5 m respectively (top to bottom panel), colorbar indicates elevation in m (light is shallow, dark is deep).

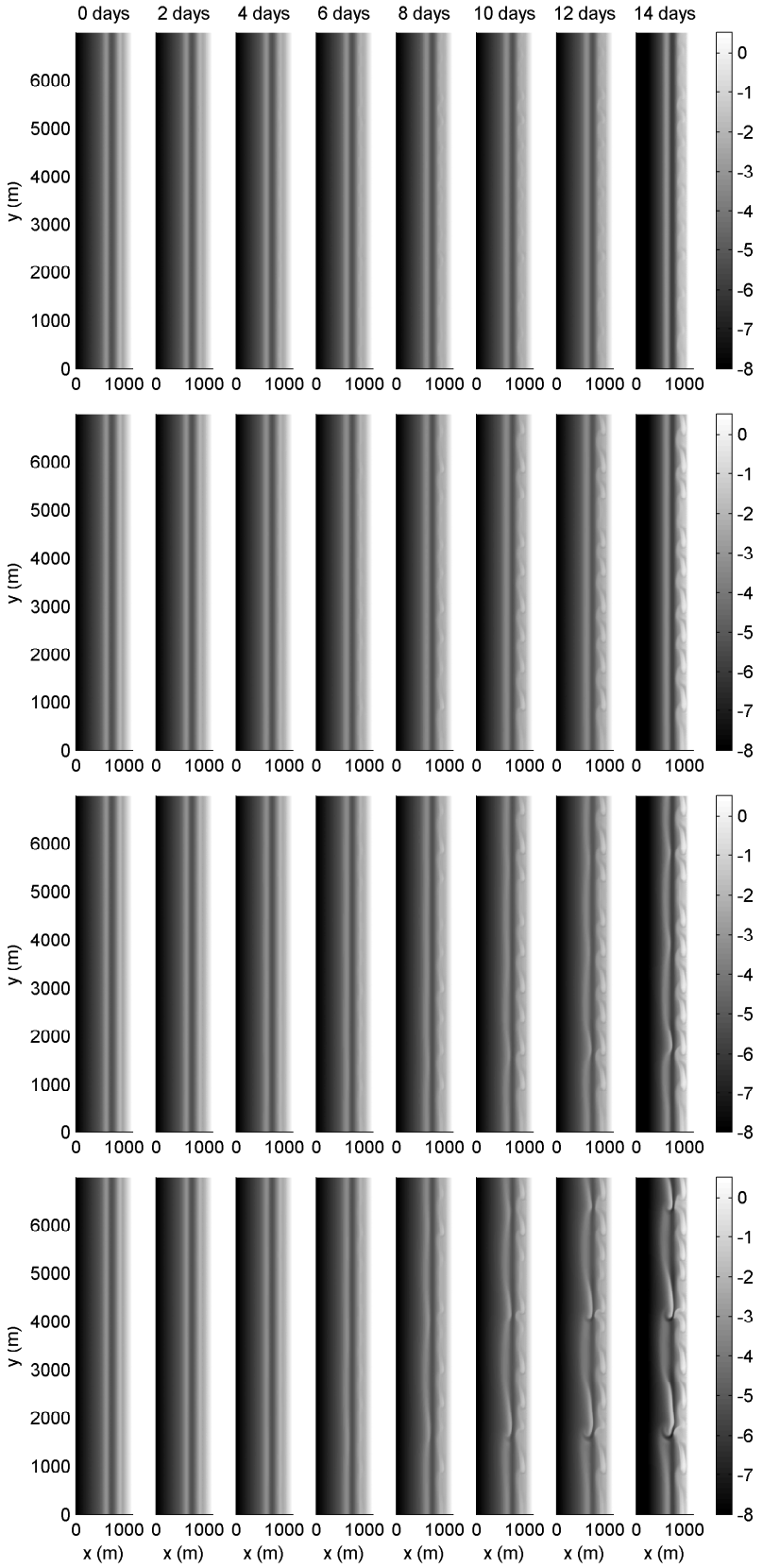

Figure B.4: Morphological evolution of initially alongshore uniform bathymetry with random initial perturbation 1 (O cm), forced with wave conditions with $\theta = 30^{o}$, $H_s = 1$, 1.5, 2, 2.5 m respectively (top to bottom panel), colorbar indicates elevation in m (light is shallow, dark is deep).

Appendix C

Length scale definitions

In Chapter 2 the length scale was defined using the contours of the bathymetry and taking a Fourier transform of the locations of this contour line. This definition gives objective length scale values that can be reproduced easily and is therefore very applicable to time series of bathymetrical evolution.

In other modelling studies (e.g. Reniers et al., 2004) and the analysis of field observations (e.g. Holman et al., 2006), the length scales are often determined by manually interpreting the lengths of the individual crescents. The subjectivity of this method can be accounted for by inviting several people for the manual laborious interpretation of crescent lengths (e.g. Holman et al., 2006). Van Enckevort et al. (2004) used an automated method to indicate the horns and bays of the observed dissipation pattern in time-exposure video images, thus indicating the horns and bays of the underlying crescentic bathymetry. Their detection of horns and bays (HBD) is a well suited technique to automatically obtain individual crescent lengths from video images and additionally provides information on the cross-shore amplitude of the crescents.

Below, the length scales obtained when using HBD are compared with the weighted length scales based on Fourier analyses as described in this paper. This gives information on the applicability of these methods and their differences. The same contour lines are used for both methods. In this comparison, the length scales are computed for the inner bar at the end of the computations of all 16 hydrodynamic conditions and for all five perturbations, as shown in e.g. Figure 2.5a.

Figure C.1 compares the HBD based length scales with $\overline{\lambda}_{end}$. Both methods result in similar length scales. Also the variations in the length scales for the five different perturbations are similar in most cases. The largest difference can be found for one hydrodynamic condition (see 725, 550 in Figure C.1). The HBD method found four length scales ranging from 500 to 600 m and one of around 1000 m, thus resulting in both an offset and a very large standard deviation. In general, however, the figure demonstrates that the mean lengths are similar, which makes the methods interchangable to determine the mean length scales.

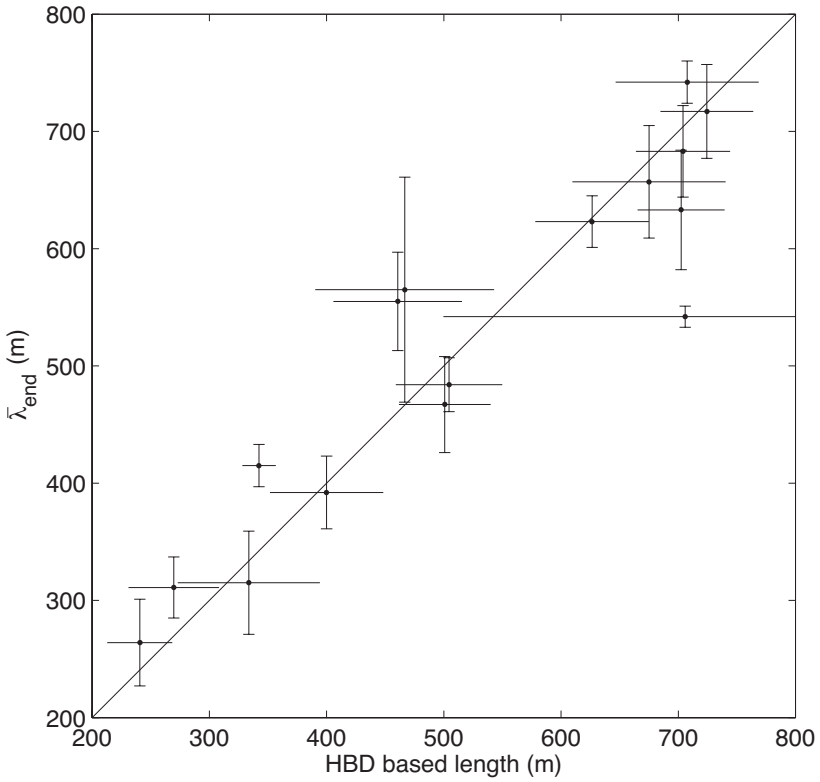

Figure C.1: $\overline{\lambda}_{end}$ as used in this paper versus length scales based on HBD. Each marker indicates a mean length scale value for one hydrodynamic condition. Vertical lines indicate ± 1 standard deviation for the five different length scales found for the five different perturbations. The diagonal line indicates a perfect fit.

Appendix D

Addition to Chapter 3: Bathymetries at $t = t_T$ and $t = 20$ days

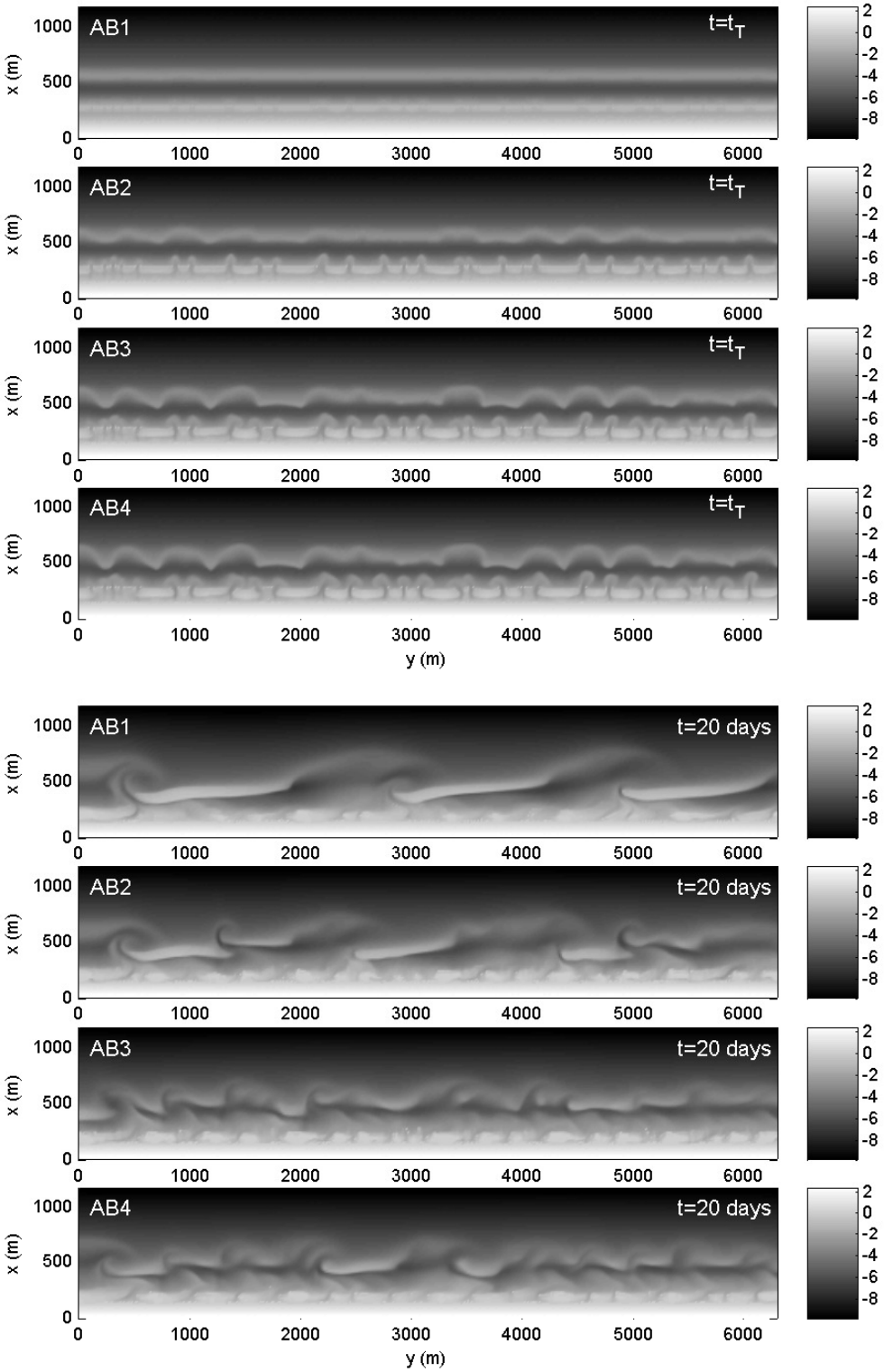

Figure D.1: The bathymetries at t_T for AB1..4, i.e. after condition A. The most upper panel is at the first transition moment, after 1.5 days of condition A. The second panel is the bathymetry at the second moment (4 days), the third panel the third moment of transition (6.5 days) and the lowest panel the bathymetry at the fourth moment of transitions (7.5 days).e-end: Final bathymetries for AB 1..4 computations. All after 20 days of morphological evolution. t_T of the upper panel was after 1.5 days of normal wave incidence (1.5 m height), of the second panel after 4 days, the third after 6.5 days and of the lowest panel after 7.5 days.

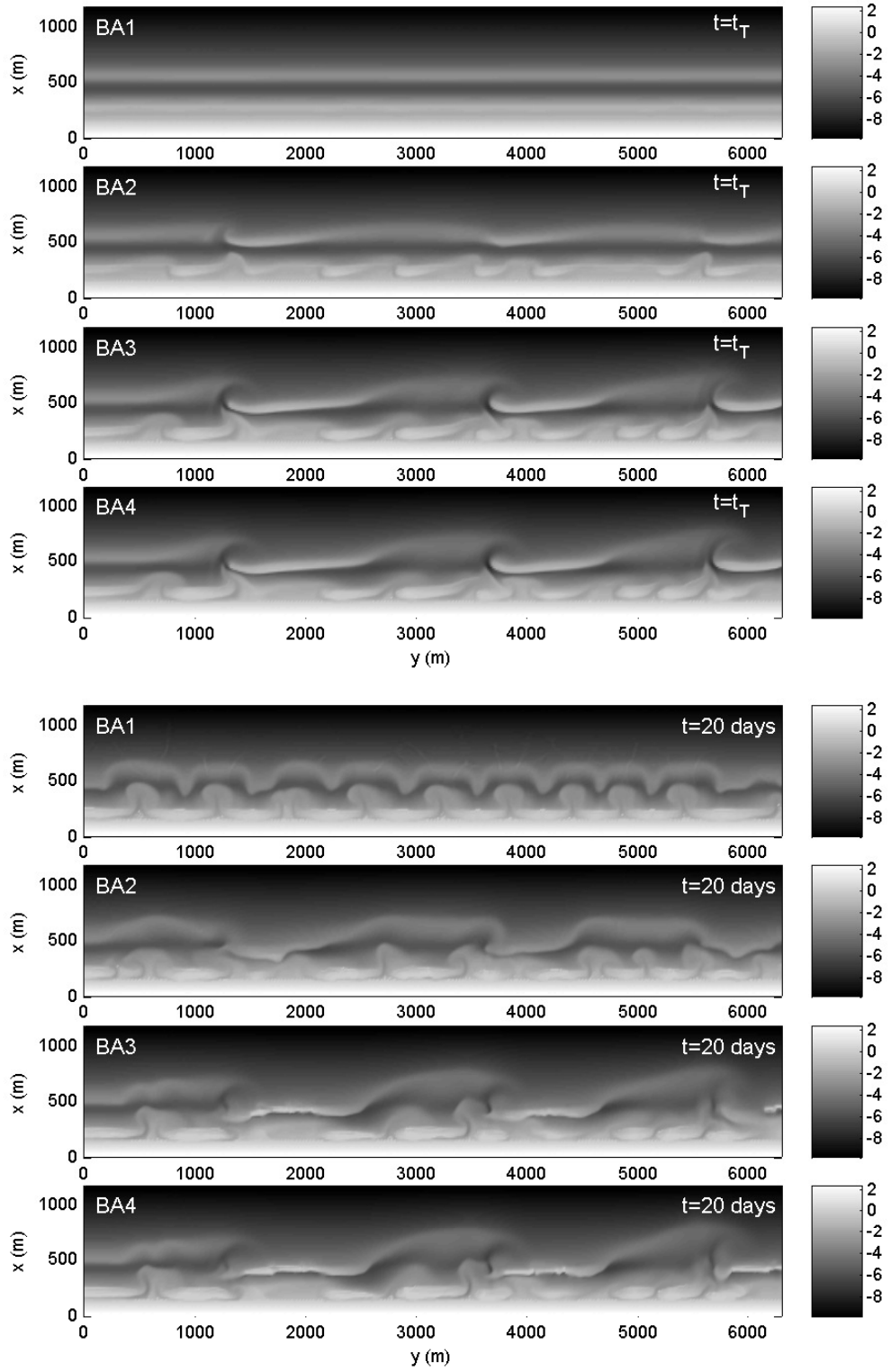

Figure D.2: The bathymetries at t_T for BA1..4, i.e. after condition B. e-end: Final bathymetries for BA 1..4 computations. All after 20 days of morphological evolution.

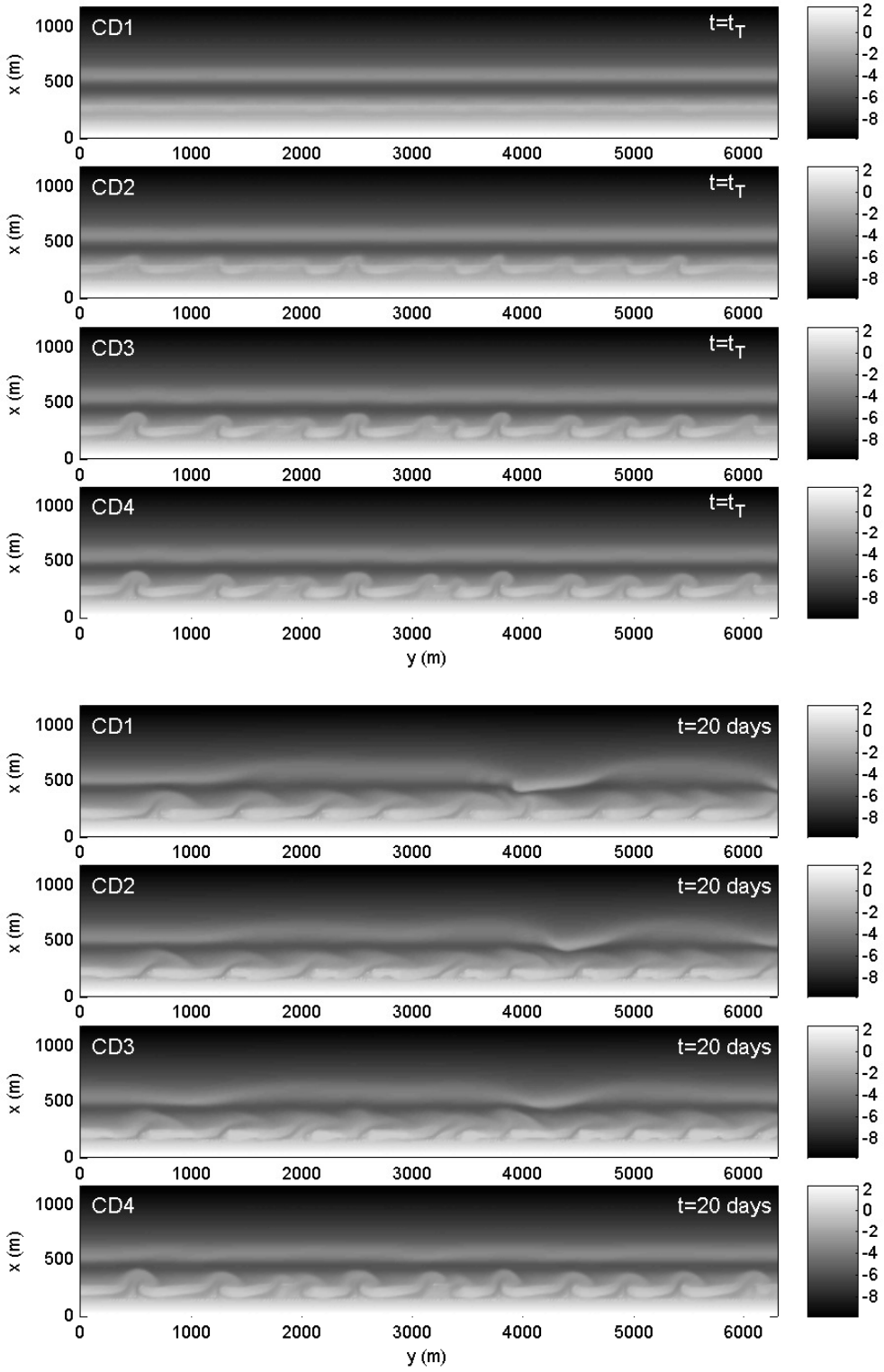

Figure D.3: The bathymetries at t_T for CD1..4, i.e. after condition C. e-end: Final bathymetries for CD 1..4 computations. All after 20 days of morphological evolution.

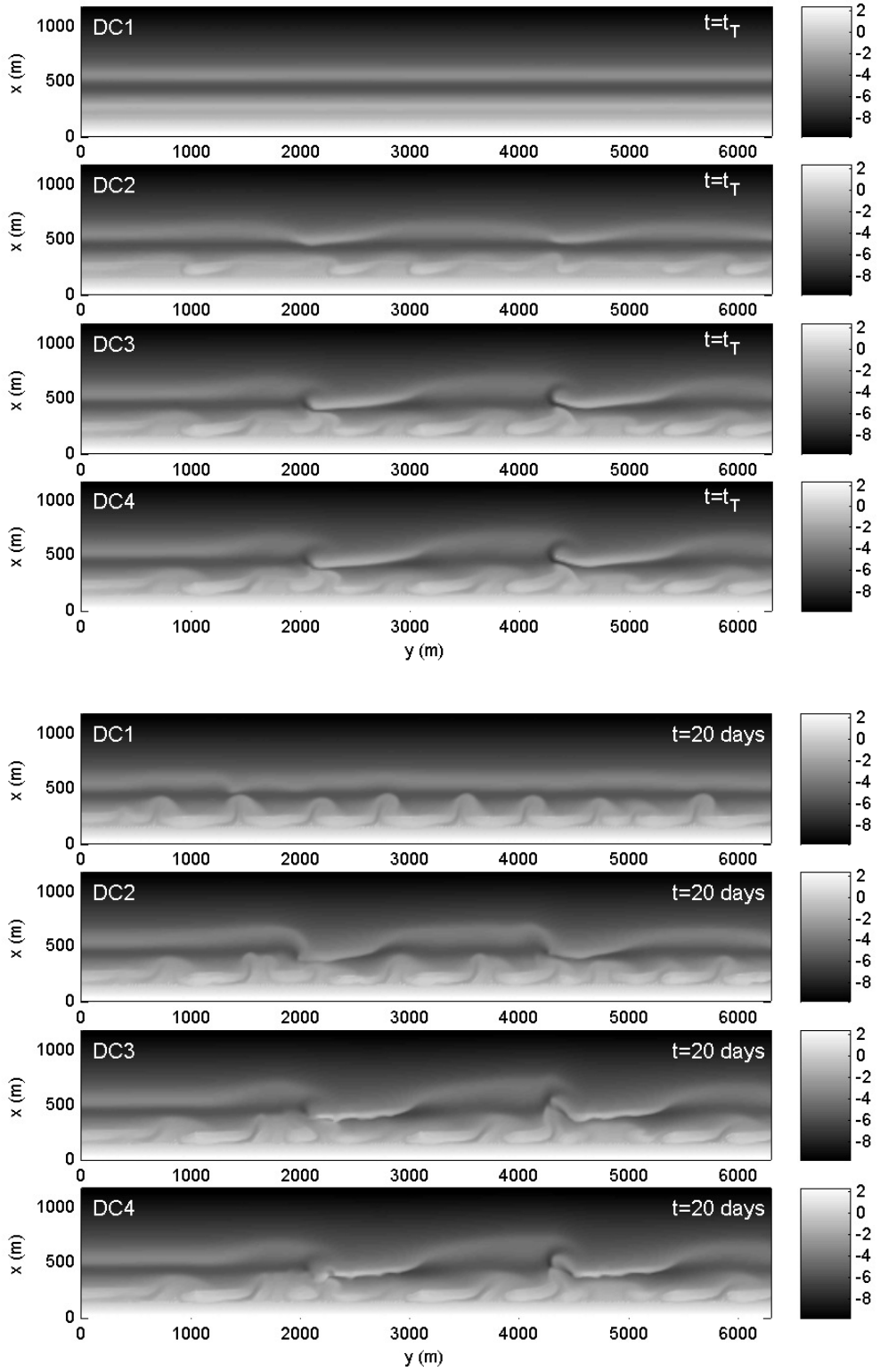

Figure D.4: The bathymetries at t_T for DC1..4, i.e. after condition D. e-end: Final bathymetries for DC 1..4 computations. All after 20 days of morphological evolution.

Appendix E

Addition to Chapter 3: $\overline{\lambda}$ evolution and $\overline{\lambda}Score(comp(k,t))$

The figures below present the evolution of $\overline{\lambda}$ and $\overline{\lambda}Score(comp(k,t))$ for both inner and outer bar, all for the computations with initial perturbation nr 1.

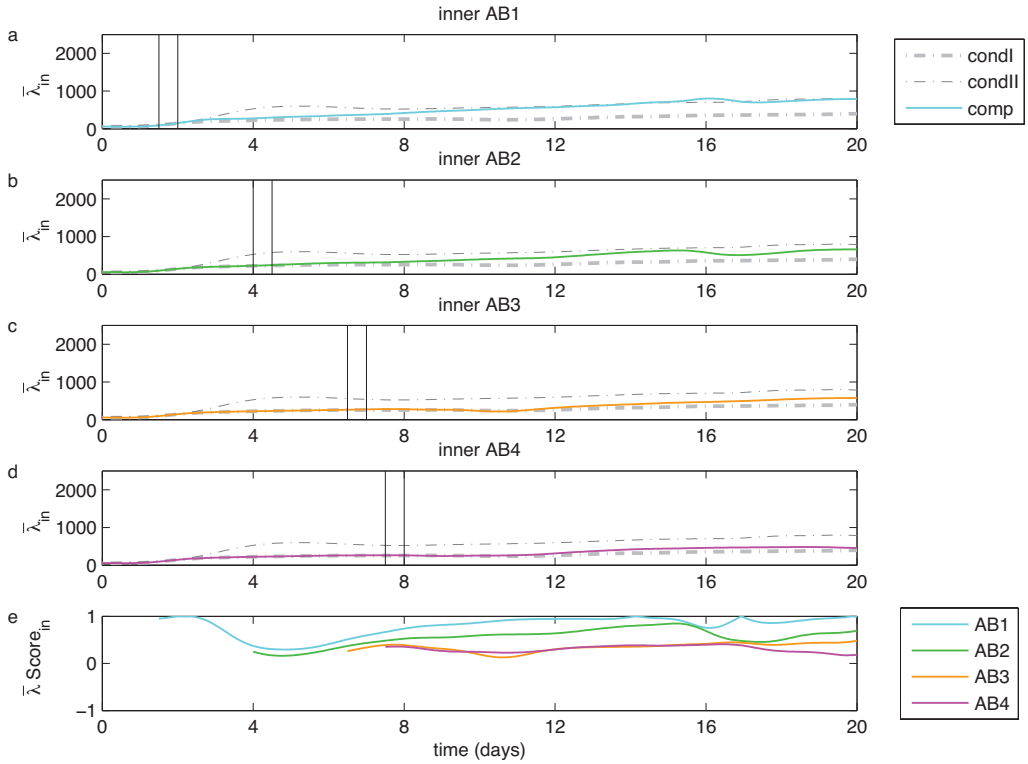

Figure E.1: a-d: $\overline{\lambda}_{in}(t)$ [m] for AB computations; e: $\overline{\lambda}Score(AB(k,t))$

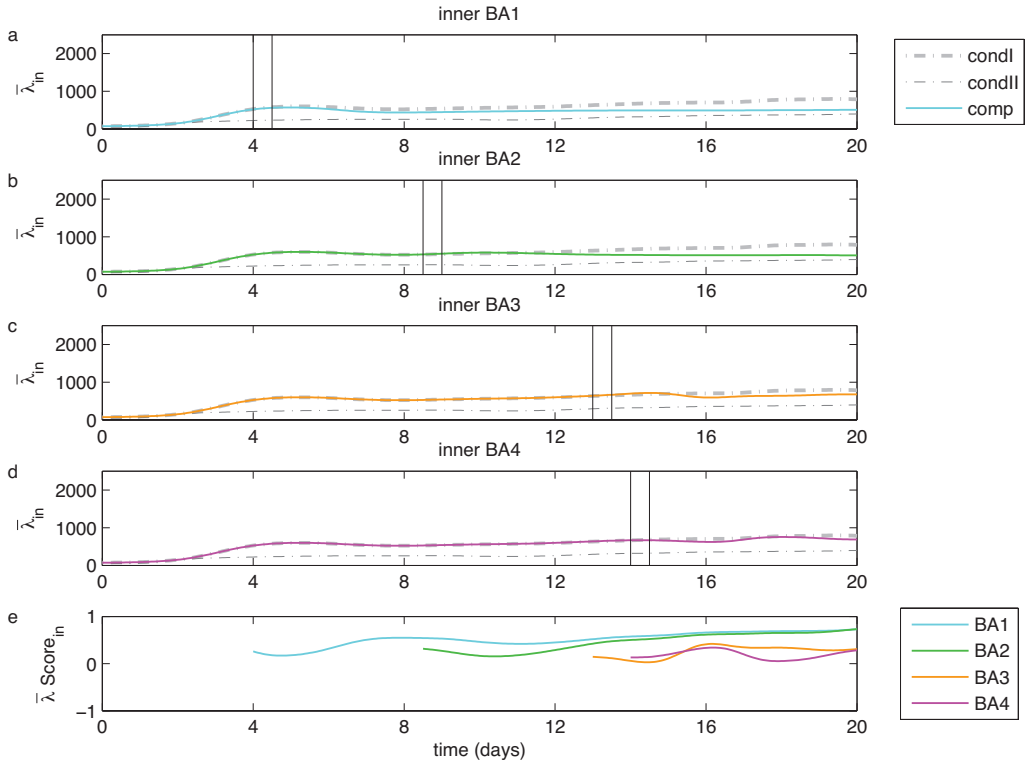

Figure E.2: a-d: $\overline{\lambda}_{in}(t)$ [m] for BA computations; e: $\overline{\lambda}Score(BA(k,t))$

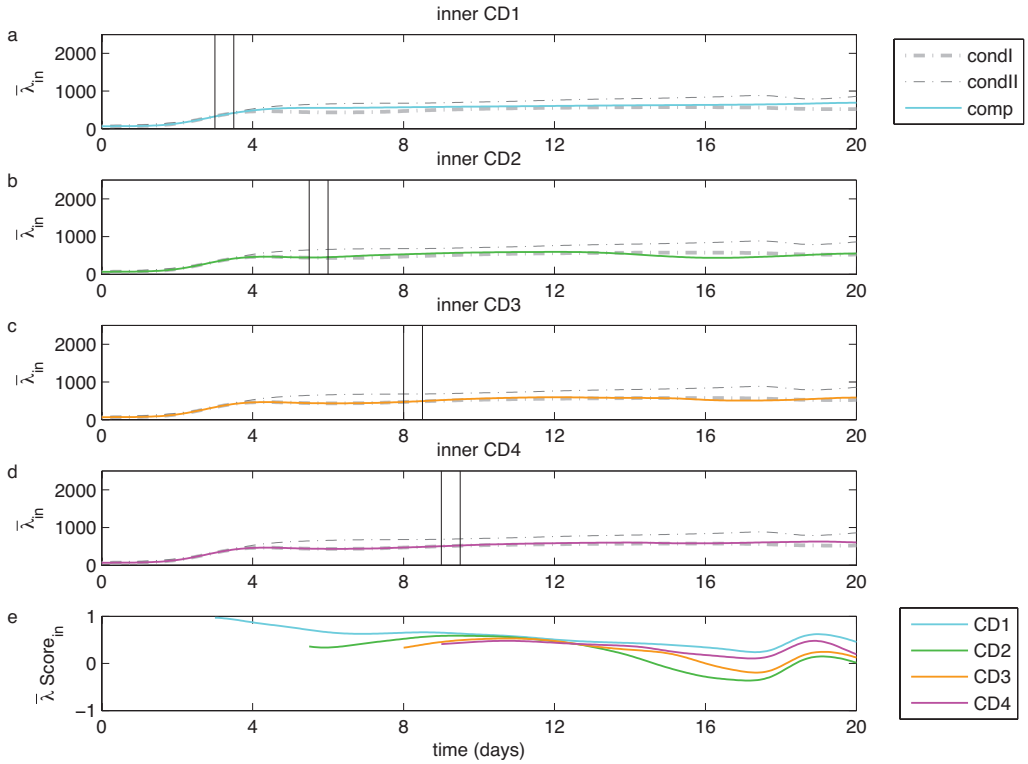

Figure E.3: a-d: $\overline{\lambda}_{in}(t)$ [m] for CD computations; e: $\overline{\lambda}Score(CD(k,t))$

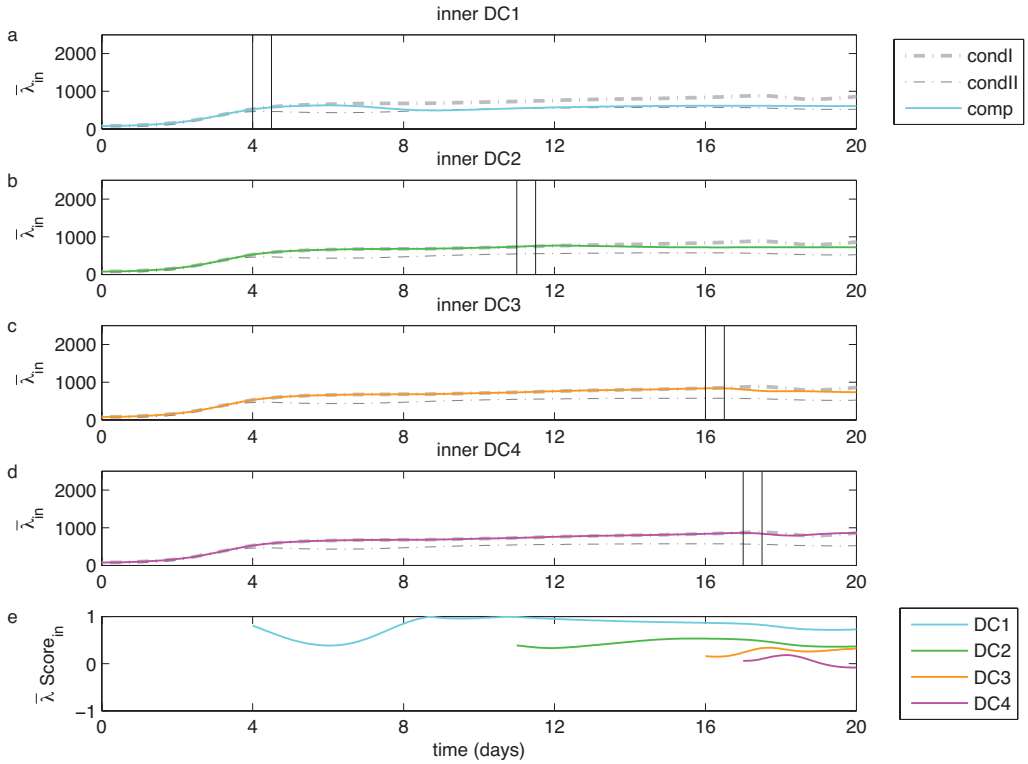

Figure E.4: a-d: $\overline{\lambda}_{in}(t)$ [m] for DC computations; e: $\overline{\lambda}Score(DC(k,t))$

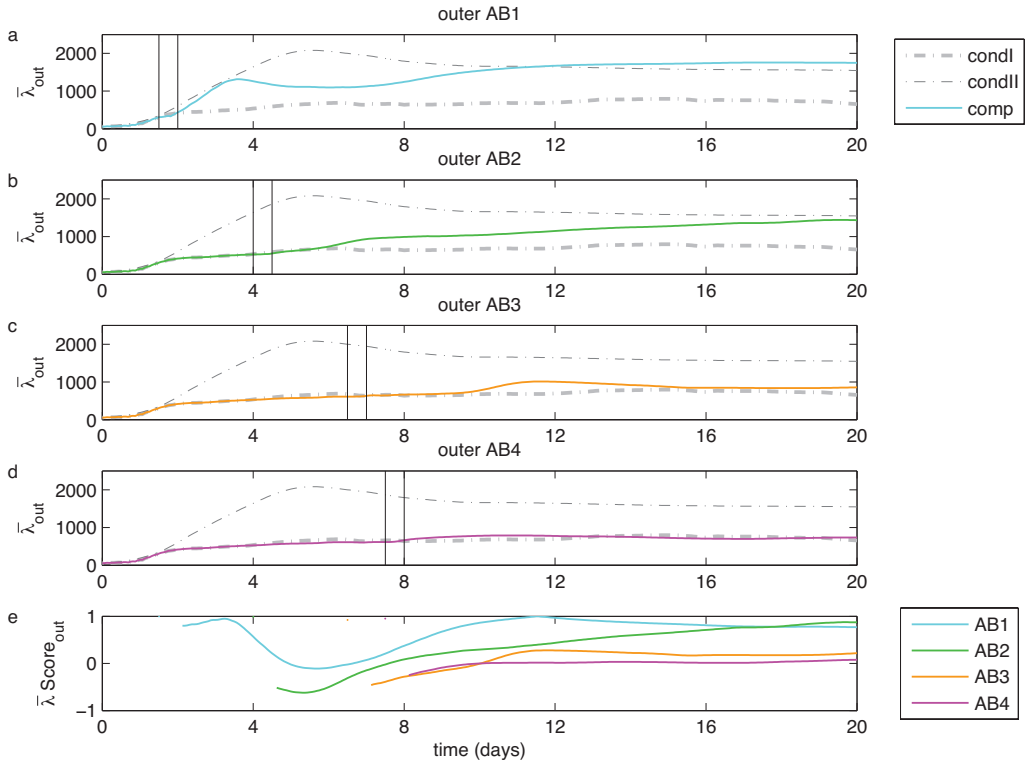

Figure E.5: a-d: $\overline{\lambda}_{out}(t)$ [m] for AB computations; e: $\overline{\lambda}Score(BA(k,t))$

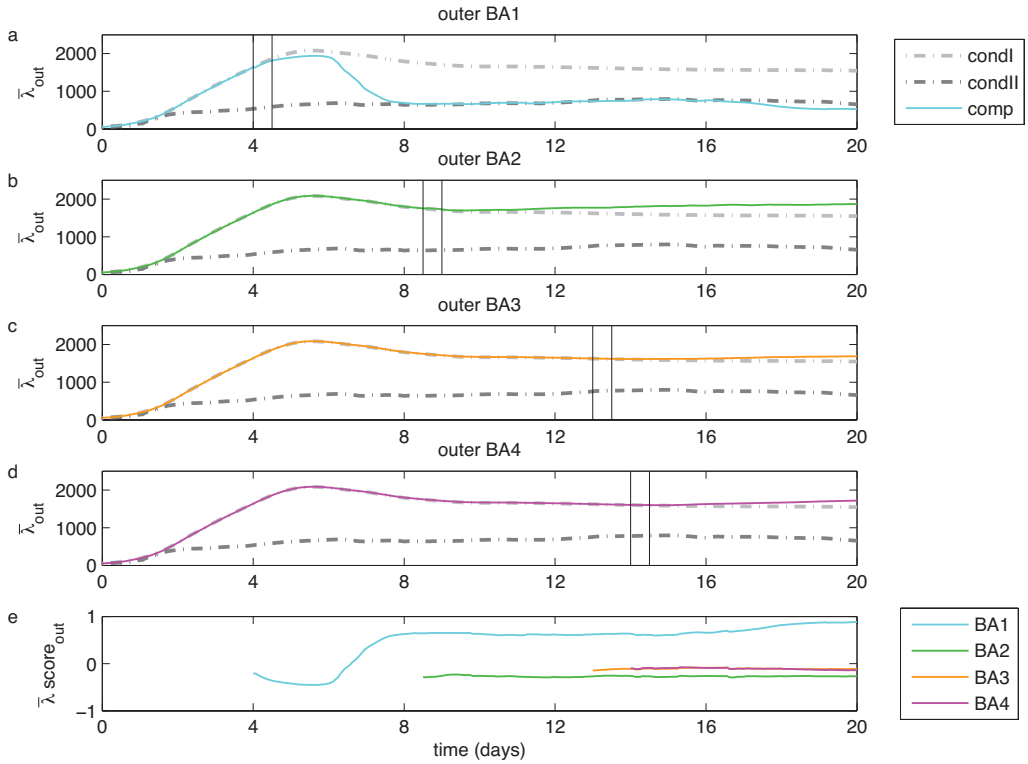

Figure E.6: a-d: $\overline{\lambda}_{out}(t)$ [m] for BA computations; e: $\overline{\lambda}Score(BA(k,t))$

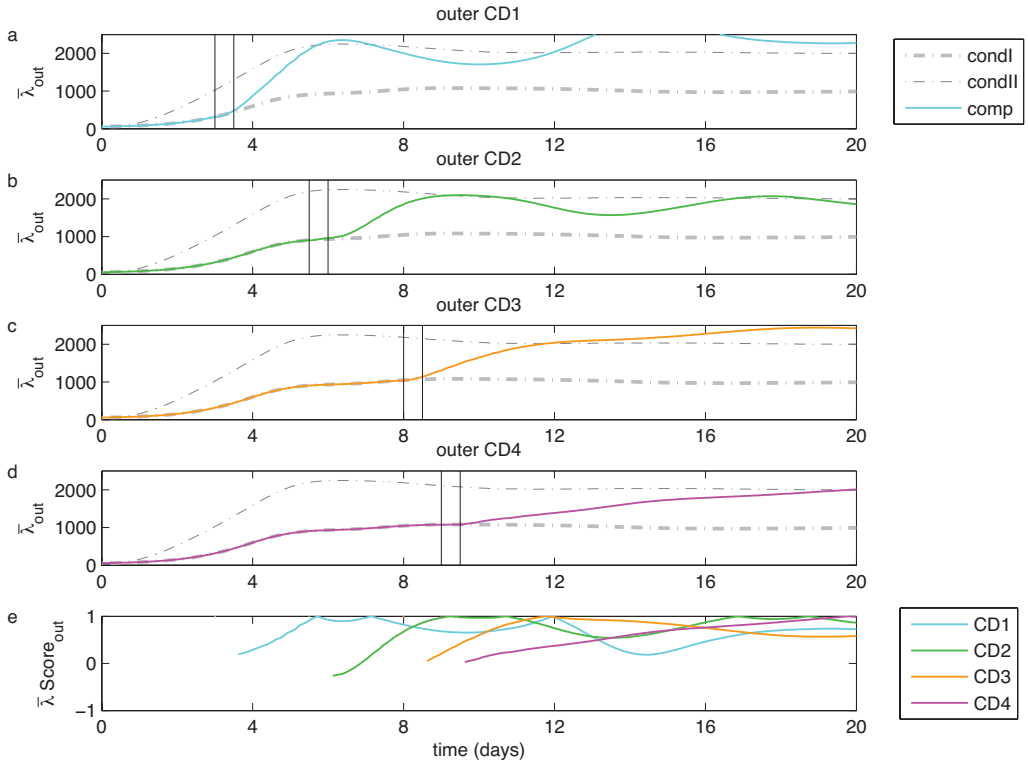

Figure E.7: a-d: $\overline{\lambda}_{out}(t)$ [m] for CD computations; e: $\overline{\lambda}Score(CD(k,t))$

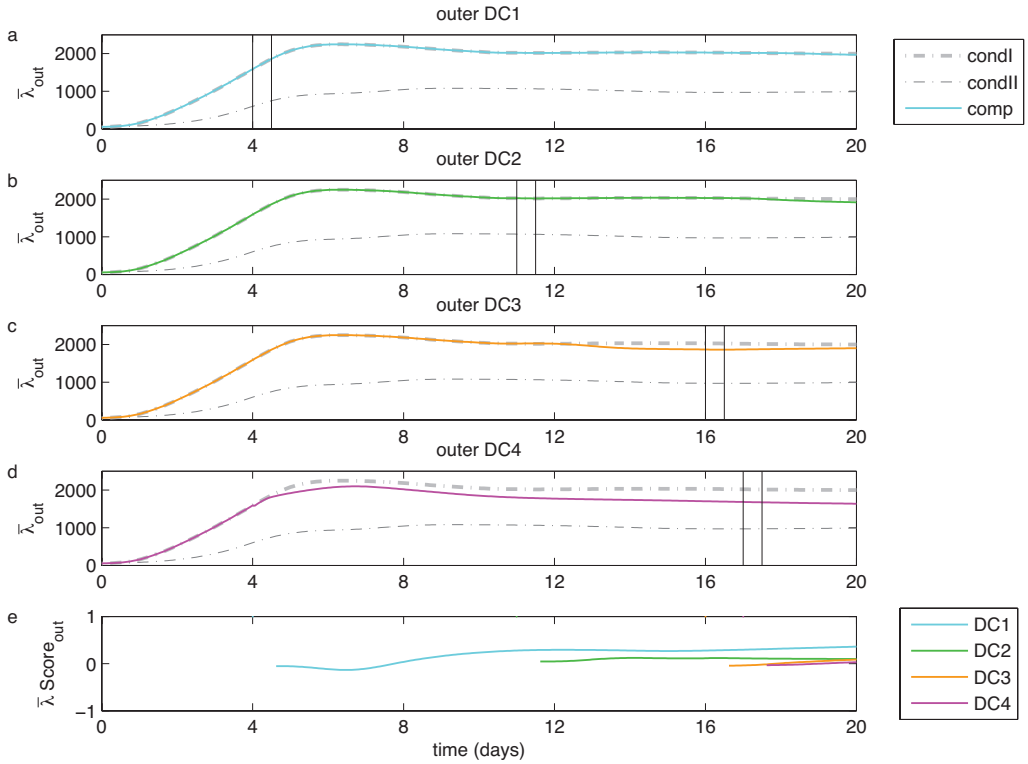

Figure E.8: a-d: $\overline{\lambda}_{out}(t)$ [m] for DC computations; e: $\overline{\lambda}Score(DC(k,t))$

Appendix F

Model set-up waves

F.1 Waves in Chapter 2 and 3

In chapter 2 and 3 the frequency-directional wave energy density spectrum, ($S_{\eta\eta}(f,\theta)$), is computed in each location with the third generation wave model SWAN (Booij et al., 1999; Ris et al., 1999). Input for the SWAN wave module are the significant wave height (H_{m0}), the mean angle of wave incidence ($\overline{\theta}$), the peak period (T_p), the directional spreading ($DSPR$) and the shape of the spectrum (in this case we choose Jonswap) at the offshore boundary from which $S_{\eta\eta}(f,\theta)$ is constructed. Given the fact that wave action is conserved in the presence of currents (whereas wave energy is not) the stationary wave action balance to describe the evolution of the wave spectrum:

$$\frac{\partial}{\partial x}c_x N + \frac{\partial}{\partial y}c_y N + \frac{\partial}{\partial \sigma}c_\sigma N + \frac{\partial}{\partial \theta}c_\theta N = \frac{D}{\sigma} \tag{F.1}$$

where the wave action density is given by:

$$N = \frac{S_{\eta\eta}(x,y,f,\theta)}{\sigma} \tag{F.2}$$

with σ the intrinsic radial frequency and c_x, c_y, c_σ, c_θ represent the propagation velocities in the x-, y-, σ- and θ-space respectively, and t being time. $D(f,\theta)$ is the source/sink term, representing the effects of generation, dissipation and non-linear wave-wave interactions as function of frequency and direction. The corresponding significant wave height is obtained from the spectrum by integrating over directions and frequency:

$$H_{m0}(x,y) = 4\sqrt{\int_\theta \int_f S_{\eta\eta}\left(x,y,\theta,f\right) \mathrm{d}f \mathrm{d}\theta} \tag{F.3}$$

and the mean wave angle is obtained from the first order moment:

$$\overline{\theta}(x,y) = \frac{\int\int \theta S_{\eta\eta}(x,y,\theta,f)\,\mathrm{d}t\mathrm{d}\theta}{\int\int S_{\eta\eta}(x,y,\theta,f)\,\mathrm{d}f\mathrm{d}\theta} \tag{F.4}$$

The stationary wave forces in the non-linear shallow water equations are computed from the spatial gradients in the radiation stresses within the flow domain where the latter are given by:

$$S_{xx}(x,y) = \rho g \int_f \int_\theta \left\{(1+n(x,y,f))cos^2\theta - \frac{1}{2}\right\} S_{\eta\eta}(x,y,\theta,f)\,\mathrm{d}f\mathrm{d}\theta \tag{F.5}$$

$$S_{yy}(x,y) = \rho g \int_f \int_\theta \left\{(1+n(x,y,f))sin^2\theta - \frac{1}{2}\right\} S_{\eta\eta}(x,y,\theta,f)\,\mathrm{d}f\mathrm{d}\theta \tag{F.6}$$

$$S_{xy}(x,y) = S_{yx}(x,y) = \rho g \int_f \int_\theta \left\{n(x,y,f)sin\theta cos\theta\right\} S_{\eta\eta}(x,y,\theta,f)\,\mathrm{d}f\mathrm{d}\theta \tag{F.7}$$

F.2 Waves in Chapter 4

The model approach in Chapter 4 takes into account the wave group variation of the radiation stresses to calculate the flow response with the non-linear shallow water equations. As a result Equation F.5, F.6 and F.7 can no longer be used to calculate the radiation stresses. Instead the frequency-directional spectra at the flow boundary are used to construct surface elevation time series with a random phase model:

$$\eta = \sum_i \sum_j a(\theta_i, f_j)\sin(2\pi f_{jt} - k\cos\theta_i x - \sin\theta_i y + \varphi_{ij}) \tag{F.8}$$

with φ_{ij} the random phase. The amplitudes are given by:

$$a(\theta_i, f_j) = \sqrt{2S_{\eta\eta}(i,j)\Delta f \Delta\theta} \tag{F.9}$$

where Δf and $\Delta\theta$ represent the spectral frequency and directional resolution. Taking the Hilbert transform to compute the wave envelope, A, the corresponding wave-group varying energy is calculated as:

$$E = \frac{1}{2}\rho g A^2 \tag{F.10}$$

which is used as the boundary condition in the calculation of the evolution of the wave energy, being no longer a function of direction and frequency, with the non-stationary wave energy balance:

$$\frac{\partial E}{\partial t} + \frac{\partial E c_g \cos\overline{\theta}}{\partial x} + \frac{\partial E c_g \sin\overline{\theta}}{\partial y} = -D \tag{F.11}$$

where $\overline{\theta}$ is obtained from the SWAN output within the flow domain and c and c_g are calculated from the mean wave period also provided by SWAN. The corresponding radiations stresses are calculated from:

$$S_{xx}(x,y,t) = (1 + n(x,y,t)\cos^2\overline{\theta}(x,y) - \frac{1}{2})E(x,y,t) \tag{F.12}$$

$$S_{xy}(x,y,t) = n(x,y,t)E(x,y,t)\sin\overline{\theta}(x,y)\cos\overline{\theta}(x,y) \tag{F.13}$$

$$S_{yy}(x,y,t) = (1 + n(x,y,t)\sin^2\overline{\theta}(x,y) - \frac{1}{2})E(x,y,t) \tag{F.14}$$

which are used to calculate the wave-group varying wave forcing in the non -linear shallow water equations. The wave group modulation in the wave forcing results in infragravity waves and very low frequency motions (Reniers et al., 2004).

Appendix G

Model process descriptions

G.1 Introduction

Chapter 4 describes the effect of various different process settings: the basic setting (base), no wave asymmetry (NA), no long wave induced stirring (NLW) and no wave groups (NWG) as well as of the variation of the diffusion ($facvisc$) and the rate of morphological change ($ACAL$). The description of these process settings are explained in detail below.

In general, in the conducted morphological computations, the bed level changes are computed as a result of a sequence of processes. First, wave energy and its dissipation is computed (Wave module). This results in local wave direction and energy dissipation and radiation stresses The depth-averaged velocity field is then computed using nonlinear shallow water equations (flow module). These velocities are used as input to compute the equilibirum concentration, which, combined with the computed velocities, using a depth-averaged advection diffusion equation, results in sediment concentrations. Computing both bed load (using the velocities) and the suspended load (using both the concentration, velocities and diffusion) transports, results in the total transport, which, using continuity, results in bed level updates (morphological module).

G.2 Wave equations

This text contains excerpts from Reniers et al. (2004).

(begin excerpt from Reniers et al. (2004)).

Motions on the time scale of wave groups are considered. To that end, all quantities have been averaged over the time scale of the incident wave period. The incident short-wave spectrum is assumed to be narrow in both frequency and direction. the balance for short wave energy E_w, describing the propagation of the obliquely incident short-wave groups on a variable bathymetry is then given by:

$$\frac{\partial E_w}{\partial t} + \frac{\partial E_w c_g \cos(\theta)}{\partial x} + \frac{\partial E_w c_g \sin(\theta)}{\partial y} = -D_w \tag{G.1}$$

where c_g represents the group velocity associated with the peak period of the waves, D_w the wave energy dissipation, x the distance in the cross-shore, y the distance alongshore (following the cartesian convention) and θ the mean wave incidence angle with respect to the x-axis. The spatially and temporally varying wave energy is defined along the upwave boundary. To model the wave energy dissipation due to wave breaking, the dissipation formulation of Roelvink (1993) is used:

$$D_w = 2\alpha f_p E_w \left[1 - exp\left[\left(\frac{E_w}{\gamma^2 E_{ref}}\right)^{\frac{n_d}{2}}\right]\right] \tag{G.2}$$

with

$$E_{ref} = \frac{1}{8}\rho g h^2 \tag{G.3}$$

where f_p is the peak frequency, γ is a wave breaking parameter representing saturation, α a coefficient of O (1), n_d a dissipation parameter corresponding to the randomness of the incident waves, ρ is the water density, g the gravitational acceleration and h represents the total water depth (including setup and infragravity surface elevation). The wave energy dissipation serves as input in the balance for the kinetic roller energy, E_r (Nairn et al., 1990; Stive and De Vriend, 1994):

$$\frac{\partial E_r}{\partial t} + \frac{\partial 2E_r c\cos(\theta)}{\partial x} + \frac{\partial 2E_r c\sin(\theta)}{\partial y} = -D_r + D_w \tag{G.4}$$

where c is the phase velocity and D_r represents the roller energy dissipation expressed by

$$D_r = \frac{2g\sin(\beta)E_r}{c} \tag{G.5}$$

Choosing β, the single unknown in Equation G.4, E_r, is solved for, which is taken to be zero at the up-wave boundary.

(end excerpt from Reniers et al. (2004)).

SWAN calculations are performed to pre-compute the refraction, i.e. θ, and yield the frequency-directional spectra at the flow boundary. These spectra are translated into wave group energy boundary conditions using the method outlined by Van Dongeren et al. (2003). From the wave and roller energy distributution the radiation stresses are computed (Reniers et al., 2004) which are the input for the further flow computations (next section).

G.3 Flow equations

(begin excerpt from Reniers et al. (2004)).

The short-wave averaged, depth-averaged velocity field is computed with nonlinear shallow water equations. The wave group varying velocities, u and v in the x- and y-direction respectively, include the wave-induced drift velocity (Stokes, 1847):

$$u = u^E + u^S \tag{G.6}$$

where the superscripts E and S stand for Eulerian and Stokes respectively, and a similar expression is used for the v component. This allows differentiating between the onshore velocity near the surface owing the waves and flow beneath that can include the offshore undertow. Separating the velocities in this manner is important in specifying the mass flux and the bottom shear stress. The continuity equation is given by:

$$\frac{\partial \eta}{\partial t} + \frac{\partial (hu)}{\partial x} + \frac{\partial (hv)}{\partial y} = 0 \tag{G.7}$$

where η represents the mean and infragravity surface elevation. The cross-shore momentum balance is given by:

$$\frac{\partial u}{\partial t} + u\frac{\partial u}{\partial x} + v\frac{\partial u}{\partial y} = -F_x - g\frac{\partial \eta}{\partial x} + \nu_t \left(\frac{\partial^2 u}{\partial x^2} + \frac{\partial^2 u}{\partial y^2} \right) - \frac{\tau_x}{h} \tag{G.8}$$

where the first term of the RHS represents the wave-induced forcing, the second term the cross-shore pressure gradient, the third term the turbulent lateral mixing and τ_x represents the combined short-wave and (Eulerian) current bottom shear stress (Soulsby et al., 1993) operating in the cross-shore direction. The alongshore momentum equation is given by:

$$\frac{\partial v}{\partial t} + u\frac{\partial v}{\partial x} + v\frac{\partial v}{\partial y} = -F_y - g\frac{\partial \eta}{\partial y} + \nu_t \left(\frac{\partial^2 v}{\partial x^2} + \frac{\partial^2 v}{\partial y^2} \right) - \frac{\tau_y}{h} \tag{G.9}$$

where τ_y represents the combined short-wave and current bottom shear stress in the alongshore direction. The wave- and roller induced forces F_x and F_y are defined as:

$$F_x = \frac{1}{\rho h} \left(\frac{\partial S_{xx}}{\partial x} + \frac{\partial S_{yx}}{\partial y} \right) \tag{G.10}$$

$$F_y = \frac{1}{\rho h} \left(\frac{\partial S_{yy}}{\partial y} + \frac{\partial S_{xy}}{\partial x} \right) \tag{G.11}$$

where the subscripts refer to the direction in which the forces act and the radiation stress tensor, S_{ij}, is obtained from linear wave theory including the roller contribution (Reniers et al., 2002).

The turbulent eddy viscosity, ν_t, associated with lateral mixing is assumed to be related to wave breaking (Battjes, 1975):

$$\nu_t = h\left(\frac{D_r}{\rho}\right)^{\frac{1}{3}} \tag{G.12}$$

where the roller energy dissipation, D_r, is obtained from the wave transformation Equation (G.4). The friction coefficent used in the bed shear stress formulation is kept constant and is based on the succesful comparisons with both mean flow conditions (Reniers et al., 2001) and infragravity conditions (Reniers et al., 2002, 2006).

(end excerpt from Reniers et al. (2004)).

G.4 Sediment transport and bed changes

In general, the same formulations have been used as in the model described in Reniers et al. (2004). In the computation of sediment transport and bottom changes, the following adaptations have been made.

The suspended sediment transport is modelled with a depth-averaged advection diffusion equation including horizontal diffusion terms (which were omitted in Reniers et al. (2004)):

$$\frac{\partial}{\partial t}hC + \frac{\partial}{\partial x}hCu^E + \frac{\partial}{\partial y}hCv^E - \frac{\partial}{\partial x}D\frac{\partial hC}{\partial x} - \frac{\partial}{\partial y}D\frac{\partial hC}{\partial y} = \frac{hC_{eq} - hC}{T_s} \tag{G.13}$$

in which h is the local water depth, C is the depth averaged sediment concentration, D is the horizontal diffusion coefficient, C_{eq} is the depth averaged equilibrium concentration, T_s is the adaptation time, representing the vertical diffusion of the sediment and u^E, v^E are the Eulerian velocities containing both wave-group averaged and long wave motions. The Gallapatti Time scale T_s (Gallapatti, 1983) is given by,

$$T_s = max\left(0.05\frac{h}{w_s}, 1\right) \tag{G.14}$$

where w_s is the sediment fall velocity (here $w_s = 0.016$ m/s) and h is the water depth. The equilibrium concentration (C_{eq}) is a function of sediment stirring by the wave-group averaged, long wave and short wave orbital velocities:

$$C_{eq} = A_{ss}\left(\left(u_{tot}^2 + \frac{0.018u_{rms}^2}{C_d}\right)^{1/2} - u_{cr}\right)^{2.4} \tag{G.15}$$

where A_{ss} is the suspended load coefficient, which is a function of the sediment grain size, relative density of the sediment and the local water depth (see Soulsby (1997) for details). C_d represents the drag coefficient, u_{cr} the threshold velocity, u_{rms} the short wave near bed orbital

velocity including breaking induced turbulence (Equation 16, Reniers et al., 2004) and u_{tot} represents the combined wave-group averaged and long wave Eulerian velocity magnitude:

$$u_{tot} = \sqrt{(u^E)^2 + (v^E)^2} \tag{G.16}$$

where:

$$u^E = \bar{u}^E + u_L^E \tag{G.17}$$

with $\bar{u}^E$ the velocity averaged over many groups and u_L^E the long wave velocity. The eulerian velocities (u^E and v^E) are obtained by subtracting the Stokes drift from the computed velocities (Reniers et al., 2004).

G.5 Adjustments for selected process settings

G.5.1 Wave asymmetry

Wave asymmetry: due to the asymmetric shape of waves, the onshore orbital motion under the wave crest is larger than the offshore motion under the wave trough: this results in net onshore sediment transport.

In the process-based model used in the computations in chapter 4 (Palm Beach), the wave asymmetry is included in the sediment transport. The bed level up-date is computed with continuity and the sediment transports used in this equation include bed transport, suspended load, and sediment transport due to wave asymmetry.

The suspended sediment transport is given by (using Equation G.13):

$$S_{s,x} = hCu^E - D\frac{\partial hC}{\partial x} \tag{G.18}$$

Bedload is computed locally using the transport formulation by Soulsby-van Rijn (Soulsby, 1997) (Equation G.19):

$$S_{b,x} = A_{sb}u^E \left(\left(u_{tot}^2 + \frac{0.018{u_{rms}}^2}{C_d} \right)^{1/2} - u_{cr} \right)^{2.4} \tag{G.19}$$

The wave asymmetry sediment transport is represented by:

$$S_{a,x} = \frac{1}{T} \int [\alpha_w u_b' \left(A_{sb} + A_{ss}\right) \left(u_{tot}^2 + \frac{0.018{u_b'}^2}{2C_d} \right)^{2.4} \cos\theta] dt \tag{G.20}$$

where u_b' is the instantaneous near bed velocity obtained with Rienecker and Fenton (1981), the prime denotes intra-wave variables, T is the mean wave period, α_w is a calibration parameter, and θ is the mean wave direction with respect to the x-axis (i.e. cross-shore). α_w is used to account for errors made as the used intra-wave values are in reality not in phase with the instantaneous velocities. Equivalent expressions are used for the alongshore transport components.

The bottom changes are obtained from continuity:

$$(1 - \varepsilon_{por}) \frac{\partial z_b}{\partial t} + ACAL \left(\frac{\partial S_x}{\partial x} + \frac{\partial S_y}{\partial y} \right) = 0 \tag{G.21}$$

in which z_b is bed level, $S_{x,y}$ are the combined suspended load ($S_{s,x}$ from Equation G.18), bed load ($S_{b,x}$ from Equation G.19) and wave asymmetry ($S_{a,x}$ from Equation G.20), transport rates in x- and y-direction and $ACAL$ is a calibration coefficient (-) which is set to 1 unless stated otherwise.

G.5.2 Long wave induced stirring

When long wave induced stirring is excluded (NLW), only stirring due to wave groups averaged velocities and short wave orbital motion is included. In the equations this means that the long wave induced velocities (u_L^E) are excluded from u^E and thus from u_{tot}, which therefore affects the computation of C_{eq}, $S_{s,x}$, $S_{b,x}$, $S_{a,x}$. u_{tot} represents the combined wave-group averaged and long wave Eulerian velocity magnitude:

$$u_{tot} = \sqrt{\bar{u}^{E2} + \bar{v}^{E2}} \tag{G.22}$$

where:

$$u^E = \bar{u}^E \tag{G.23}$$

with $\bar{u}^E$ the velocity averaged over many groups. The eulerian velocities (u^E and v^E) are obtained by subtracting the Stokes drift from the computed velocities (Reniers et al., 2004). Only in the advection diffusion equation the used u_{tot} contains contributions from long wave velocities (Equation G.17).

G.5.3 No wave groups

This option (NWG) excludes all wave group effects in all processes. Starting from the wave energy balance, which means no wave groups, no long waves, no eddies. Also in the advection diffusion equation, u^E does not include long wave velocities (in contrast to the NLW option, see above).

List of symbols

Roman symbols

$ACAL$	calibration parameter in bed continuity equation
A_{ss}	suspended load coefficient
A_{sb}	bed load coefficient
b	calibration factor (Equation 2.6)
c	propagation velocity
C	depth-averaged sediment concentration
C_d	drag coefficient
C_{eq}	depth averaged equilibrium concentration
c_f	longshore current friction parameter
$C1$	dimensional scaling coefficient
Cg	wave group velocity
Ch	Chézy coefficient
d	water depth with respect to MSL
D	horizontal diffusion coefficient
D_{50}	mean grain diameter
D_r	roller energy dissipation
$dZ2$	Z minus 2nd order polynomial per cross-shore location
EC_g	energy flux
g	gravitational acceleration
$facvisc$	calibration parameter in diffusion description
F	external forces
Fzy	variance
h	local water depth
h_{crest}	depth of the bar crest
H_{rms}	root mean square wave height
H_s	significant wave height
H_t	height of the active part of the bar
k	wave number, and here also: computation, clashes .. rename to do
k	computation number (1..4)
k_y	wave number
L	length scale (Chapter 5)
L_y	length scale (Chapter 2)

$meanZ$	alongshore mean of Z
$modelpar$	parameter obtained from model result
N	wave action density spectrum
$obspar$	observation based parameter value
q	flow velocity magnitude
RMS	morphological variability
$RMSscore$	score of the RMS
S	sediment transport
S	source/sink term (Equation 2.1)
S	score indicating model performance
S_a	wave asymmetry transport
S_s	suspended sediment transport
S_b	bed load transport
$stdZ$	alongshore std($dZ2$)
$stdZmean$	alongshore mean $stdZ$
t	time
T	mean wave period
t_0	initial moment
T_{resp}	response time
T_s	adaptation time
t_T	moment of transistion
u	depth-averaged velocity in x-direction
$u_b^{'}$	instantaneous near bed velocity
u_{cr}	threshold velocity
u^E	Eulerian velocity in x-direction
$\bar{u}^E$	wave group averaged u
u_L^E	long wave velocity
u_{rms}	short wave near bed orbital velocity
u_{tot}	wave group averaged and long wave Eulerian velocity magnitude
v	depth-averaged velocity in y-direction
V_{crit}	critical velocity
v^E	Eulerian velocity in y-direction
V_y	alongshore current velocity at bar crest
Vol_a	active volume of the bar
W	width of active part of the bar
w_s	sediment fall velocity
x	cross-shore location
$x5$	cross-shore location on rectified 5x5m grid
$X_{std,max}$	cross-shore location with highest $stdZ$
y	alongshore location
$y5$	alongshore location on rectified 5x5m grid
z_b	bed level

Z	depth of shoreline rectified bathymetry

Greek symbols

α_w	calibration parameter
β	roller dissipation coefficient
γ	breaker index
ϵ_{por}	porosity
η	water level with respect to MSL
θ	angle of wave incidence
$\overline{\lambda}$	weighted length scale
$\overline{\lambda}$ Score	performance of model on $\overline{\lambda}$
$\overline{\lambda}_y$	weighted length scale averaged over 10 overlapping alongshore sections (Chapter 4)
ν_t	turbulent eddy viscosity
ρ_w	water density
σ	relative frequency
τ	bed shear stress
ω	wave frequency

Subscripts

bar	either inner or outer bar
end	end of computation
i	computational setting
in	inner bar related parameter
obs	osbervation
par	parameter (*bathy*, *meanZ* or *stdZ*)
out	outer bar related parameter
T	transition
whole	whole model area

Acknowledgements

Nearshore sandbar morphology was the field I chose for my research, partly because of my love for water and partly because it concerns an area that can hardly ever be fully observed as it lays beneath the water surface. This intrigues me and remains a challenge. During this whole adventure many occasions and people have come across my path and motivated me in several ways. I would like to mention most of them personally below.

Ad Reniers, thank you for your great support, and lots of feedback in the whole process as well as your input on the numerical aspects of the job. I am very grateful for the time you were making for all the questions I had. When I came running into your office with another set of new graphs, you patiently waited until my gibberish calmed down into understandable sentences. Thank you for the great hospitality you and your family showed during my three month visit to Miami, Florida. With a big smile I remember the conversations we had during lunch breaks, overlooking the turquoise waters and spotting whatever weird fish would be swimming by. Stella, thank you for sharing the warmth of your family -the great joys of the presence of Femke and Lennart- during my stay there.

Marcel Stive, your enthusiasm has been motivating from the beginning. Thank you for the opportunities and support throughout the various phases. You gave me a lot of freedom and guidance at crucial moments. I highly appreciate your open communication.

Gerben Ruessink, thank you for the discussions and support throughout my PhD. You have advised me at several moments and were always available for constructive feedback, which I have always highly appreciated. Graham Symonds, thank you for inviting me to spend time at CSIRO in Perth, Western Australia, the intended three months quickly changed into six and I am thankful for every moment of it. It was inspiring to collaborate with someone who was answering my model-based questions with a more field-based perspective. It has been very valuable. I would like to express my sincere gratitude toward the other members of the committee: Prof. Dr. Ir. Dano Roelvink, thank you for developing Delft3D code on the spot when I got pretty stuck with existing code. Prof. Dr. Huib de Swart thank you for all the constructive comments on my thesis and the great discussions. Prof. dr. Wim Uijttewaal, thank you for reviewing my thesis.

Great thanks also go to Delft University of Technology, the Dr. Lely Foundation, ONR, Deltares

for the software support and the NIOO for understanding the hectic phase I was in, while finishing my PhD and starting a new position.

Several people and moments have been crucial in the snowball effect of getting to know more and more people in this field of science. They are all having similar mindsets when it comes to sharing a good time, enjoying the moment and being simply kind with one another. This ever spreading network seems to guarantee the greatest moments during workshops and conferences. Thanks to all, it is a pleasure! Two events in the early days of my PhD had a large spin-off in this network of people I quickly got to know: participating in the Coastview project and The Renesse Summerschool in 2003. Thanks to: Stefan Aarninkhof, Mark van Koningsveld, Mark, Ken, Howard, Nigel, Clara, Paolo, José Jiménez, Rob Holman, Kathelijne, and all the others of the Coastview crew who introduced me into the great habit of having the greatest workshops and meetings. The summercourse in Renesse was great. Thanks for the great times and constructive discussions, Nick Dodd and Albert Falqués. Rodrigo, Bruno, Roland, Cesca, Maitane, and all the others thank you for all the great laughs. Ismael you became a very valuable friend, unaware that you are always reminding me to enjoy life even more. Knowing you, connected me to the Mexicans, who I've met at several occasions and in various situations. You guys always suprise me with your endless energy to create little fiestas. It is a gift to be hanging out with you. Christian, thank you for your hospitality in San Diego, you are a very warm person. Adrian thanks for the hospitality in Plymouth. Tona and Elena -half a Mexican by now- you are two of the most wonderful people I know, thank you for the good times and for connecting me to Gemma and Tim! Guys, let's have many more shared moments -surf and pancakes! The Truc Vert experiment was great: Jamie MacMahan, all the people in the house and the other people in Truc Vert, we shared great times after hard days work trying not to get too caught in rip currents. Lindino and Raquel, muito obrigada for the hospitality and shared sessions in Florida. Giovanni and Sandrine, thank you for inviting me to your house in Hamilton and showing me around. I treasure the moments I have spent in New Zealand. Brad and Ana, thank you for your hospitality in Sydney, inviting me to stay at your place during the fieldwork at Palm Beach. You are both such great and relaxed people, I enjoyed spending some time amongst you. Thank you Nathaniel Plant, Yohama, Nicolas Bruneau, Mitch, Ian. Irene, vielen Dank for the great time in Karrinyup, living in your house during my stay in Perth, you provided me with a very relaxed home.

From the Hydraulic Engineering section: My buddies in Delft: The Boysz!!!! Thanks for all the good times we had, especially Martijn and Matthieu. We had great times that first winter I got back from Australia and we were heading towards the beach together on cold wintery mornings for great sessions with snow or sun and warm cups of tea afterwards. I treasure those moments and the shared smiles. Martijn, thanks for being a great room mate and for letting me win with office soccer once in a while :). Matthieu, you are a special person, thanks for the great times. Jaap it was great organising two bike tours, you are a big support for people in general.

Jasper, thanks for the good times in Delft and during conferences (Baja California!). Fedor, I admire your great will and actions to learn, thank you for the LaTeX support. Thank you for all the good times in these years: Wim Kanning, Ronald, Bianca, Madelon, Zhu, Ruben, Mathijs, Anneke, Martin, Stefan, Paul Sistermans, Mark, Saskia, Edwin, Hans Bonekamp, Henk Schuttelaars, Joep, Jan van de Graaff, Dirk Jan, Sierd, Chu, Sebi, Tomo, Li, Tung, Kees, Xui Fei, and all the others. Thanks for the great support, even when I was calling for help from somewhere over an ocean, Mark Voorendt, Chantal, Inge, Adeeba and the others. Thanks for the nice sessions in PSOR with the people from the fluid mechanics section: Gerben, Michel, Wim, Bas -running from The Hague to Delft was definitely more fun with two-, Walter, Petra, André van der Westhuysen: you are my birthday buddy, it was great to be sharing cups of tea and chocolate while both still working at the TU on weird hours. In my new working environment at the NIOO, Ellen, Eduardo, Christian and the others, you guys crack me up.

To my beloved friends who I at times hardly saw. Thank you for still being my friends: Jurjen -always good for sharing smiles and great laughs, you are creative in both your work and humour; Esther and Arend, it is always nice to be around you, you are great people; Carla, Jorrit and your kiddo's Hidde and Sjoerd, I am always happy with moments I could spend with you, thank you for all the support you give me; Annemaartje, I enjoy having you as a friend and catching up thoroughly from time to time. Tessa and your family, thank you for all the large and small e-mail conversations we have had, both in length and contents. It is not always easy both having busy lives and living in separate countries, I am happy we are sharing the contact that we have. Thank you, Klemm! To my other friends who may stay or may pass, I enjoy and treasure moments and smiles -and surf sessions- together, thank you. A special thanks goes to those whose names I may not know, that give me a smile on my way, lifting my day.

The biggest thanks goes to my family. Dear grote broer Arnout and Anneloes. Thank you both. Anneloes it is a great joy to have you in the family, I couldn't be more happy with such a partner for my brother. Arnout, thank you for pushing me and supporting me especially and specifically in the last phase of finishing this piece of work. I appreciate you highly. My papa and mama. Thank you for making and taking my hand to learn me to walk and letting go as soon as my feet are moving forward. I am continuously learning from you and your approaches to life. Dankjulliewel.
Jullie weten
dat mijn dank
ook staat geschreven
in al het wit
wat rond de woorden zit.
Marije

Curriculum Vitae

Marije Welmoed Joanne Smit was born the 8th of September 1975 in Berlin, Germany. She grew up in and near Deventer and Hilversum where she graduated from secondary school, the Comenius College in 1993. She started studying Civil Engineering and Management at Twente University in Enschede. During her fourth year, she spent a year in Great Britain at the University of Southampton. After a traineeship on Texel (NIOZ) and her MSc project in The Hague at the TNO Physics and Electronics Laboratory, she graduated in 1999 under the supervision of Prof.dr.ir. H.J. De Vriend. She then worked for an environmental consulting company, Iwaco, later named Royal Haskoning, for two and a half years in the field of ground water.

In 2002 she commenced her PhD at Delft University of Technology at the section of Hydraulic Engineering of the faculty of Civil Engineering and Geosciences. During her PhD she was involved in the European Coastview project and the Beach Wizard project, funded by ONR. As part of the latter project she spent six months at CSIRO, in Perth, Western Australia. From August 2008 she worked part time on the European funded MICORE project.

September 2009 she started a postdoc position at NIOO-CEME in Yerseke at the Spatial Ecology department investigating Salt Marsh Dynamics.